UNIVERSIDADE DO ALGARVE

Faculdade de Ciências e Tecnologia

Design and implementation of microstrip filters for a radio over fiber network demonstrator

Paulo Roberto Ferreira da Rocha

Master in Electrical Engineer and Telecommunications

2009

UNIVERSIDADE DO ALGARVE

Faculdade de Ciências e Tecnologia

Design and implementation of microstrip filters for a radio over fiber network demonstrator

Paulo Roberto Ferreira da Rocha

Supervisor:

Professora Doutora Maria do Carmo Raposo de Medeiros

Master in Electrical Engineer and Telecommunications

2009

Declaration

Paulo Roberto Ferreira da Rocha, Universidade do Algarve student declares that he is the author of this master dissertation.

Student:

Paulo Roberto Ferreira da Rocha

Supervisor:

Professora Doutora Maria do Carmo Raposo de Medeiros

Supervisory committee:

Abstract

The need for networks able of integrating services such as voice, video, data and mobility is growing. To satisfy such needs wireless networks with a high data transmission capacity are required.

An efficient solution for these broadband wireless networks is to transmit radio signals to the Base Stations (BS) via optical fiber using Wavelength Division Multiplexing (WDM). The WDM usage helps this growing, allowing the use of a single optical fiber to feed several BSs using for each one a different wavelength (or WDM channel). Additionally, in the RoFnet project in order to improve radio coverage within a cell, it is considered a sectorized antenna interface. The combination of subcarrier multiplexing (SCM) with WDM, further simplifies the network architecture, by using a specific wavelength channel to feed an individual BS and different subcarriers to drive the individual antenna sectors within the BS.

This dissertation reports the design and simulation of the microstrip bandpass filters used at the BS on of the RoFnet demonstrator. These bandpass filters are used for the filtering of fours subcarrier multiplexed channels located at (9, 11, 13, 15 and 17 *GHz*). The design and simulation of the lowpass root raised cosine filter required for testing is also discussed. Additionally, the design and testing of two power splitter is reported. Finally, all the designed components were brought together and the overall BS performance is assessed.

The microstrip components have been designed and simulated using both ADS (Agilent's Advanced Design System) and Momentum simulators.

Kewords: microstrip filter, lowpass filter, bandpass filter, power divider, power combiner, Wilkinson power divider, Radio over Fiber and Advanced Design System.

Resumo

Sistemas de Rádio sobre Fibra (RoF - *Radio over Fiber*) que operam na gama de frequências milimétricas (*mm-wave*), apresentam muitas vantagens para a implementação de sistemas de acesso das redes sem fios. No entanto, devido às suas características de propagação estes sistemas apresentam tamanhos de células pequenos e consequentemente necessitam de um grande número de estações base (BS-*Base Station*) para cobrir uma determinada área geográfica. Uma rede RoF, é composta por várias BSs ligadas a uma estação central (CO-*Central Office*) por uma rede de acesso de fibra óptica. Dentro de cada BS o sinal necessita de ser filtrado através de filtros passa banda e formatado através do filtro passa baixo *Raised-Cosine,* na banda base de modo a minimizar a interferência inter-simbólica na transmissão dos sinais. Divisores de potência também são considerados na arquitectura proposta para a BS.

Nesta dissertação é apresentada a implementação dos componentes necessários á tecnologia Rádio sobre Fibra utilizando a tecnologia microstrip. Esta tecnologia consiste num condutor assente num substrato com um respectivo dieléctrico e é usada para construir antenas, acopladores, filtros e divisores de potência a um preço reduzido quando comparado aos componentes que operam na gama de frequências tradicional. Outras vantagens são a reduzida dimensão dos componentes assim como o seu baixo custo. Por outro lado, são dispositivos com facilidade de perda de potência e muito susceptíveis a radiações e/ou efeitos electromagnéticos entre as linhas de transmissão adjacentes e o substrato em que assentam.

A implementação dos componentes do projecto é feita no software *Advanced Design System* (ADS). Este software incorpora ferramentas de simulação bastante úteis para a análise dos componentes implementados neste mestrado. O *Momentum* é um simulador determinante na construção de dispositivos em microstrip devido á densidade de efeitos electromagnéticos ao longo das linhas de transmissão. Esta ferramenta identifica efeitos de *coupling*, produz resultados próximos da realidade e permite visualizar radiações e variações de corrente no circuito.

Os filtros têm como objectivo obter uma determinada largura de banda, atenuando todas as frequências fora deste intervalo. Na banda passante do filtro idealmente não existe atenuação e no intervalo rejeitado a atenuação será máxima. No caso dos condensadores,

bobines e linhas de transmissão a atenuação na banda passante está sempre presente. Esta atenuação só pode ser melhorada pela escolha correcta dos componentes do filtro, minimizando assim a atenuação na banda passante e melhorando a eficácia de filtragem. Em baixas frequências, os condensadores e bobines são usados para o desenho dos filtros. No entanto, em altas frequências o uso de secções de linhas de transmissão que têm um funcionamento equivalente ao dos condensadores e bobines é mais o método de desenho mais habitual, ou seja *microstrip*.

As técnicas utilizadas para o desenho dos filtros podem ser *Image Parameter Method* ou *Insertion loss Method*. *Image Parameter Method* tem a desvantagem de não se poder controlar a resposta na banda passante e na banda de rejeição. O segundo método começa com um protótipo de filtros passa baixo baseado nas curvas de atenuação dos filtros Butteworth ou Chebyshev. A atenuação na banda passante e de rejeição pode ser controlada com base no número de secções de linhas de transmissão escolhido e nas características dos componentes usados tais como a espessura do substrato, do condutor e o dieléctrico do mesmo.

O filtro passa baixo com uma resposta equivalente ao *Square Root Raised Cosine* (SRRCOS) foi implementado e posteriormente simulado no *Momentum* no qual não deferiu significativamente. A construção deste tipo de filtros tem como base um filtro passa baixo que consiste em linhas de grande e baixa impedância consecutivamente ligadas entre si. No entanto, para conseguir trazer a resposta para zero como no *square root raised cosine filter* (SRRCOS) foi utilizado um *Open Circuit Stub* com um comprimento de $\lambda/4$ na frequência do filtro. Este componente é transformado num curto-circuito e a impedância de entrada na direcção do *Stub* torna-se zero. O curto-circuito à saída do filtro cria o zero pretendido pela resposta do SRRCOS.

A implementação dos filtros passa banda é efectuada recorrendo ao efeito de *coupling* entre duas linhas de transmissão próximas uma da outra. O método utilizado para implementar os filtros passa banda chama-se *parallel coupled lines*, e consiste numa cascata de secções de linhas de transmissão contendo cada uma delas duas linhas em paralelo, em que o número de secções determina a ordem do filtro. Esta estrutura é analisada pelo método de simetria *Even and Odd mode* que consiste em obter os parâmetros-S do componente.

Nas altas frequências os filtros passa banda implementados apresentam bastantes oscilações devido ao facto da construção estar no limite de largura de banda suportada pelo método utilizado, devido aos efeitos de *coupling* das linhas de transmissão paralelas entre si e

devido à necessidade acrescida de processamento nesta gama de frequências. A tecnologia *Microstrip* apresenta uma limitação na construção de filtros passa banda estreitos. Para este efeito é necessário um grande espaçamento nas linhas de transmissão paralelas entre si, provocando uma maior atenuação na resposta do filtro. Na implementação deste filtro aumentou-se a largura de banda e deslocou-se o filtro para a zona do espectro que não contem informação relevante.

Para dividir o mesmo sinal e obter a mesma potência nas duas saídas normalmente utiliza-se o *Wilkinson power divider*. Este divisor pode ter uma ou mais secções consoante a largura de banda pretendida e tamanho disponível no substrato. A sua análise é também efectuada através do método *Even and Odd mode*. É usual na construção deste dispositivo a implementação de uma resistência ao longo das diversas secções, para fornecer um melhor isolamento nas portas de saída do divisor. As resistências utilizadas na dissertação chamam-se *thin film resistors*. A análise do *power divider* consiste no estudo dos parâmetros-S, mais precisamente na análise de isolamento entre as portas, *port matching* e *insertion loss.*

Os divisores de potência foram devidamente implementados e co-simulados no *Momentum*. Co-simulados pois o *Momentum* só por si, não considera os elementos físicos de circuitos tais como as resistências. Para este efeito, o componente foi gerado no *layout* e foram inseridas portas internas no circuito para posteriormente poder-se ligar os componentes. Depois foi gerado um componente com base na arquitectura e importado para o *schematic* para se poder efectuar a simulação electromagnética com as resistências integradas. O último divisor desenhado em vez de resistências ideais utiliza uma resistência do tipo *thin film resistor*. Este tipo de resistência, devido à sua constituição foi simulado apenas no *Momentum*.

Na simulação geral é possível ver todos os elementos desenhados em *microstrip* em conjunto com os restantes dispositivos presentes na arquitectura deste projecto. Inicialmente é gerada uma sequência aleatória de bits. Estes dados são filtrados e situados no espectro nas frequências 9,11,13,15 e 17 *GHz*. Posteriormente o sinal é dividido e filtrado pelos primeiros filtros passa banda de banda larga. O sinal é novamente dividido para posteriormente ser filtrado pelos filtros passa banda especificamente desenhados para cada uma das frequências do espectro (9, 11, 13, 15 e 17 *GHz*). Após este processo é aplicado novamente o filtro *Square Root Raised Cosine* para se proceder à análise da qualidade de serviço da rede através do

diagrama de olho. Outra análise efectuada é a visualização do espectro de frequências em determinados pontos fulcrais da arquitectura da BS.

Palavras-chave: Filtros em *Microstrip*, filtros passa baixo, filtros passa banda, divisores de sinal, *Wilkinson Power Divider*, *Radio over Fiber, Advanced Design System*.

Acknowledgements

In these years I have benefited a lot from the extensive knowledge and experience of my supervisor Prof. Maria Carmo Raposo de Medeiros. It has been pleasure learning from her and being motivated by her.

This work could not be achieved without the precious help and guidance of Prof. Izzat Darwazeh. His excellent support and work methodology were fundamental for the accomplishment of this dissertation.

Special thanks to my parents João Rocha and Neyde Rocha who always supported me, my girlfriend Ida Gaspar, my friends Mark Guerreiro, Ricardo Avó, José Coimbra and Hélio Vargues. Their help was very important for the accomplishment of this project.

Table of contents

List of figures

Abbreviations

ADS   Advanced Design System

BS   Base Station

CO   Central Office

EM   Electromagnetic

IL   Insertion Loss

ISI   Inter-Symbol Interference

LTE   Long Term Evolution

MMIC   Monolithic Microwave Integrated Circuit

NRZ   Non Return to Zero

PCB   Printed Circuit Board

PDA   Personal Digital Assistance

RF   Radio Frequency

RL   Return Loss

RoFnet   Reconfigurable Radio over Fiber network

RSOA   Reflective Semiconductor Optical Amplifier

SCM   Subcarrier Multiplexing

TEM   Transverse Electromagnetic

TM   Transverse Magnetic

TE   Transverse Electric

VSWR   Voltage Standing Wave Ratio

WDM   Wavelength Division Multiplexing

WLAN   Wireless Local Area Network

Wifii   Wireless fidelity

Wimax   Worldwide Interoperability for Microwave Access

1. Introduction

1.1. Introduction

Currently wireless and mobile communications are witnessing a great development. In most developed countries, mobile phone penetration exceeds that of fixed phones. Wireless communications are entering a new phase where the focus is shifting from voice to multimedia services. Present mobile network users want to be able to use their mobile terminals and enjoy the same user experience as they do while connected at their fixed network at work or at home. WLAN hot-spots based on IEEE802.11 are a reality, and many consumer devices (Laptop PCs, mobile telephones, PDAs, etc) have Bluetooth so they can establish a Wireless Personal Area Network (WPAN). Due to the need of integrated broadband services (voice, data and video) wireless networks will need higher data transmission capacities well beyond the present day standards of wireless systems. Nowadays the main technologies vary from IEEE802.11 a/b/g (54Mbps) at 2.4 GHz and 5 GHz (Wi-Fi) until Wimax 802.16 (72 Mbps) between 2 and 66 GHz. Currently international standard bodies such as IEEE 802.15.3c working group are working on the standard for 60 GHz WPAN transmission systems. WPAN networks cover relatively short distances (10-30 meters) and can support high data rate applications (480 $Mbit/s - 3\ Gbit/s$).

The limited propagation characteristics of mm-wave operating in the 60 GHz region lead to small cell sizes, therefore a large number of cells, served by base stations (BSs), are necessary to cover an operational area. This requirement has led to the development of system architectures where functions such as signal/routing/processing, handover and frequency allocation are carried out at the central office (CO). The best solution for connecting the CO with BSs in such radio network is via an optical fiber network, now known as radio over fiber (RoF) network [1]. By exploiting high bandwidth wavelength division multiplexing (WDM) networks, an integrated efficient fiber radio backbone network can be realized, where mm-wave carriers are modulated with data, placed on a particular wavelength channel and delivered to a specific BS (Figure 1.1).

The multiple BSs providing wireless connectivity to users via mm-wave radio links are connected with a central office (CO) via an optical fiber access network, i.e. employing Radio over Fiber (RoF) technology.
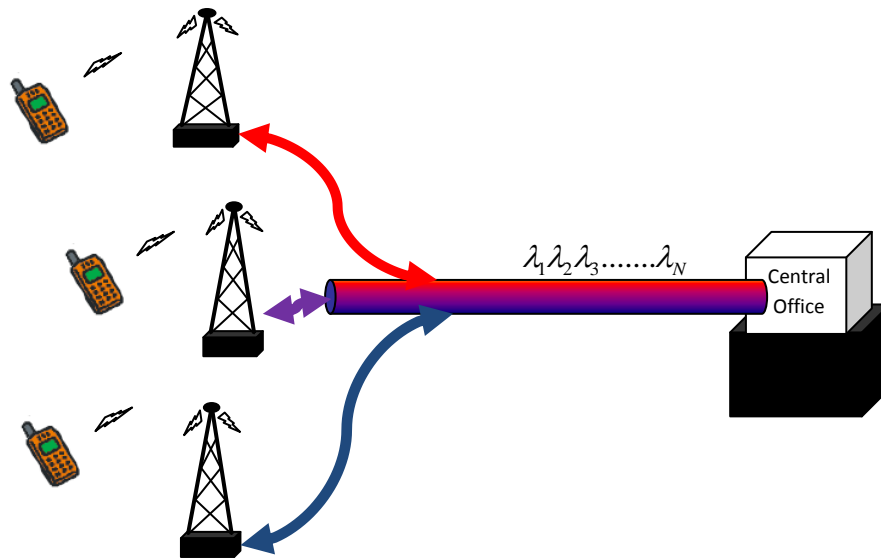
Figure 1.1 - Radio over Fiber (RoF) network architecture

1.2. RoFnet Project

The RoFnet-Reconfigurable Radio over Fiber network is a project supported by the Portuguese Foundation for Science and Technology. This project proposes an innovative radio over fiber optical access network architecture, which combines a low cost Base Station (BS) design, incorporating reflective semiconductor optical amplifiers, with fiber dispersion mitigation provided by optical single sideband modulation techniques. Optical wavelength division multiplexing (WDM) techniques are used to simplify the access network architecture allowing for different Base Stations to be fed by a common fiber. Different wavelength channels can be allocated to different BSs depending on user requirements. Additionally, in order to improve radio coverage within a cell, it is considered a sectorized antenna interface. The combination of subcarrier multiplexing (SCM) with WDM, further simplifies the network architecture, by using a specific wavelength channel to feed an individual BS and four different subcarriers to drive the individual antenna sectors within the BS.

1.3. Downlink operation

A BS receives the downlink RF signal on a specific wavelength channel. The downlink signal is composed by *4* multiplexed subcarrier channels (11 *GHz*, 13 *GHz*, 15 *GHz* and 17 *GHz*) combined with an un-modulated RF (9 *GHz*) carrier as shown in Figure 1.2. The un-modulated RF carrier and the downlink signals are generated at the CO. At the BS, the

downlink optical signal is split. One part is directed to the RSOA (Reflective Semiconductor Optical Amplifier), and the other part is detected by a high bandwidth receiver and delivered to the antennas. The four SCM channels are delivered to the four antenna sectors after being photo detected, split by a splitter designed in this dissertation and filtered by bandpass filters designed in this dissertation. The un-modulated RF carrier is filtered and used in the uplink operation.
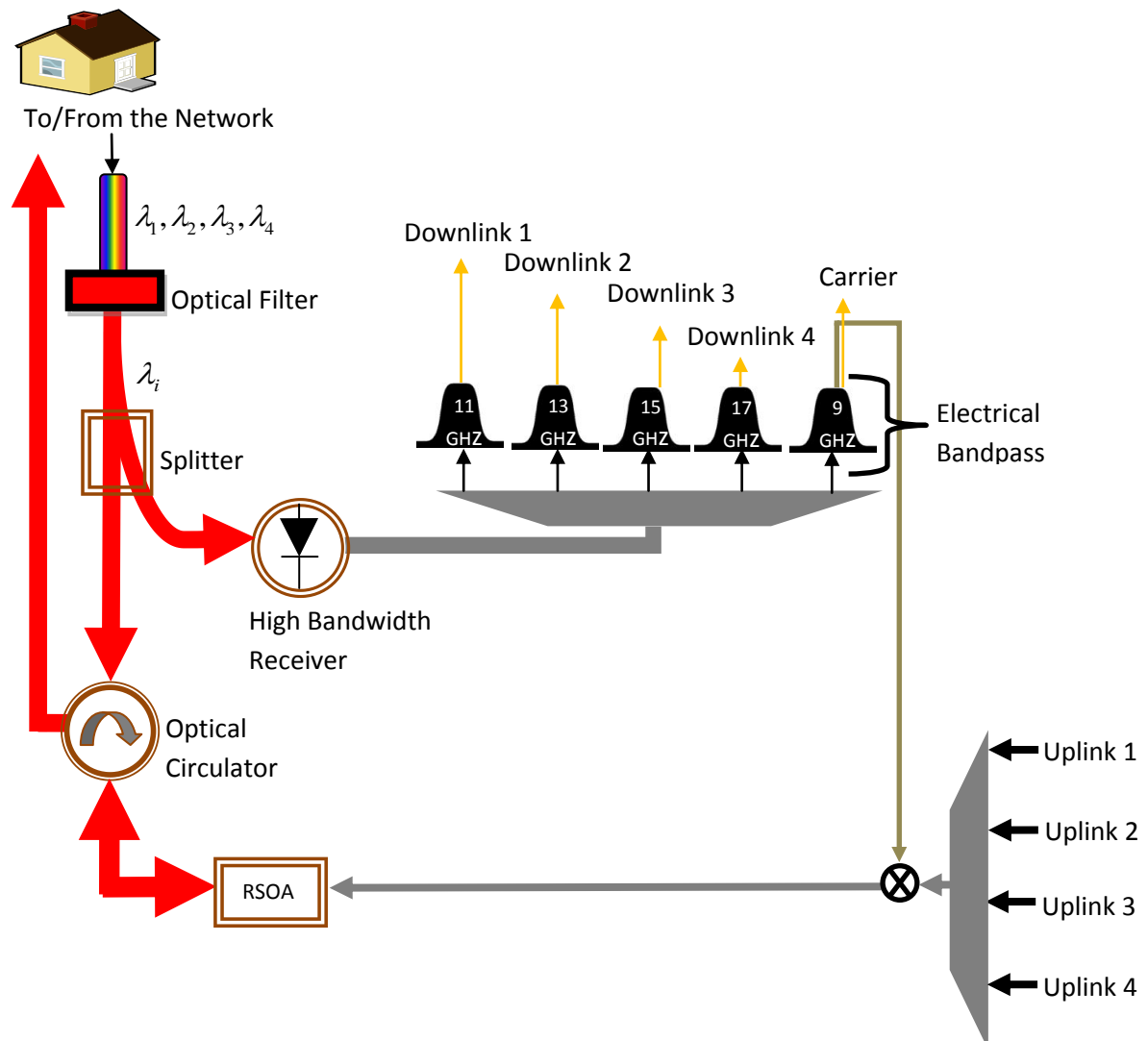
Figure 1.2 - RoFnet BS architecture

1.4. Uplink Operation

The downlink optical carrier travels through the RSOA, where it is amplified and modulated by the uplink data channels, which has been combined and down converted to an Intermediate Frequency (IF). The un-modulated RF carrier act as local oscillators (LO) and is

used to down-convert the uplink data to an Intermediate Frequency (IF), within the electrical bandwidth of the RSOA (1.2 *GHz*). The RSOA is directly modulated by the SCM uplink down-converted signals.

Using this technique, the uplink optical signal is generated by recovering a portion of the optical carrier used in the downlink transmission.

1.5. Dissertation Goals

The goal of this dissertation is to design, implement and test several lowpass and bandpass filters and one power divider that will be used in the RoFnet demonstrator. The work plan involves:

- Installation and familiarization with EEsof Advanced Design System (ADS);
- Bandpass and lowpass filters design;
- Filters optimization;
- Microstrip implementation and optimization;
- Performance analysis using simulation methods.

1.6. Dissertation Organization

Following this short introductory section, chapter 2 discusses the theoretical fundaments needed for the work reported in this dissertation such as: transmission lines, scattering matrix, ABDC parameters, Richard's transformation, Kuroda's identities and digital transmission over bandlimited channels.

Chapter 3 describes the design procedure off both the lowpass and the bandpass filters required for this dissertation. Both filters design start from the choice of the appropriate lumped-element lowpass prototypes, followed by the transformation of these prototypes and the implementation in microstrip. An overview about power dividers is also given namely the Wilkinson power divider design approach.

The design environment (Advanced Design System) is described in chapter 4.

Chapter 5 reports to the design and implementation of the microstrip components. The BS filtering scheme is projected and the substrate is selected. The implementation of the lowpass filter, bandpass filters and power divider are also described in this chapter.

Momentum results are presented in chapter 6 as well as performance evaluation of the designed microstrip components.

After simulating each component separately, all the network components were brought together and simulated in chapter 7.

In chapter 8 conclusions regarding the accomplished work are presented as well as suggestions for future work.

2. Theoretical fundaments

2.1. Introduction

This chapter gives an overview of the theoretical background of microwave engineering used in this dissertation. The chapter starts with the basic definitions followed by a discussion of the propagations modes that exists in microstrip technology as well as discontinuities and stub tunes that may occur. Scattering matrix is also introduced as well as ABCD parameters, Richard's transformation, Kurodas's Identities and some construction methodologies regarding the projected filters and power splitters.

2.2. Microwave

Microwave means alternate current signals with a range of frequencies between 300 *MHz* and 300 *GHz*, corresponding to a wavelength (λ) between $\lambda = c/f = 1\,m$ (300 *MHz*) and $\lambda = 1\,mm$ (300 *GHz*). Most of the present research and wireless communications cover this frequencies range. When using these frequencies there are several aspects that have to be taken into account, i.e. radiation, coupling electromagnetic issues and frequency response of lumped (discrete entities that approximate the behavior of the distributed system under certain assumptions) circuit elements [2].

Standard circuit theory cannot solve the usual microwave problems for high frequencies (short wavelengths). Most of the times microwave components are distributed elements were phase and current change significantly with the physical dimensions of the device due to a dependence related to the microwave length. Thus, at low frequencies the wavelength is larger and there are not significant changes in the phase values across the component. On the other hand when dealing with high frequencies the wavelengths are much shorter than the dimensions of the component [3].

2.3. Transmission lines

Transmission lines are a very important factor in the design of integrated/high frequency circuits. Their length is expressed as a multiple or sub multiple of an electric or electromagnetic propagating signal wavelength and it can be expressed by degrees or radians.

Circuit theory and transmission line theory essentially differ in the electrical size. Circuit analysis assumes the physical dimension of a network much smaller then electrical wavelength. On the other hand, a transmission line may be a significant part of one or several wavelengths.

Important parameters that define a RF/microwave design are cost, electric performance, power and reliability. Costs can be reduced through the use a cheap technology, a cheap substrate, a set of simple components and a minimum number of interconnection.

Every printed transmission lines have their conductors impressed in a relatively small substrate. These lines can be uniform or non uniform, homogeneous or non homogeneous, lossy or lossless, protected or non protected, monolayer or multilayer and can be based in one or several substrates, i.e. different dielectrics. In uniform lines the characteristic impedance does not vary throw the line (opposite in the non uniform lines). In practice we can vary this impedance by changing the strip width.

When transmission lines have different dielectric (ex. microstrip lines), the transmission velocity depends on the transversal geometry of the line and the dielectric constants of the different mediums (ex. air and substrate material). Considering the dielectric constant of the line higher than the dielectric constant of the air and lower then the substrate material then the propagation of the electromagnetic waves is not realized as in a TEM (Transverse Electromagnetic) environment.

In a low loss transmission line the conductor thickness is 3 to 5 times higher than the human skin. Lossy transmission lines (conductor thickness smaller than the layer composation) can be used in the construction of terminals and atenuators.

When combining diferent transmission lines it is usefull to use multiple layers. With multiple layers it is possible to combine radio-frequencies and digital functions in an single module, i.e. the final circuit will be smaller, light, more reliable and will have more performance and lower costs [4].

Unshielded transmission lines are in direct contact with the air so they have to be protected from external radiation and electromagnetic interference (EMI) as Figure 2.1 illustrates.
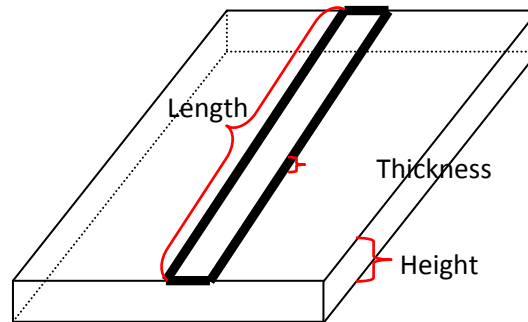
Figure 2.1 – Unshielded transmission line

This protection is provided by a shield around the transmission line [5].

2.3.1. Propagation

TEM (Transverse Electromagnetic waves) is the Stripline propagation mode. The conductor path is surrounded by similar dielectric materials, i.e. there are none electric or magnetic fields in the propagation direction. Thus, it has a phase velocity equal to the speed of light. One other common example beside Stripline that supports TEM propagation is the coaxial medium.

Microstrip lines propagation is characterized by a combination of TM (Transverse Magnetic) and TE (Transverse Electric). TM means that magnetic fields in the propagation direction do not exist, and TE means that there are not any electric fields in the propagation direction. Notice that the dielectric of the upper part of the microstrip line is air and the bottom is a PCB (Printed Circuit Board). In this case the TEM is not supported because the waves phase velocity of the air is different from the velocity in the PCB. However in a lower frequency (<=66 GHz) the magnetic and electric fields are sufficiently small in a way that these two propagation modes join themselves (quasi-TEM).

With low frequencies most of the electromagnetic field is distributed through the air, and with high frequencies the electromagnetic field travels in the PCB dielectric direction [4].

Therefore, a transmission line filled with a uniform dielectric can support a single and well-defined mode of propagation over a specified range of frequencies. This happens in TEM for coaxial lines, TE for waveguides, etc.

2.3.2. Microstrip transmission lines

A microstrip transmission line consists on a dielectric material sandwiched between metalized conductor(s) with a specific metallization circuit conductor on top and ground-plane on the back, as illustrated in Figure 2.2 .
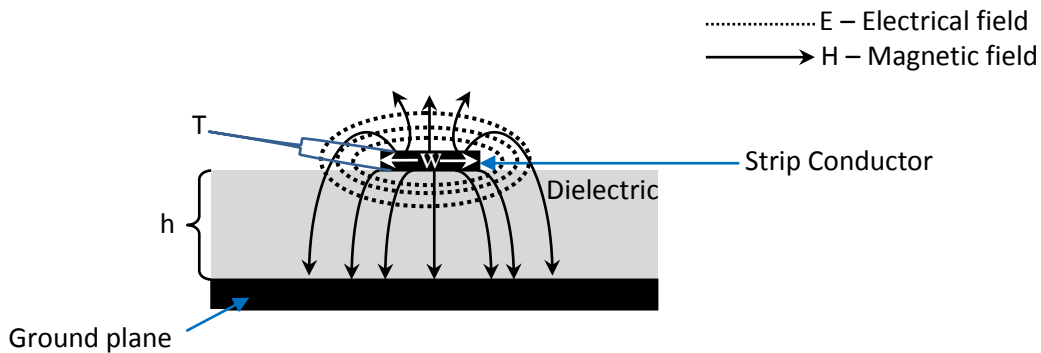
Figure 2.2 - Microstrip line details

This technology that can be easily integrated with other passive and microwave devices. The conductor with a specific Thickness (T) is printed on a thin grounded dielectric substrate with a specific height (h) and relative permittivity[i] (ε_r).

Microstrip transmission lines characteristics include:

- Good geometry that provides power handling, moderate radiation loss and reasonable dispersion over a wide characteristic impedance range (about 15 to 150 Ohms) [7].
- Easy incorporations of active devices, diodes and transistors;
- Transmission of DC and AC signals;
- Line wavelength is considerably reduced from its free-space value due to the substrate fields;
- The structure can support moderately high voltages and power levels [6].

Concerning the design issues there are a few variables of high importance such as characteristic impedance and the propagation coefficient.

Therefore, a microstrip transmission line is a distributed parameter network where voltages and currents can vary in magnitude and phase along the line length.

The voltage (*V*) and current (*I*) on a transmission line along the *z* axis are given by:

$$V(z) = V_0^+ e^{-\gamma z} + V_0^- e^{+\gamma z} \tag{2.1}$$

$$I(z) = I_0^+ e^{-\gamma z} + I_0^- e^{+\gamma z} \tag{2.2}$$

The $e^{-\gamma z}$ term describes wave propagation in the $+z$ direction and the $e^{+\gamma z}$ term represents the propagation in the $-z$. The complex propagation constant γ is given by

$$\gamma = \alpha + j\beta = \sqrt{(R + j\omega L)(G + j\omega C)} \tag{2.3}$$

where α represents the attenuation coefficient given by *neper.m*$^{-1}$, β the phase coefficient give by *radians.m*$^{-1}$, R and L are the series resistance and inductance per unit length and G and C are the shunt conductance and capacitance per unit length. The real part α causes signal amplitude to decrease along the transmission line and the imaginary part or phase constant β determines the sinusoidal amplitude/phase of the signal along the transmission line at a constant time [9].

These terms are not constants because they depend on the material, frequency or geometry in use.

Another important issue is the characteristic impedance. If we consider a travelling wave in the transmission line regardless its path (forward or backwards), the ratio of voltage to current is the characteristic impedance. Meaning that the impedance can be defined as:

$$Z_0 = \frac{R + j\omega L}{\gamma} = \sqrt{\frac{R + j\omega L}{G + j\omega C}} \; \Omega \tag{2.4}$$

Assuming a lossless line with perfect conductors and dielectric material i.e. if no conducting currents exists between the two conductors and for that matter G=0 and R=0, then the propagation coefficient is:

$$\gamma = \alpha + j\beta = j\omega\sqrt{LC} \tag{2.5}$$

where at sufficiently high ratio frequencies the phase constant is given by equation (2.6).

$$\beta = \omega\sqrt{LC} \tag{2.6}$$

For a lossless transmission line (attenuation constant $\alpha = 0$) the characteristic impedance can be written as:

$$Z_0 = \sqrt{\frac{L}{C}} \ \Omega \tag{2.7}$$

A wider microstrip line occupies more area in the dielectric which results in larger capacitance per length. Considering C_d the capacitance of the transmission line with dielectric filing and C_{free} the capacitance that has no dielectric filing we have the following relation:

$$C_d = \varepsilon_r C_{free} \tag{2.8}$$

However, the inductance per unit length is independent of the line's dielectric and is given by:

$$L = \frac{1}{c^2 C_{free}} \tag{2.9}$$

In the above equation c is the propagation velocity of the electromagnetic wave in free space ($\approx 3 \times 10^8 \ m/s$).

Equation (2.9) can be used in equation (2.7) to obtain equation (2.10).

$$Z_0 = \sqrt{\frac{L}{C}} = \frac{1}{c\sqrt{\varepsilon_r} C_{free}} \tag{2.10}$$

The phase velocity for a TEM wave can be written as:

$$v_p = \frac{c}{\sqrt{\varepsilon_r}} \tag{2.11}$$

The wavelength of such propagation type is defined as:

$$\lambda = \frac{\lambda_0}{\sqrt{\varepsilon_r}} \tag{2.12}$$

where λ_0 is the free space wavelength. Therefore the wavelength is proportioned to the square root of the relative permittivity of the uniform dielectric material in which the line is implemented. So, for large permittivity materials the distributed components became shorter resulting in less occupied space [8].

Still, a microstrip line cannot support a pure TEM wave (phase velocity varies from the dielectric region ($v_p = c/\sqrt{\varepsilon_r}$) to the air region ($v_p = c$), so the exact fields in a microstrip environment (quasi-TEM propagation mode) constitute a hybrid TM-TE wave, and for these matter approximations for the phase velocity, propagation constant and characteristic impedances will be obtained by the following quasi-static solutions[10]:

$$v_p = c/\sqrt{\varepsilon_{eff}} \tag{2.13}$$

$$\beta = k_0\sqrt{\varepsilon_{eff}} \tag{2.14}$$

$$k_0 = w\sqrt{\mu_0\varepsilon_0} \tag{2.15}$$

In the above equations v_p is the phase velocity and β is the propagation constant. Phase velocity also depends on the effective dielectric constant (ε_{eff}) of the microstrip line which has a value between the air dielectric (1) and the region dielectric (ε_r). It also depends on the conductor width (w) and the substrate thickness (h) as follows [3]:

$$\varepsilon_{eff} = \frac{\varepsilon_r + 1}{2} + \frac{\varepsilon_r - 1}{2} \times \frac{1}{\sqrt{1 + 12 \times h/w}} \tag{2.16}$$

Once the dielectric constant is known the characteristic impedance of the line can be calculated by equation (2.17).

$$Z_0 = \begin{cases} \dfrac{60}{\sqrt{\varepsilon_{eff}}} \ln\left(\dfrac{8h}{w} + \dfrac{w}{4h}\right) & \text{para } \dfrac{w}{h} \leq 1 \\[3mm] \dfrac{120\pi}{\sqrt{\varepsilon_{eff}}\left(w/h + 1.393 + 0.667\ln\left(w/h + 1.444\right)\right)} & \text{para } \dfrac{w}{h} \geq 1 \end{cases} \tag{2.17}$$

The ratio $\dfrac{w}{h}$ based on specific characteristic impedance and dielectric constant takes the following form [3]:

$$\frac{w}{h} = \begin{cases} \dfrac{8e^A}{e^{2A}-2} & \text{for } \dfrac{w}{h} < 2 \\[2mm] \dfrac{2}{\pi}\left[B-1-\ln(2B-1)+\dfrac{\varepsilon_r-1}{2\varepsilon_r}\left(\ln(B-1)+0.39-\dfrac{0.61}{\varepsilon_r}\right)\right] & \text{for } \dfrac{w}{h} > 2 \end{cases} \tag{2.18}$$

$$A = \frac{Z_0}{60}\sqrt{\frac{\varepsilon_r+1}{2}}+\frac{\varepsilon_r-1}{\varepsilon_r+1}\left(0.23+\frac{0.11}{\varepsilon_r}\right) \tag{2.19}$$

$$B = \frac{377\pi}{2Z_0\sqrt{\varepsilon_r}} \tag{2.20}$$

Notice that with the previous equations it is also possible to calculate the width of the microstrip line. Substrate definition include the ε_r and the h, by stipulating a characteristic impedance for the microstrip line will give access for the width calculation of the microstrip line.

Due to this propagation method the wavelength in a microstrip medium is given by:

$$\lambda_g = \frac{\lambda_0}{\sqrt{\varepsilon_{\text{eff}}}} \tag{2.21}$$

Considering two points in the same transmission line separated by one wavelength we can say that they have a phase difference of 2π. With this it becomes possible to determine the wavelength along the transmission line:

$$\begin{aligned} wt - \beta z &= wt - \beta(z+\lambda)+2\pi \Leftrightarrow \\ \Leftrightarrow 0 &= -\beta\lambda+2\pi \Leftrightarrow \beta\lambda = 2\pi \Leftrightarrow \\ \Leftrightarrow \qquad \lambda &= \frac{2\pi}{\beta} \end{aligned} \tag{2.22}$$

Meanwhile, velocity of propagation (v_p) can be expressed by the wavelength along the transmission line at the operation frequency:

$$v_p = f\lambda \tag{2.23}$$

$$v_p = \frac{w}{\beta} \tag{2.24}$$

Using equation (2.6):

$$v_p = \frac{1}{\sqrt{LC}} \tag{2.25}$$

The capacitance of a line that is uniformly filled with dielectric material is proportional to ε_r. And the velocity in an air-filled transmission line is approximately the velocity of light in free space, so:

$$v_p = \frac{c}{\sqrt{\varepsilon_r}} \; m/s \tag{2.26}$$

Where c is the free space velocity of light.

The total voltage and current of the line is a superposition of the incident and the reflected wave (standing waves). The voltage reflection coefficient is defined as the ratio of the amplitude of the reflected voltage by the amplitude of the incident voltage:

$$\Gamma = \frac{V_0^-}{V_0^+} = \frac{Z_L - Z_0}{Z_L + Z_0} \tag{2.27}$$
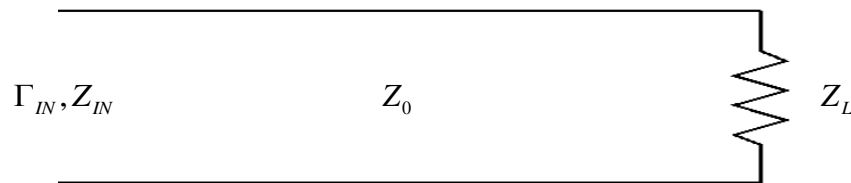
Figure 2.3 - Transmission line with load termination

When $\Gamma = 0$ there is no reflected wave. In order to achieve $\Gamma = 0$, the load impedance Z_L must be equal to Z_0. In this case the load is matched to the line, since there is no reflection of the incident wave.

When $Z_L \neq Z_0$ (mismatch), the line voltage magnitude is not constant and this voltage magnitude will oscillate along the line. The ratio of maximum voltage magnitude V_{max} to the minimum voltage magnitude V_{min} is defined as the *voltage standing wave ratio* (VSWR).

$$VSWR = \frac{V_{max}}{V_{min}} = \frac{1 + |\Gamma|}{1 - |\Gamma|} \tag{2.28}$$

The input impedance of a lossless transmission line with length $l = \lambda/2$, propagation constant β and characteristic impedance Z_0, terminated by arbitrary load impedance Z_L is given as

$$Z_{in} = Z_0 \frac{Z_L + jZ_0 \tan \beta \ l}{Z_0 + jZ_L \tan \beta \ l} \tag{2.29}$$

The electrical length (βl) is normally given in degrees. If there is a short circuit in the line then $Z_L = 0$ and from (2.29):

$$Z_{sc} = jZ_0 \tan \beta l \tag{2.30}$$

When $Z_L = \infty$ (open circuit), using equation (2.26) the input impedance is:

$$Z_{oc} = -jZ_0 \cot \beta l \tag{2.31}$$

2.3.3. Lossless terminated lines (Short and Open circuit transmission lines)

How transmission lines are terminated is an important issue in practical designs. Consider a line terminated by a short circuit as follows:
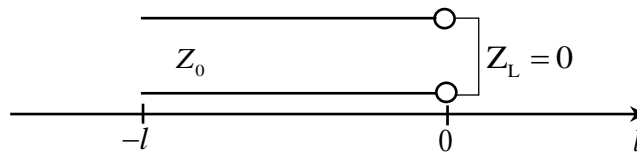
Figure 2.4 - Short circuited transmission line

One very important issue to consider regarding a transmission line is its impedance. And the impedance of a short circuit line has the following behavior:
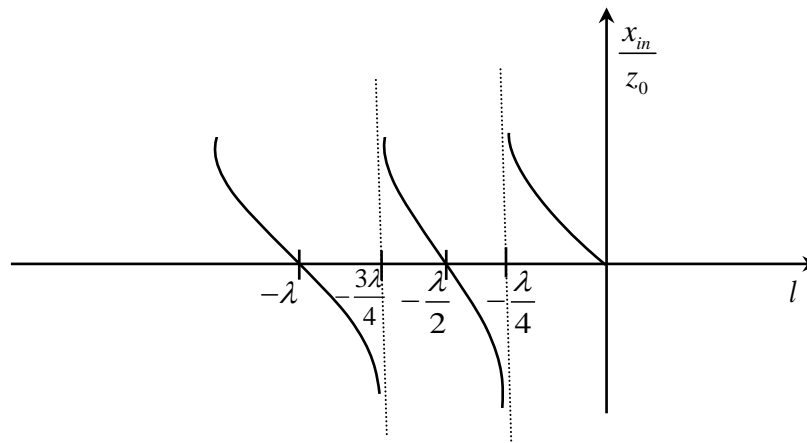
Figure 2.5 - Impedance behavior along a short circuit transmission line

For $l = 0 \Rightarrow z_{in} = 0$, however for $l = \lambda/4 \Rightarrow z_{in} = \infty$ (open circuit). So, it is periodic in multiples of $\lambda/2$ [3]. For $l < \lambda/4$ the line becomes inductive, and for $\lambda/4 < l < \lambda/2$ it shows a capacitive response [11].

An open circuit terminated line is illustrated in Figure 2.6.
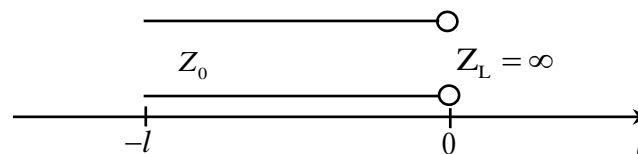
Figure 2.6 - Open-circuited transmission line

And the impedance behavior along an open circuit line is given by Figure 2.7.
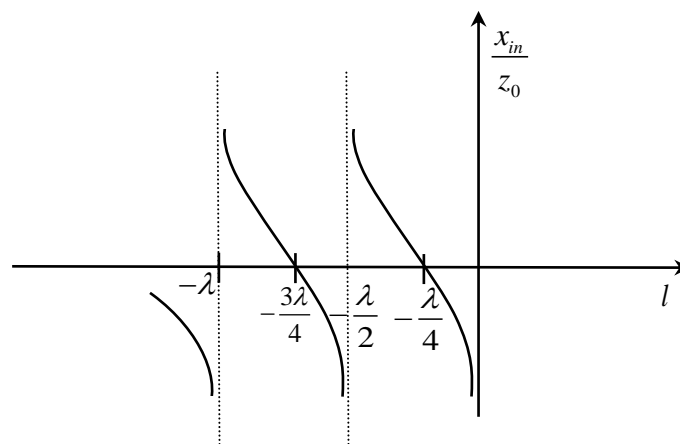
Figure 2.7 - Impedance behavior along an open circuit transmission line

Notice that any multiple of $\lambda/2$ does not change the load impedance as seen above. However if the transmission line is a quarter wavelength length long, or $l = \lambda/4 + n\lambda/2$ with $n = 1, 2, 3....$ it will transform/invert the load impedance [3].

For $l < \lambda/4$ the line has a capacitive behavior, and for $\lambda/4 < l < \lambda/2$ it shows an inductive response [11].

As seen, passive circuit elements can be represented by short-circuited or open-circuited lines. If an open-circuit is proposed, for different length values the correspondent circuits are illustrated in Figure 2.8.

$l < \lambda/4 \qquad l = \lambda/4 \qquad \lambda/4 < l < \lambda/2 \qquad l = \lambda/2$
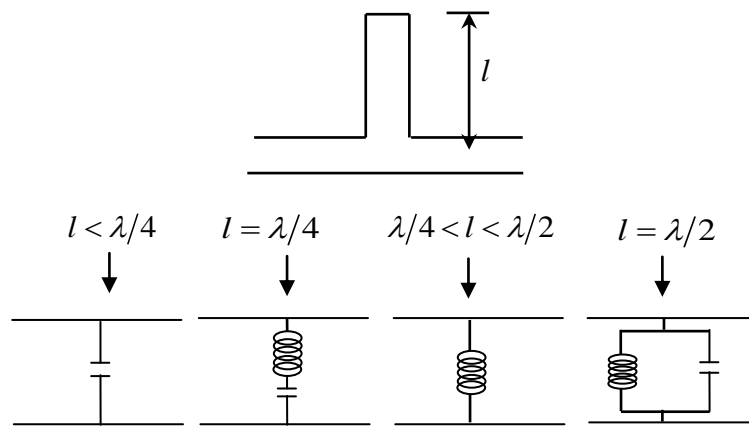
Figure 2.8 - Representation of capacitance and inductance of microstrip lines [12]

If a short circuit line is used then length variation presents the following behaviours:

$\lambda/4 < l < \lambda/2 \qquad l = \lambda/2 \qquad l < \lambda/4 \qquad l = \lambda/4$
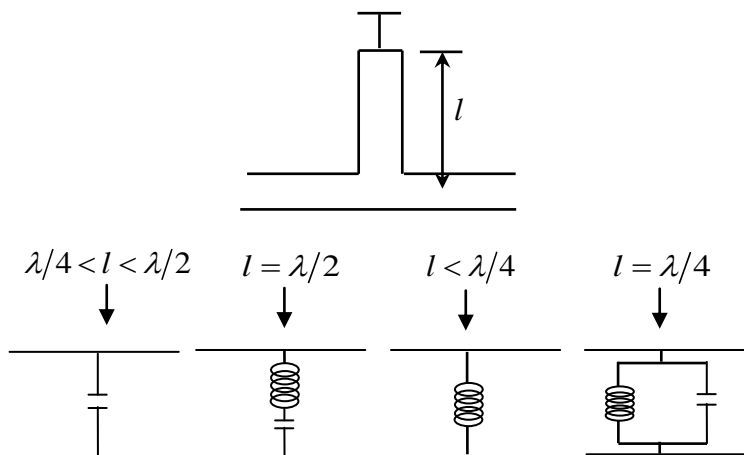
Figure 2.9 - Inductive and capacitive reactance example in microstrip line [12]

Thus, for different lengths values different behaviours will occur. This methodology is also used for line series resonant circuits as seen in Figure 2.10:
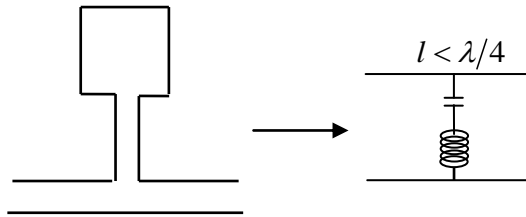
Figure 2.10 - Inductive and capacitive reactance example in microstrip line [12]

2.3.4. Discontinuities

Transmission lines present several types of discontinuities. Sometimes discontinuities results from mechanical or electrical transitions from one medium to another. Normally the effect of discontinuity is seen as an undesirable event, however sometimes discontinuities are deliberately implemented into the circuit in order to provide a certain electrical function. Either way, the discontinuities can be represented by an equivalent circuit. For this purpose usually the T or Π equivalent circuit is used [3].

Common microstrip discontinuities are the open ended that consist on a line over the substrate that which produces capacitor behaviour as illustrated in Figure 2.11.
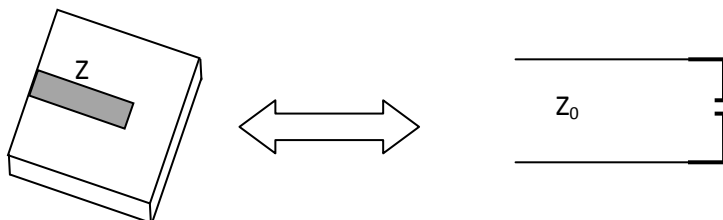
Figure 2.11 - Open-ended discontinuity

The Gap discontinuity consists in two lines with open ended behaviours plus the additional coupling effect between them both as exemplified in Figure 2.12:
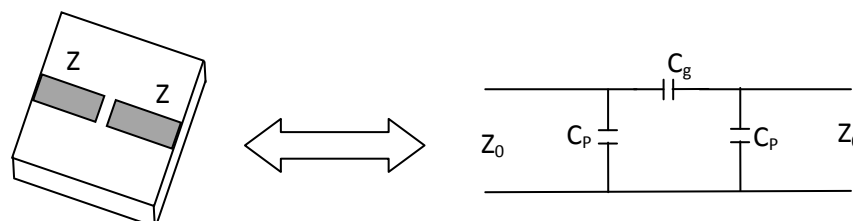
Figure 2.12 - Gap discontinuity

When different line sections have different width values then discontinuities effects appear in the circuit as well. Notice that common microstrip structures are based on this

oscillating effect (example: lowpass filters). This event can be characterized with Figure 2.13 circuit [3].
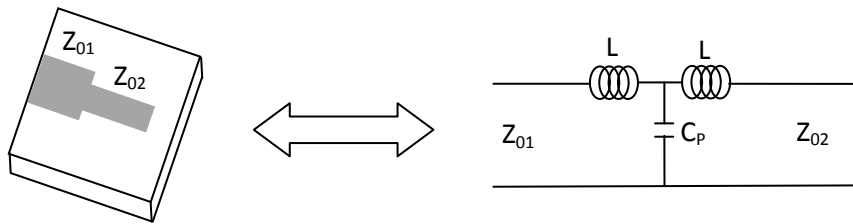
Figure 2.13 - Change in width discontinuity

Note: Other topologies can be consulted in [3].

Discontinuities at bends, step changes in widths and junctions cause degradations in circuit performance. These discontinuities introduce parasitic reactance that can lead to phase and amplitude errors, input or output mismatch and other undesirable effects. As seen, one approach is to include an additional circuit to adjust the circuit performance. However another approach can be taken. It consists on minimizing the effect of the discontinuities by slightly modifying the design structure. Consider Figure 2.14:

Figure 2.14 - Bend effect

The right angle has a parasitic discontinuity capacitance caused by the increased conductor area near the bend. To eliminate this effect it is made a smooth bend with radius $r \geq 3w$ or a slice of the corner must be taken off. This will reduce the excess capacitance of the bend (Figure 2.15). The optimums bend value depends on the characteristic impedance and the angle, so a miter length equal to 8 times the frequency used is a reasonable bend [3].
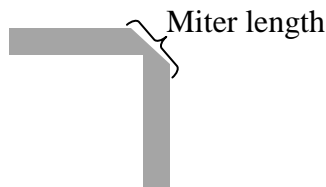
Miter length

Figure 2.15 - Mitering the bend

2.3.5. Stub tuning

Stub tuning is a matching technique that uses open-circuit or short-circuits length of transmission line connected at a curtained distance from the load. There are two important parameters to take into account with this methodology, i.e. the distance from the load and the value of reactance provided by the stub [3].

For practical consideration this method optimizes the circuit response and brings it back to zero.

2.4. Scattering Matrix

In microwave frequencies the idea of voltage, current and impedances is less descriptive when high networks are analysed. Instead, an analysis of incident and reflected waves is used.

The scattering matrix provides a good and complete description of a high frequency network as seen by its N ports, in terms of incident/reflected voltage travelling waves. For this matter this matrix becomes a valuable tool to evaluate per example the filters performance.

S-parameters can be measured by a network analyzer or calculated using network analysis techniques [3].
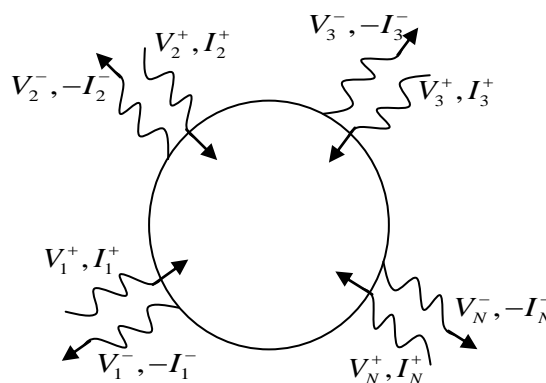
Figure 2.16 - N-port microwave network

As seen in Figure 2.16 the V_n^+ is the amplitude of the incident voltage wave on port n and V_n^- is the amplitude of the reflected wave from port n. The scattering matrix $[S]$ is defined as:

$$\begin{bmatrix} V_1^- \\ V_2^- \\ \vdots \\ V_N^- \cdot \end{bmatrix} = \begin{bmatrix} S_{11} & S_{12} & \dots & S_{1N} \\ S_{21} & S_{22} & \dots & S_{2N} \\ \vdots & & & \vdots \\ S_{N1} & S_{N2} & \dots & S_{NN} \end{bmatrix} \begin{bmatrix} V_1^+ \\ V_2^+ \\ \vdots \\ V_N^+ \end{bmatrix} \tag{2.32}$$

An element of the $[S]$ matrix is defined as:

$$S_{ij} = \frac{V_i^-}{V_j^+} \Bigg|_{V_k^+ = 0 \text{ for } k \neq j} \tag{2.33}$$

Meaning that S_{ij} (transmission coefficient) can be found by putting through port j an incident voltage wave of amplitude V_j^+ and measuring the reflected wave amplitude V_i^- from port i. To avoid reflections all ports except port j should terminate in matched loads.

In the same manner S_{ii} is the reflection coefficient seen through port i when all other ports are terminated in matched loads [3].

Consider a two port network. If we want to measure S_{11}, we inject a signal at port one and measure its reflected signal. In practical experiments it is advised to only inject one signal at a time. If measuring S_{21}, it is injected a signal at port 1, and then the resulting signal existing at port 2 is measured. For S_{12} a signal is injected into port 2, and measured in the leaving port 1, and for S_{22} it is injected a signal at port 2 and the reflected signal is measured at port 2 as well [13].

2.5. ABCD parameters

A large group of microwave networks consist of a cascade connection of two or more two-port networks. When this happens it is defined a 2x2 transmission or ABCD matrix for each two-port network.

The ABCD matrix is defined by:

$$V_1 = AV_2 + BI_2 \tag{2.34}$$

$$I_1 = CV_2 + DI_2 \tag{2.35}$$

Or:

$$\begin{bmatrix} V_1 \\ I_1 \end{bmatrix} = \begin{bmatrix} A & B \\ C & D \end{bmatrix} \begin{bmatrix} V_2 \\ I_2 \end{bmatrix}$$

(2.36)

These equations represent the following system:
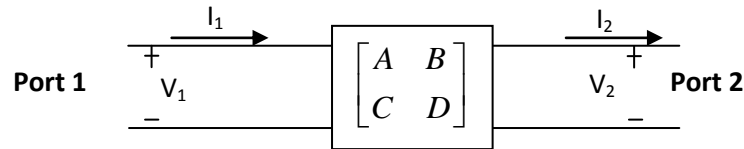
Figure 2.17 - ABCD system

Looking at the cascade network:
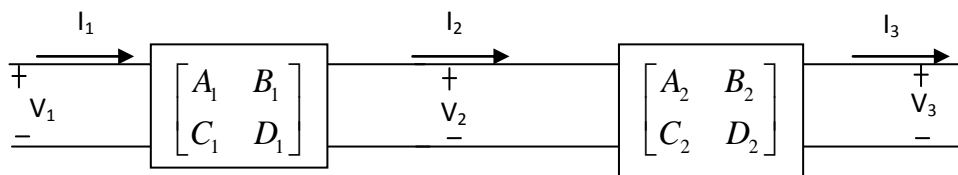
Figure 2.18 - Cascade network example

Which means that ABCD matrix of the cascade connection is equal to the product of the ABCD matrices representing individual ports.

$$\begin{bmatrix} V_1 \\ I_1 \end{bmatrix} = \begin{bmatrix} A_1 & B_1 \\ C_1 & D_1 \end{bmatrix} \begin{bmatrix} A_2 & B_2 \\ C_2 & D_2 \end{bmatrix} \begin{bmatrix} V_3 \\ I_3 \end{bmatrix}$$

(2.37)

This is a useful method when a more complicated microwave network that consists of cascades of this simpler two-ports need to be analyzed [3].

2.6. Richard's Transformation

Richard's transformation equals the behavior of lumped elements (L or C) and a given stub with respective characteristic impedance and length at precisely one frequency as illustrated in Figure 2.19.
The input impedance of short and open circuit transmission lines is given by equations (2.30) and (2.31).

However, transmission line stubs mathematically differs from the reactance of lumped inductors and capacitors as seen in equations:

$$Z_L = jwL \tag{2.38}$$

$$Z_C = \frac{-j}{wC} \tag{2.39}$$

Meaning that the impedances of transmission line stubs and lumped elements differ regarding its frequency, which leads to the following:

$$Z_{IN}^S \neq Z_L \tag{2.40}$$

$$Z_{IN}^O \neq Z_C \tag{2.41}$$

where Z_{IN}^S is the input short circuit transmission line impedance and Z_{IN}^O refers to the open circuit transmission line impedance. On the other hand if a single frequency is used than these functions will equalize and a transformation can be developed.

So, if a frequency (w_C) satisfies the following equation:

$$jw_C = jZ_0 \tan\beta_C l \Leftrightarrow$$
$$= jZ_0 \tan\left[\frac{w_C}{v_P} l\right] \tag{2.42}$$

Or similarly in the lumped capacitor case:

$$\frac{-j}{w_C C} = jZ_0 \cot\beta_C l \Leftrightarrow$$
$$= -jZ_0 \cot\left[\frac{w_C}{v_P} l\right] \tag{2.43}$$

Considering a stub transmission length of $\lambda/8$ and equation (2.22) the following wavelength is achieved:

$$\lambda_C = \frac{v_P}{w_C} = \frac{2\pi}{\beta_C} \tag{2.44}$$

Equation (2.30) will achieve the following expression:

$$jw_C = jZ_0 \tan\beta_C l = jZ_0 \tan\left[\frac{\pi}{4}\right] = jZ_0 \tag{2.45}$$

Similarly, equation (2.31) acquires the referred expression:

$$\frac{-j}{w_C C} = jZ_0 \cot \beta_C l = -jZ_0 \qquad (2.46)$$

A short circuit stub with the same impedance as an inductor L at frequency w_C can be achieved if the characteristic impedance of the stub is set to $w_C L$. Likewise an open circuit stub can be designed if his characteristic impedance has the value $\dfrac{1}{w_C C}$.

Richard Transformations:
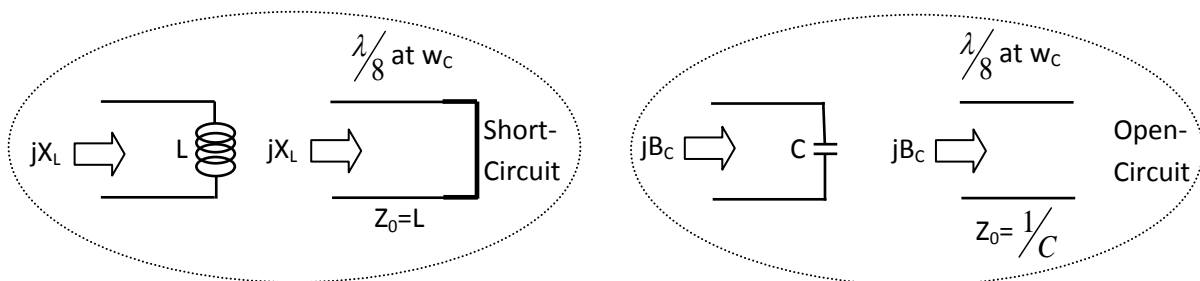
Figure 2.19 - Richard Transformations

Richard's Transformations do not result in perfect replacements for lumped elements i.e. the stubs do not behave like capacitors and inductors. What happens is that the transformation is perfect and impedances are equal at a certain frequency w_C. This w_C is also known as the cutoff frequency of a lumped element filter design whose inductors and capacitances were replaced by Richard's transformations [3].

2.7. Kurodas's Identities

The four Kuroda identities use redundant transmission line sections to allow implementation of microwave filters. They separate transmission line stubs, transforms series stubs into shunt stubs and vice-versa and replaces characteristic impedances that are difficult to implement with more practical ones. The additional transmission line segments are called unit elements and are $\lambda/8$ long at the cutoff frequency and they are commensurate (all lengths of all the stubs are the same) with the stubs that realize the inductors and capacitors of the prototype design. The four identities within each specific box representing a unit element (transmission line) of the specified characteristic impedance and length $\lambda/8$ at ω_c are

available in [3]. For every identity the equivalence between the two networks can be proved demonstrating that their *ABCD* matrices are equal [3].

2.8. Digital transmission

2.8.1. Digital transmission trough band limited channels

The transfer function of a transmission channel, H(f) may be expressed in the form of equation (**2.47**).

$$H(f) = |H(f)|e^{j\beta(f)} \tag{2.47}$$

where $|H(f)|$ is the amplitude response and the phase response. A channel is ideal or non-distorting if within the bandwidth W occupied by the transmitted signal, $|H(f)|$ is constant and $|\beta(f)|$ is a linear function of the frequency. Real transmission channels, such as coaxial cables or optical fibers are band limited and non ideal. Therefore when a digital signal with infinite bandwidth, such as a sequence of rectangular pulses is transmitted through the channel it becomes distorted causing inter-symbol interference (ISI).

2.8.2. Nyquist criteria for zero ISI

Typically, the transfer function of the channel and the transmitted pulse shape are specified, and the problem is to determine the transfer functions of the transmitter and receiver filters so as to obtain at the decision circuit zero ISI.

Let p(t) to be the pulse shape at the output of the receiving filter. In the absence of noise and assuming no transmission loss, the output waveform is given by equation (2.48).

$$y(t) = \sum_k a_k p(t - t_d - KT) \tag{2.48}$$

a_k represents the amplitude of the k pulse and *p(t)* is the shape of the elementary pulse, in order to have ISI=0,

$$p(t) = \begin{cases} 1 & t = 0 \\ 0 & t = \pm T, \pm 2T, ... \end{cases} \tag{2.49}$$

Imposing the additional requirement that the pulse spectrum be band limited, such that

$$P(f) = 0 \quad |f| \geq W \tag{2.50}$$

where,

$$W = \frac{1}{2T} + \alpha \quad 0 \leq \alpha \leq \frac{1}{2T} \tag{2.51}$$

The Nyquist vestigial-symmetry theorem states that equation (2.49) is satisfied if p(t) has the form of equation (**2.52**).

$$p(t) = p_\alpha(t)\,\text{sinc}\left(\frac{t}{T}\right) \tag{2.52}$$

with,

$$\Im\left[p_\alpha(t)\right] = P_\alpha(f) = 0 \quad |f| > \alpha$$
$$p_\alpha(0) = \int_{-\infty}^{+\infty} P_\alpha(f)\,df = 1 \tag{2.53}$$

Infinitely many functions satisfy the Nysquist conditions, including the case when $p_\beta(t) = 1$ and $p(t) = \text{sinc}\left(\dfrac{t}{T}\right)$. This pulse shape allows band limited signaling at the maximum rate r=2W. However, synchronization and practical implementation are an issue.

2.8.3. Raised Cosine shaping

Raised cosine shaping filters are used to minimize inter symbol interference (ISI) and to avoid the synchronization problem mentioned in the previous section. It eliminates ISI as its impulse response is zero at all nT (except n=0, and T the sampling interval). For this matter a good choice is to use a square root raised cosine filter (SRRCOS) at transmitter and receiver end of the communication system, so the final shape will be raised cosine [14].

The spectrum of the raised cosine filter shows odd symmetry about $1/2T$. The   raised cosine frequency response can be written as [15]:

$$H(f) = \begin{cases} T, & 0 \le |f| \le \dfrac{1-\alpha}{2T} \\[2mm] \dfrac{T}{2}\left[1+\cos\left(\dfrac{\pi T}{\alpha}\left[|f|-\dfrac{1-\alpha}{2T}\right]\right)\right], & \dfrac{1-\alpha}{2T} \le |f| \le \dfrac{1+\alpha}{2T} \\[2mm] 0, & |f| > \dfrac{1+\alpha}{2T} \end{cases} \tag{2.54}$$

where α is the roll-off factor, which is the measure of the bandwidth occupied beyond the Nyquist bandwidth of $\dfrac{1}{2T}$ also called excess bandwidth. The roll-off factor is given by:

$$\alpha = \frac{\Delta f}{\dfrac{1}{2T}} = \frac{\Delta f}{\dfrac{R_s}{2}} = 2T\Delta f \tag{2.55}$$

Plus, Δf is the excess bandwidth and R_s the symbol rate given by:

$$R_s = 1/T \tag{2.56}$$

The bandwidth is given in expression (**2.57**).

$$W = \frac{1}{2}R_s(1+\alpha) \tag{2.57}$$

The roll of factor varies from zero to one and along with this variation the frequency domain response takes the form of Figure 2.20.
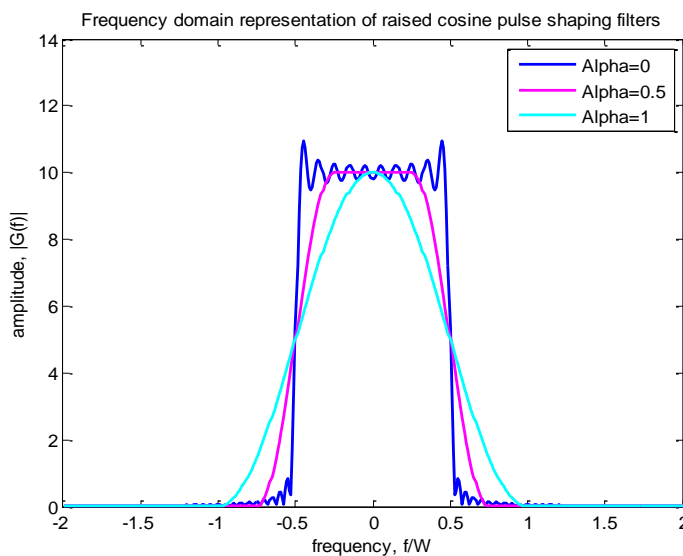
Figure 2.20 - Frequency response of raised-cosine filter.

The impulse response has its zeros in T, 2T, 3T and by varying the roll off factor the harmonics of the response become more or less flatten as it can be seen in Figure 2.21.
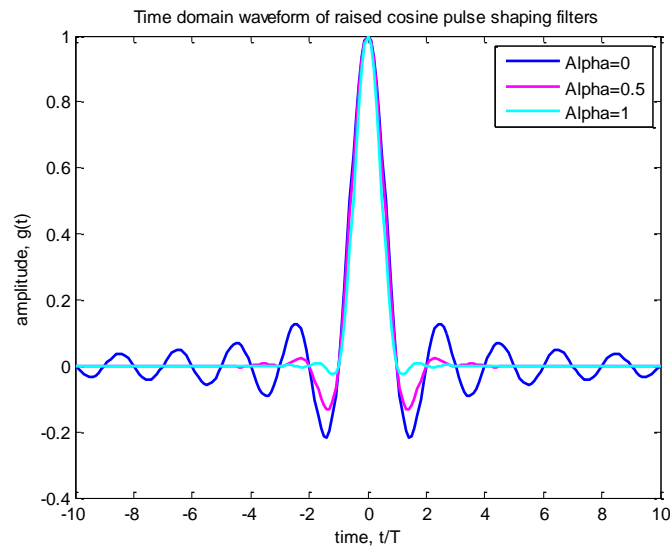
Figure 2.21 - Impulse response of raised-cosine filter.

When $\alpha = 1$, the non-zero portion of the spectrum is a pure raised cosine:

$$H(f) = \left\{ \frac{1}{2}\left[1 + \cos(\pi f T)\right], \qquad |f| \leq \frac{1}{T} \right. \tag{2.58}$$

When α approaches zero:

$$H(f) \approx rect(fT) \tag{2.59}$$

In the equation above $rect(fT)$ refers to a rectangular function [15][17].

2.9. Chapter Summary

Microwave transmission lines were explained, as well as their importance in the design of integrated/high frequency circuits. Short and open circuit transmission lines are studied and the respective impedance behavior regarding the length of these transmission lines are discussed.

Eventually, discontinuities results from mechanical or electrical transitions from one medium to another and is normally considered as an undesirable effect, however, in certain cases discontinuities are deliberately implemented into the circuit in order to provide a certain

electrical function. Either way, the discontinuities can be represented by equivalent circuits that were demonstrated in this chapter.

Matching techniques that use an open-circuit or short-circuits length of transmission line connected at a curtained distance from the load are also reviewed.

The scattering matrix is introduce to evaluate the performance of the microstrip circuits as well as other important tools in this field, as the ABCD parameters, Richard's transformation and Kurodas's identities.

Theoretical fundaments regarding digital transmission are also described namely the use of the raised cosine shaping witch minimizes inter symbol interference (ISI) and synchronization problems.

---

[i] Permittivity describes how an electric field is affected and affects a dielectric medium.

3. Lowpass and bandpass filtering

3.1. Introduction

This chapter describes the design procedure off both the lowpass and the bandpass filters required for this dissertation. Lowpass filters consists on alternating sections with very high and very low characteristics impedances. At first a suitable lowpass lumped-element prototype filter is designed according to the filter specifications. This lowpass prototype is then scaled to the desired frequency and characteristic impedance and the lumped-element components are finally replaced by transmission lines for implementation at microwave frequencies.

The design of bandpass filters starts with the design of a prototype lowpass filter with the required passband and attenuation characteristics. Once a prototype is available it is possible to transform the values using simple algebraic identities to give highpass and bandpass filters with the same shape. Several structures of bandpass filters are taken into account such as parallel coupled filters and edge coupled filters.

An overview about power dividers is also given namely the Wilkinson power divider design approach.

3.2. Filtering

A filter is a frequency selective device that is used to limit the spectrum of a signal to some specified band of frequencies. Its frequency response is characterized by a passband and a stopband. The frequencies inside the passband are transmitted with little or no distortion, whereas those in the stopband are rejected. The filter may be of lowpass, highpass or bandstop type.

3.3. Microstrip filters

The following subsections will introduce the microstrip configurations used to form lowpass and bandpass filter designed in this dissertation

Microstrip filters design can take many forms. A useful one is achieved by using classical filter prototypes and converting them to the microstrip form using the equivalence of short lengths of transmission line to inductance or capacitance.

3.4. Lowpass filters

Lumped elements, capacitors and inductors, in microwave filters normally have a limited range of availability, and therefore are very difficult to implement in microwave frequencies. Plus the distances between filter components can be a problem. To overcome these barriers Richard's transformation can be used to convert lumped elements to transmission line sections and Kuroda's identities to specifically separate filter elements using transmission line sections. These sections are often used to improve filters response once their inclusions do not affect the filter response (redundant filter synthesis).

3.4.1. Stepped-impedance methodology

The stepped-impedance method illustrated in Figure 3.1 consists on alternating section with very high and very low characteristics impedances. This method has the advantage of being relatively easy to build. Additionally, it takes less space than a similar lowpass filter using stubs. The disadvantage is the electrical performance. This method of construction is often indicated to applications were a sharp cutoff frequency is not required. More specifically because of the radiations, transverse resonances and other undesirable effects, the stepped-impedance method is not suitable for microwave frequencies higher than 20 *GHz*. However, bellow 20 *GHz*, with the actual technologies and simulators available to engineers this disadvantage becomes a minor issue.
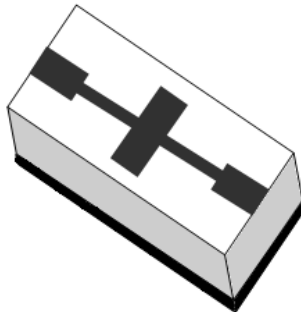
Figure 3.1 - Lowpass microstrip filter using stepped-impedance method

The main idea is to find the *T*-equivalent circuit for a short length of transmission line (electrical length $\beta\ell << \pi/2$) with either very large or very small characteristic impedance (Figure 3.2).
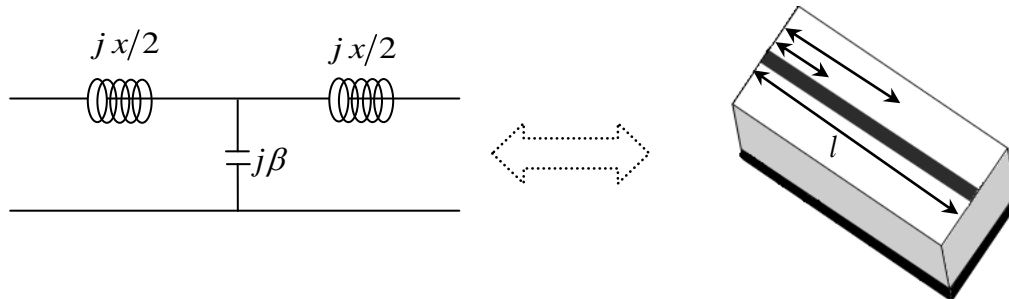
Figure 3.2 - T-equivalent circuit for a short length transmission line

Regarding the cases where large characteristic impedance exist the T-equivalent circuit transforms itself to a series inductor (Figure 3.3). On the other hand if the transmission medium has small characteristic impedance then the T-equivalent reduces to a shunt capacitor (Figure 3.4).
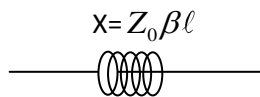
Figure 3.3 - High characteristic impedance circuit equivalent
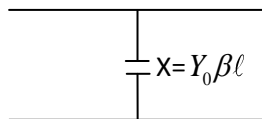
Figure 3.4 - Low characteristic impedance circuit equivalent

These high and small impedances lines into the prototype will produce the final ladder configuration (see Figure 3.1). It is proved that the ratio between the highest and lowest characteristic impedance should be in the interval 9-200 [18]. However in reality these values cannot be followed, and instead of this relation, an optimum value is discovered based on the substrate and its specific characteristics.

3.4.2. LowPass Realization

Normally lowpass filters are implemented using lumped elements such as capacitors, resistors and inductors. It is common to use two syntheses techniques:

- **Image-parameter method (IPM)**

The purpose of this method is to design high-order filters with reasonable performances [19].

It divides the filter into a cascade of two port networks and discovers the schematic of each two-port. Finally it combines each port and gives the required frequency response [20].

The passband and stopband characteristic for a cascade of two port networks have to be specified. This is useful for simple filters and it provides a link between infinitive periodic structures and practical filter design [3]. This method has the disadvantage that an arbitrary frequency response cannot be incorporated in the design and at the same time if a good filter response is not succeeded there is no direct way to improve the design.

- **Insertion-loss method (ILM)**

An arbitrary frequency response can be incorporated into the design with the Insertion Loss method. ILM allows a high degree of control over the passband and stopband amplitude and also over phase characteristics. This is done in a very systematic approach and pointing down to the user desired response, for example, if the goal is to have the minimum insertion loss possible then a binomial response could be used, or if the goal is to obtain the sharpest cutoff then chebyshev would the chosen.

This method has a direct relation with the filters order which equals the number of reactive elements in the circuit [3].

The design procedure of the Insertion Loss (IL) method is based on the attenuation response (insertion loss) of the filter:

$$IL = \frac{Source\,Power}{Load\,Power} = \frac{1}{1 - \left|\Gamma(w)\right|^2} \tag{3.1}$$

where Γ is the reflection coefficient when looking into the filter.

To follow this method it is necessary to design a normalized lowpass prototype (LPP). This prototype consists on several connected reactive elements as illustrated in Figure 3.5. Afterwards, impedance transformations and frequency scaling are applied to transform the LPP.
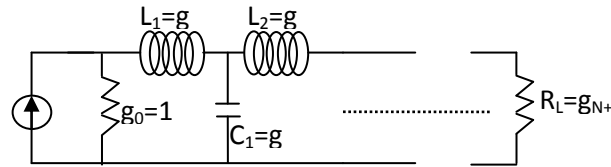
Figure 3.5 - Lowpass filter prototype

The order of this ladder network (Figure 3.5) corresponds to the number of reactive elements. The goal is to approximate the ideal amplitude response of an amplifier ($|H(\omega)|^2$) using polynomials such as Butterworth, Chebyshev, etc.

Consider the following schematic and equation for the amplitude response discussed:
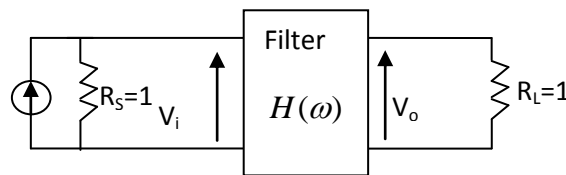
Figure 3.6 - LPP for amplitude response calculation

$$H(\omega) = \frac{V_o(\omega)}{V_i(\omega)} = \frac{K_o}{1 + C_o P_N(\omega)} \qquad (3.2)$$

In the equation K_0 and C_0 are constants that depend on the polynomial used and $P_N(w)$ is a polynomial in w of order N.

Regarding the polynomials choice there are some important issues to take into account. Chebyshev provides rapid cut off frequency, Bessel provides the slowest cut off frequency, and Butterworth's response remains between them. Butterworth is also known for its flattest response. After choosing the appropriate polynomial the respective inductance and capacitance can be obtained. This is done regarding a specific order and referring to tabulated values presented by several authors [3]. There are alternative approaches than can be seen in [21], and [22].

If we want to achieve a maximally flat response than the tabulated values of the respective LPP are the following [23]:

N	g_1	g_2	g_3	g_4	g_5	g_6	g_7	g_8	g_9	g_{10}	g_{11}
1	2.0000	1.0000									
2	1.4142	1.4142	1.0000								
3	1.0000	2.0000	1.0000	1.0000							
4	0.7654	1.8478	1.8478	0.7654	1.0000						
5	0.6180	1.6180	2.0000	1.6180	0.6180	1.0000					
6	0.5176	1.4142	1.9318	1.9318	1.4142	0.5176	1.0000				
7	0.4450	1.2470	1.8019	2.0000	1.8019	1.2470	0.4450	1.0000			
8	0.3902	1.1111	1.6629	1.9615	1.9615	1.6629	1.1111	0.3902	1.0000		
9	0.3473	1.0000	1.5321	1.8794	2.0000	1.8794	1.5321	1.0000	0.3473	1.0000	
10	0.3129	0.9080	1.4142	1.7820	1.9754	1.9754	1.7820	1.4142	0.9080	0.3129	1.0000

Table 1 - Element values for the maximally flat lowpass filter prototypes [3]

The letter *g* represents the lowpass prototype element values for each filter order.

After creating the specified LPP filter and attributing the correct above elements an impedance and frequency scaling must be performed. Therefore a new load impedance, cutoff frequency, resistance, capacitance and inductance are changed by the following expressions in order to transform de circuit:

$$R = R_0 R_n \tag{3.3}$$

$$L = R_0 \frac{L_n}{W_0} \tag{3.4}$$

$$C = \frac{C_n}{R_0 W_0} \tag{3.5}$$

Scaling impedances means multiplying each impedance by R_0. On the other hand frequency scaling is achieved with $w_n = w/w_0$. If a capacitor C is replaced with C/w_0 its frequency response is also scaled by w_0. However the resistor is not affected by frequency scaling because it is frequency independent.

After an appropriate impedance and frequency scaling the new elements are given by equations (3.6) and (3.7) [3]:

$$L_k = \frac{R_0 g_k}{\omega_c} \tag{3.6}$$

$$C_k = \frac{g_k}{R_0 \omega_c} \tag{3.7}$$

The circuit of the stepped-impedance method scaled will have this form:
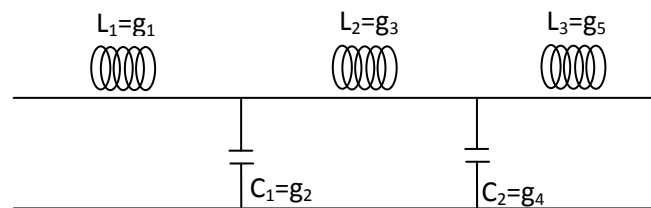
Figure 3.7 - Stepped impedance method

The final correspondent microstrip layout will have the following appearance:

Figure 3.8 - Layout of a microstrip stepped impedance circuit

A good substrate choice must be made due to the electrical performance desired, length of the circuit, price and circuit stability.

To obtain this layout the effective permittivity, width and length must be found. For a better analysis and due to the fringing fields at the end of the low impedance line sections the inclusion of a T-equivalent circuit maybe considered for these sections or/and an interactive approach correcting the modified initial design can be taken into account. So, the length for a high impedance line (or in terms of the required inductance) is given by:

$$l = \frac{\lambda_H}{2\pi} \sin^{-1}\left(wL_k / Z_H\right) \tag{3.8}$$

with the two shunt-capacitances elements:

$$C_L = \frac{1}{wZ_H} \tan\left(\pi l/\lambda_H\right)$$
(3.9)

where λ_H and Z_H are the wavelength and characteristic impedance associated with the high impedance microstrip line.

As for the low impedance line the methodology is very similar. The length of the desired capacitance is:

$$l = \frac{\lambda_L}{2\pi} \sin^{-1}\left(wC_k Z_L\right)$$
(3.10)

and the series inductances are given by:

(3.11)

$$L_C = \frac{Z_L}{w} \tan\left(\pi l/\lambda_L\right)$$

An interactive process is used until a good stable solution is found [8], i.e. the initial element length is found and the initial values are modified regarding the fringing capacitances of the high impedance lines and the inductive components of the low impedance lines.

The width is found by considering the substrate used (dielectric and thickness) and the line characteristic impedance as indicated in equations (3.12) and (3.13).

$$\varepsilon_{eff} = \frac{\varepsilon_r + 1}{2} + \frac{\varepsilon_r - 1}{2} \times \frac{1}{\sqrt{1 + 12 \times h/w}}$$
(3.12)

$$Z_0 = \begin{cases} \dfrac{60}{\sqrt{\varepsilon_{eff}}} \ln\left(\dfrac{8h}{w} + \dfrac{w}{4h}\right) & \text{para } \dfrac{w}{h} \leq 1 \\[4mm] \dfrac{120\pi}{\sqrt{\varepsilon_{eff}}\left(w/h + 1.393 + 0.667 \ln\left(w/h + 1.444\right)\right)} & \text{para } \dfrac{w}{h} \geq 1 \end{cases}$$
(3.13)

3.5. Bandpass filters

The design of bandpass filters starts with the design of a prototype lowpass filter with the required passband and attenuation characteristics. Once a prototype is available it is

possible to transform the values using simple algebraic identities to give high-pass and bandpass filters with the same shape.

The mapping from the lowpass prototype response (Butterworth) to the bandpass response is shown in Figure 3.9
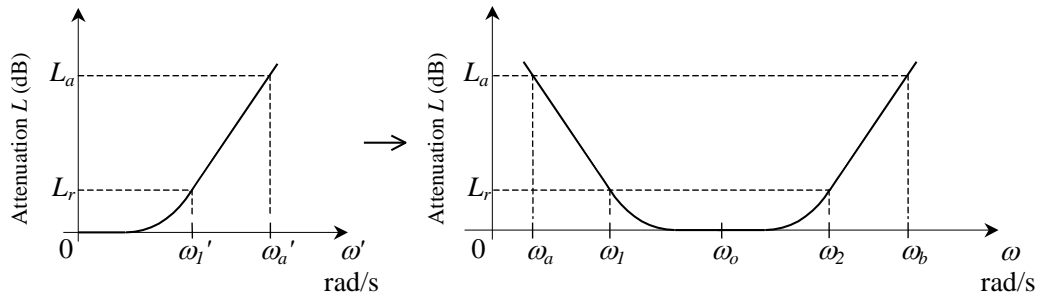
Figure 3.9 - Corresponding bandpass filter response regarding the Butterworth lowpass filter response

All elements of the lowpass prototype are replaced by tuned circuits i.e. inductors are replaced by series L-C tuned resonant circuits and capacitors are replaced by parallel L-C tuned resonant circuits.

The lowpass prototype values g_k of an nth order filter are given by [23].

$$g_k = 2\sin\left(\frac{(2k-1)\pi}{2n}\right)$$ (3.14)

The previous equation refers to maximally flat filters (Butterworth), with $g_0 = g_{n+1} = 1.0$ and attenuation $L_r = 3\ dB$ at $\omega_1' = 1$ rad/s.

The transformation from lowpass filter to bandpass filter can be expressed as:

$$\frac{\omega'}{\omega_1'} = \frac{1}{\Delta}\left(\frac{\omega}{\omega_o} - \frac{\omega_o}{\omega}\right) = \frac{1}{\Delta}\left(\frac{f}{f_o} - \frac{f_o}{f}\right)$$ (3.15)

where Δ is the 3 dB fractional bandwidth and ω_o is the centre frequency of the bandpass filter and are given by:

$$\Delta = \frac{\omega_2 - \omega_1}{\omega_o} = \frac{f_2 - f_1}{f_o}$$ (3.16)

$$\omega_o = \sqrt{\omega_2 \omega_1}$$ (3.17)

An important issue is that multiple resonances exist in a transmission line resonator resulting in additional higher frequency passbands (*spurious passbands*) that are not predicted

by equation (3.15). For broadband filter design it is necessary to use mapping functions that predict more accurately the frequency response.

For odd (Z_{oo}) and even (Z_{oe}) mode line impedance calculations it is considered a quarter wave length ($\lambda/4$) transmission line section with $1/J$ of characteristic impedance [3]:

$$Z_{0o} = Z_0\left(1 - JZ_0 + \left(JZ_0\right)^2\right) \tag{3.18}$$

$$Z_{0e} = Z_0\left(1 + JZ_0 + \left(JZ_0\right)^2\right) \tag{3.19}$$

Note that Z_0 is the characteristic impedance of the input and output connecting lines.

A bandpass filter with three cascaded coupled line sections is illustrated in Figure 33.
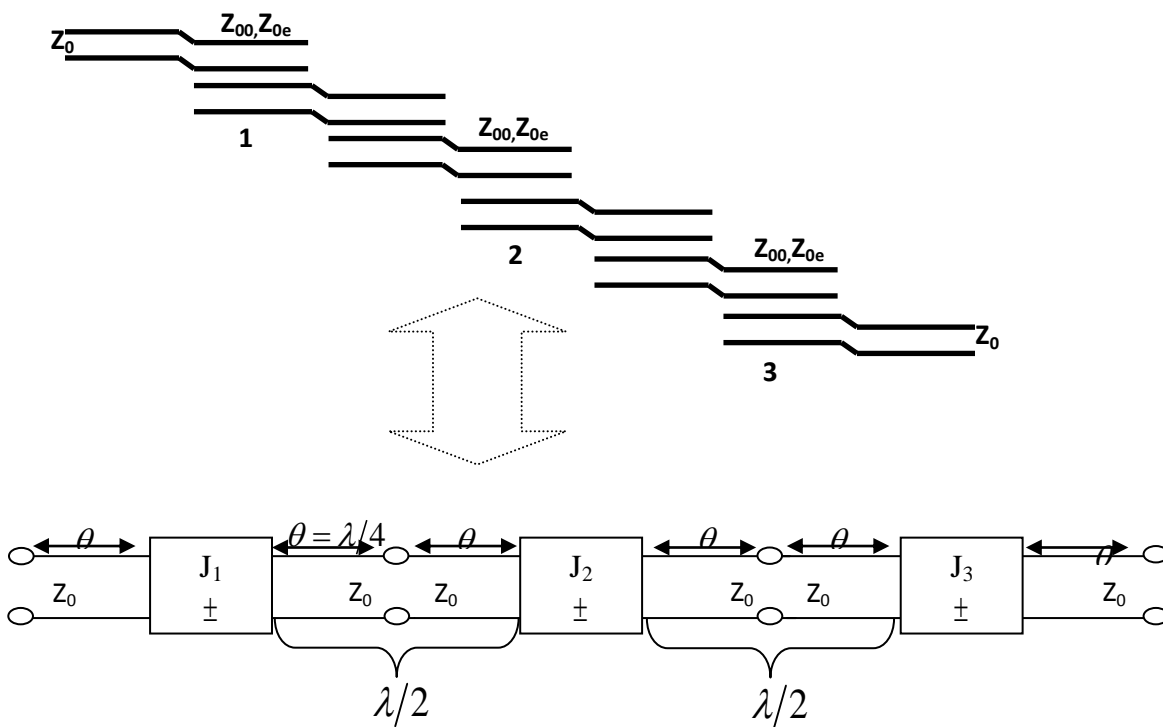
Figure 33 - Bandpass cascade with 3 coupled line sections equivalent [8]

This circuit can also be equivalent to a lumped elements circuit [3].

Between the consecutive inverters we have a transmission line section that has 2θ in length which makes it $\lambda/2$ between sections as illustrated above. They also act as resonators due to the $\lambda/4$ lines attached to the inverters.

Considering the elements (inductors or capacitors) of this prototype filter as $g_0, g_1, ..., g_N$, and that Δ corresponds to the 3 dB fractional bandwidth, from reference [3] the normalized admittance parameters are calculated through:

$$Z_0 J_1 = \sqrt{\frac{\pi\Delta}{2g_0 g_1}}$$
(3.20)

$$Z_0 J_N = \frac{\pi\Delta}{2\sqrt{g_{N-1} g_N}}, n = 2, ... N$$
(3.21)

$$Z_0 J_{N+1} = \sqrt{\frac{\pi\Delta}{2g_N g_{N+1}}}$$
(3.22)

After this, the even and odd line impedances may be calculated through equations (3.18) and (3.19).

3.5.1. Bandpass filter structures

The three common parallel-coupled microstrip structures each representing a 4th order bandpass filter are illustrated below.

Figure 3.11 - Couple resonator bandpass filters

One usual way to represent bandpass filters is to use parallel coupled microstrip structures.

The advantages from Parallel coupled filters over end coupled are [25]:

- Length (approximately half the size) of the filter;

- Symmetry in frequency response is obtained at three times the center frequency;

- Larger gap supported between adjacent microstrips.

3.6. Power Dividers

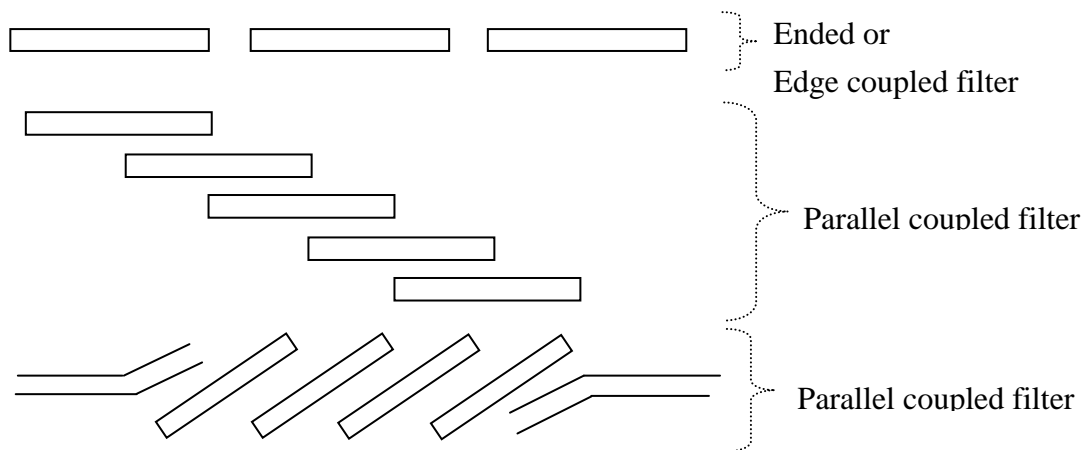Power dividers are passive microwave components normally used for two purposes:

- Power division, where the input signal P_1 is divided into 2 or more signals such as P_2 P_3 or P_N with less power than P_1 as shown in Figure 3.12.
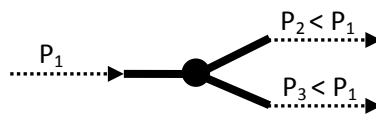
Figure 3.12 - Power divider

- Power combining or coupling which can agglomerate signals from its output ports. Directional couplers are also called four port components. Power dividers that take a form of a T-junction are the three port components as illustrated in Figure 3.13.
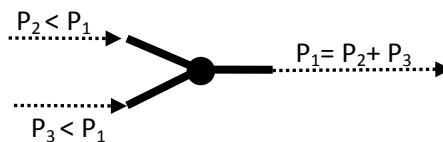
Figure 3.13 - Power divider

There are several power dividers and coupling mechanisms such as E-and H-plane waveguide tee junctions, Bethe hole coupler, multihole directional couplers, Schwinger coupler, waveguide magic-T, etc. For the microstrip line case it was invented important devices such as the Wilkinson divider, the branch line hybrid and the coupled line directional coupler [3].

3.6.1. Wilkinson power divider

The Wilkinson power divider can be used to equally divide the power through its outputs. The equal power division concept consists on dividing the input power equally in two

or more ways. The most known power divider in this field is the three port network also called 3 *dB* power divider and it takes the form of Figure 3.14.
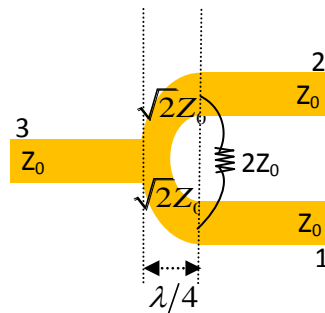
Figure 3.14 - 2-way Wilkinson power divider

It consists on the input port 3, quarter-wave transformers, resistors (isolation purposes) and outputs ports 2 and 1.

The input and output ports are scaled with the same dimensions thus with the same characteristic impedance (Zo).

The section that has the length of quarter wave means that it has one fourth of wavelength of the electromagnetic wave which is propagating in this three port network. The section lengths relates with the phase velocity[ii] (usually light speed), frequency used and matching conditions as well. A good match brings better power transfer from input to output because if output ports are matched the reflected power from input to output will be zero, i.e. all of the power is transmitted to the output.

The resistor implemented in the circuit essentially improves the isolation between the ports. It avoids coupling effects on the output ports, or in other words if transmissions on output port 2 affects transmissions on output port 1 there will be consequences on the correct splitting of the power [27].

A good S-parameters analysis must be made regarding port matching, transition, insertion loss and isolation.

Thus, considering Figure 3.14 port nomenclature, the S(3,1) and S(3,2) parameters of a power divider at 1 *GHz* with an operational bandwidth of 1 *GHz* must be linear and free of interferences which indicates a good transition between the input and output ports. Other

parameter to consider is the S(2,1) and S(1,2) which indicates good or bad isolation between the output ports. This response must be lower than the S(3,1)/S(3,2) for a good signal transition. Matched ports are also considered in this components and its response must also remain lower for good transition purposes as illustrated by Figure 3.15.
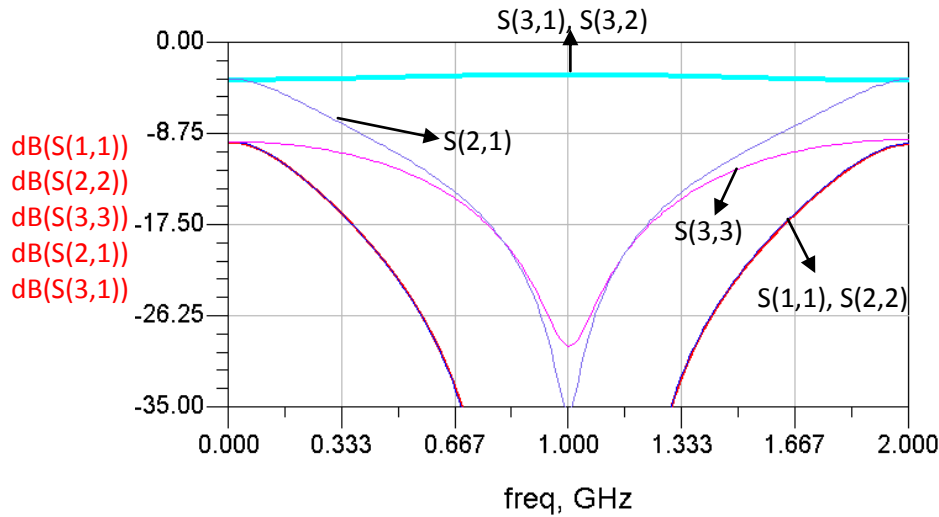
Figure 3.15 - S-parameters analysis of the Wilkinson power divider

However, for wideband power division this one stage Wilkinson power divider will not work well. As illustrated in Figure 3.15 the bandwidth available with this kind of divider is limited. One possible solution is to implement more stages to this divider in order to achieve a higher bandwidth and less distortion [28].

The circuit is based on a T junction followed by a multiplicity of cascaded pairs of quasi-TEM line lengths and interconnecting resistors. The resistors provide the output port matching and isolation. Each pair of lines and its associated resistor are referred to as a section as illustrated Figure 3.16.
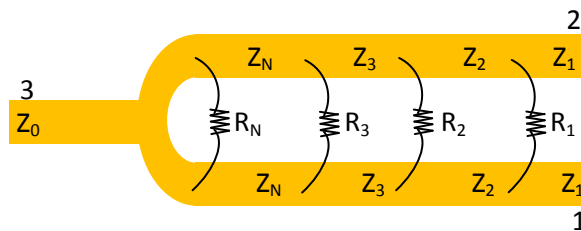
Figure 3.16 - Multistage Wilkinson power divider

The bandwidth capability increases proportional to the number of sections and resistors as proved in [28].

3.7. Chapter Summary

Microstrip transmissions lines propagation is characterized by a combination of TM (Transverse Magnetic) and TE (Transverse Electric). Still, these lines do not have a uniform dielectric filling and cannot support a single mode of propagation so the bulk of the energy is transmit along the microstrip with a field distribution almost the same as in TEM mode or quasi-TEM.

It is also important to analyze the behavior of transmission lines termination, i.e. short or open circuits. Plus, at the transmission lines terminations some events can produce discontinuities such as open-ended lines, gaps between lines, and changes in lines widths.

In microwave frequencies the idea of voltage, current and impedances is less descriptive when high frequency networks are analysed, and that is why S-parameters are used in this study.

Richard's transformation basically translates the w plane through the Ω plane and the four Kuroda's identities use redundant transmission line sections for a handier implementation of microwave filters. However, other methodologies are explained regarding lowpass filters construction such as the stepped-impedance methodology. Bandpass filters were also exposed and a few architectures such as parallel coupling were introduced as well as the knowhow to perform an even and odd mode analysis of the component

In microwave designs, electric performance, power and reliability must be always present. Thus, a good S-parameters analysis must be made.

Wilkinson power dividers were introduced and details about its S-parameters analysis were explained and demonstrated.

[ii]Wavelength * Frequency = Phase velocity (Usually the speed of light)

4. Design environment

The design of the filters and power divider was done using Agilent ADS (Advanced Design System), which enables microwave engineers to design, simulate and analyze active and passive microwave components. It is a powerful electronic design automation software system.

Some useful tools are integrated in ADS such as Linecalc that can calculate electrical and physical parameters of a transmission line and Momentum that performs an accurate electromagnetic simulation of the desired circuit [29].

4.1. LineCalc

LineCalc is an analysis and synthesis tool incorporated in ADS. A user defines the necessary parameters such as the substrate dielectric, height and cooper thickness definition as well as the characteristic impedance of one single or several lines, spacing between coupled lines, electrical lengths, characteristics impedance or even the width or length of the microstrip line. For example, if a characteristic impedance of a single line and its electrical length are known as well as the substrate characteristics then this tool can calculate the width and length of the desired microstrip line by a single click as exemplified in Figure 4.1.
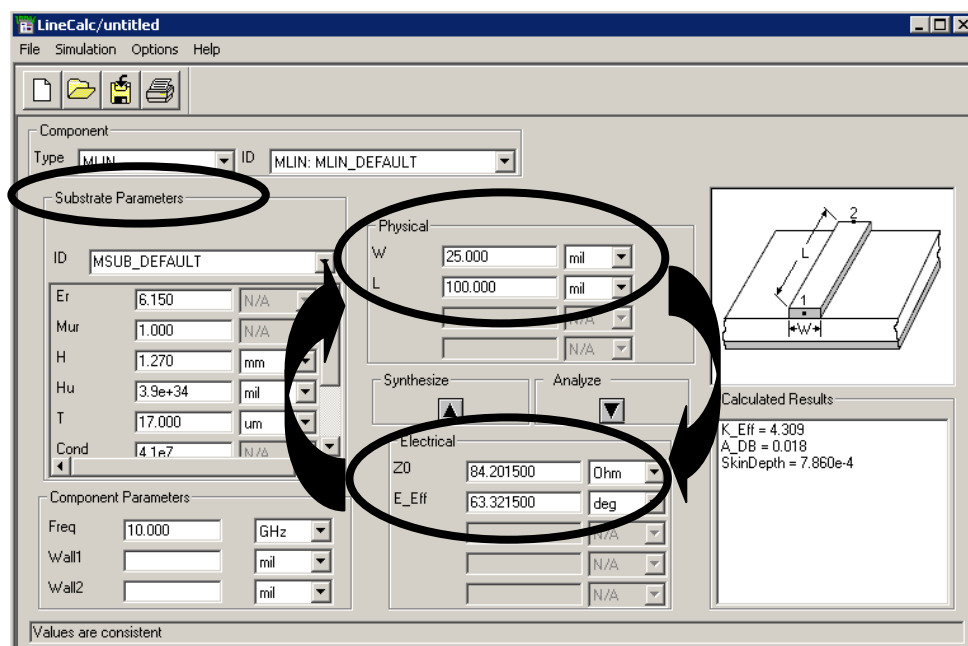

Figure 4.1 - Linecalc example

4.2. Tunning

This important tool aids the user to find his appropriate circuit response. It enables the change of one or more parameter of the design and almost simultaneously shows the output result without having to re-simulate the entire circuit [30].

4.3. Momentum

Momentum is a powerful tool incorporated in ADS. It is an electromagnetic simulator that computes S-parameters for circuits like microstrip, stripline, and other topologies. Accurate electromagnetic simulation improves passive circuit's performances and maintains a high equivalence between simulation and manufacturability.

Other option within Momentum is the Momentum RF which reduces simulation time without sacrificing accuracy on large structures under a half wavelength.

While optimizing a design it may alter the geometric dimensions to achieve the desired specifications. This tool also identify parasitic coupling between components, produces accurate and realistic results and enables the user to visualize current flow and the radiation present in the circuit with his comprehensive data display tools [31].

Since Momentum is an incorporated component of ADS, simulation setup times are reduced, and design productivity is increased [32].

4.4. Chapter summary

The three most used ADS tools in this project were as follow:

- The tuning facility - With this feature the designer doesn't need to re-simulate the entire circuit in order to view the results of his performed changes in the components parameters of the circuit;
- The Linecalc - Which calculates electrical and physical parameters of a transmission line;
- The electromagnetic simulator (Momentum) - Computes S-parameters for microstrip and stripline circuits and other topologies in a more realistic way.

5. Design and Implementation

5.1. Introduction

This chapter introduces the overall network components and then describes the design of the lowpass and bandpass filters as well as two power dividers. Methodologies used to discover the most accurate parameters of the microstrip lines as well as the substrate choice are covered in this chapter.

5.2. Base station Architecture

Figure 5.1 presents the first base station architecture. This strategy consists in dual output amplifiers which split and amplifies the signal. After the amplification the signal is filtered by the project bandpass filters.

Figure 5.1 - First architecture proposal
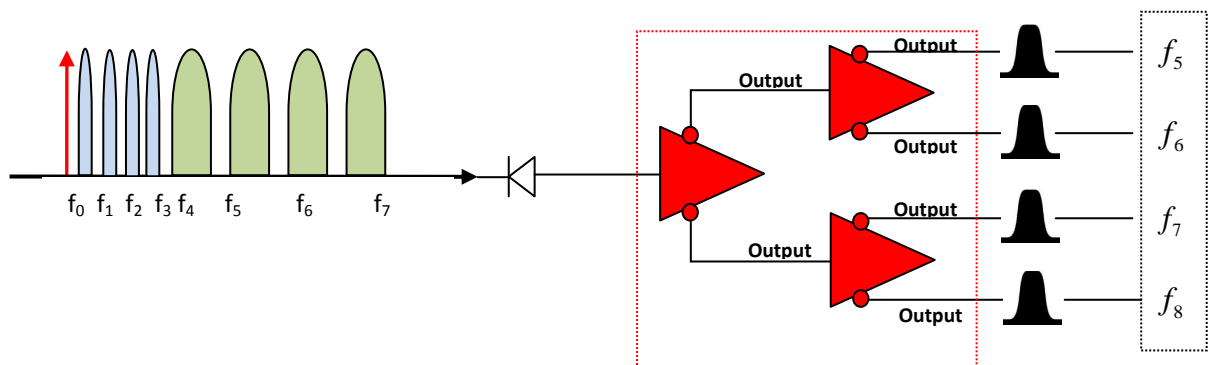
This architecture could achieve promissory results, however it was not used because these amplifiers are expensive and extremely difficult to find especially with the required frequency interval (9-18 *GHz*).Figure 5.2 shows the base station architecture that was followed in the project with one additional bandpass filter to capture the carrier that will be used for uplink operations.
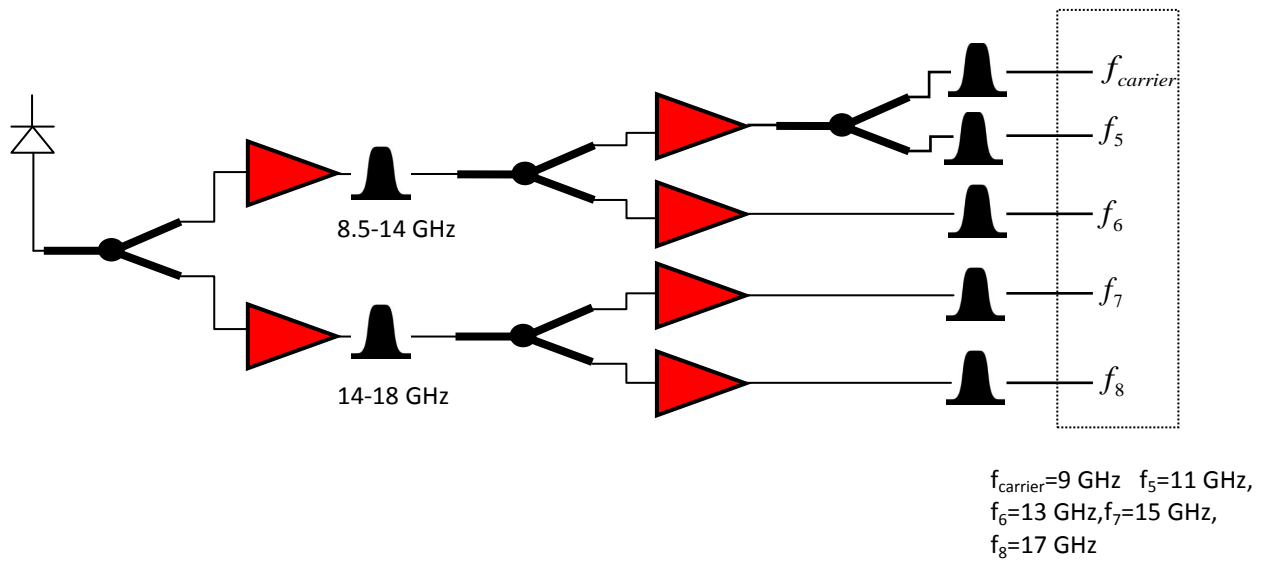
f$_{carrier}$=9 GHz f$_5$=11 GHz,
f$_6$=13 GHz,f$_7$=15 GHz,
f$_8$=17 GHz

Figure 5.2 - Architecture adopted

These broadband power dividers as well as the bandpass filters will induce undesirable power loss in the network that will be compensated by the six amplifiers attached to the respective outputs. These amplifiers are much easier to find and less expensive, while the overall architecture remains intact.

The proposed architecture presents seven bandpass filters with different bandwidths and centred frequencies plus four power dividers. The components presented in this master dissertation are designed and optimized with ADS. All the devices use the same Rogers substrate [Appendix 1] and the Hittite Microwave Corporation Low Noise Amplifiers (LNA) with 13 *dB* gain [33].

5.3. Substrate selection

The substrate selected was the RT/duroid® 6006. It has a dielectric constant of 6.15, a thickness of 1.27 *mm* and a copper cladding of 17 *μm*. These laminates are ceramic composite designed for electronic and microwave circuit applications requiring a relatively high dielectric constant. The designs take into account that the minimum fabricable dimension should be set to be 0.2 *mm*.

5.4. Lowpass filter

Alternated sections that consist in very high and very low impedances (stepped-impedance) is the method used in this dissertation for the design of the lowpass filter due to

its small size results compared to similar fabrications methods and to the relation "design difficulty vs. results quality". The major disadvantages of this method (per example. unable to get a sharp cutoff frequency and less good performance at high frequencies) were reviewed and found meaningless due to frequency used, optimizations processes and actual software tools.

5.4.1. Realization

The lowpass filter will be used for shaping 1 Gbp/s NRZ square pulses. The specifications for this Square Root Raised Cosine (SRRCOS) filter are:

- 75% raised cosine frequency response;
- Maximally flat response (Butterworth);
- 3 *dB* cutoff frequency at 500 *MHz* (bandwidth>=2 f_c, having $\alpha = 1$, the bandwidth stays at 1 *GHz* and the 3 *dB* cutoff frequency is $f_c = 500MHz$);

First the order of the filter must be found. Lowpass filter prototypes have normalized source impedance ($R_s = 1\Omega$) and cutoff frequency ($w_c = 1$).

The new cutoff frequency occurs when $w/w_c = 1$[3]. After acquiring the frequency and the desirable attenuation, the order of the filter is obtained using the data of Figure 5.3.
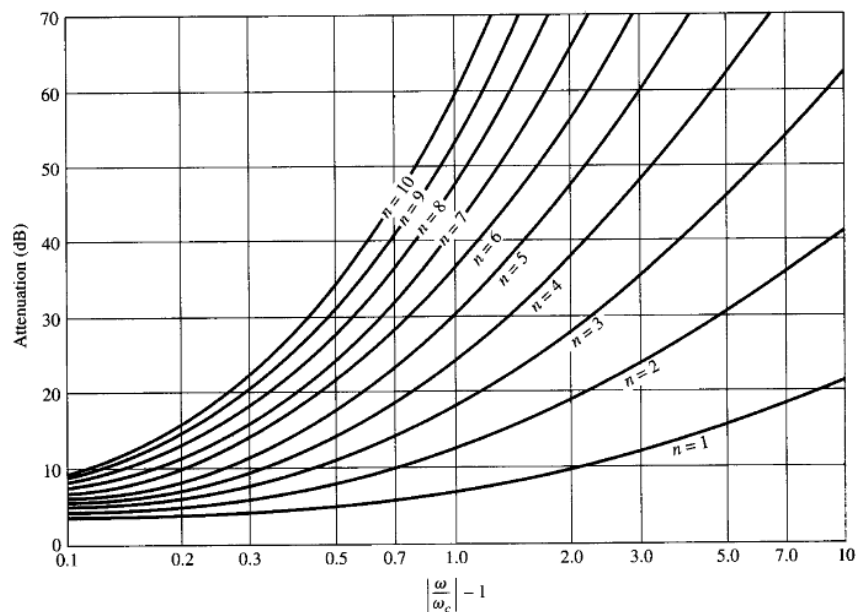

Figure 5.3 - Attenuation Vs normalized frequency for maximally flat filter prototypes [3]

The design methodology will be a slightly updated for the square root raised cosine response which is a very specific curve that needs to be brought carefully to zero. Thus, a larger value for the cut-off frequency will be chosen (2 *GHz*) to facilitate the optimization process. So, instead of finding directly the order of the filter, and taking into account the design tool (ADS), a simpler third order filter is selected for implementation. The 3rd order filter illustrated in Figure 5.4 is considered:
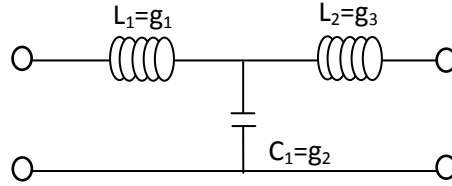

Figure 5.4 - Prototype circuit for the lowpass filter

The next step is to observe the Figure 5.4 and retrieve the element values for the maximally flat filter prototype.

The 3rd order filter (N=3) have the following elements values:

$$g1 = 1; \ g2 = 2; \ g3 = 1; \ g4 = 1;$$

(5.1)

The characteristic impedance of each line section was chosen to be $20\,\Omega$ and $100\,\Omega$ due to realizable manufacturability, i.e. line widths need to have at least a dimension of 0.2 *mm*. However, a characteristic impedance of 50Ω in the beginning and end of the transmission line section will be present in every filter with a sufficiently large length to minimize interference in the circuit.

The filter impedance is $R_0 = 50\Omega$ and the cutoff frequency as explain before has the value of $f_c = 2 \times 10^9 \ Hz$. Using equations (3.6) and (3.7), the filter lumped elements (inductive and capacitive) are:

$$g_1 = 1 \Rightarrow L_1 = \frac{R_0 g_1}{\omega_c} = \frac{50 \times 1}{2\pi \times 2 \times 10^9} = 3.98 \ \text{nH}$$

(5.2)

$$g_2 = 2 \Rightarrow C_2 = \frac{g_2}{R_0 \omega_c} = \frac{2}{50 \times 2 \times \pi \times 2 \times 10^9} = 3.18 \ \text{pF}$$

(5.3)

$$g_3 = 1 \Rightarrow L_3 = \frac{R_0 g_3}{\omega_c} = \frac{50 \times 1}{2\pi \times 2 \times 10^9} = 3.98 \text{ nH} \qquad (5.4)$$

The schematic in ADS is illustrated in Figure 5.5 after updating the calculated elements.
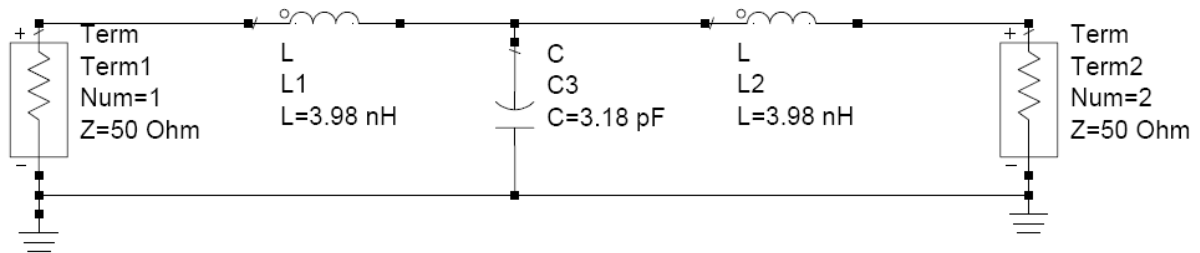
Figure 5.5 - Circuit schematic of the third order lowpass filter

Figure 5.6 presents the circuit response with the cut-off frequency exactly where stipulated.
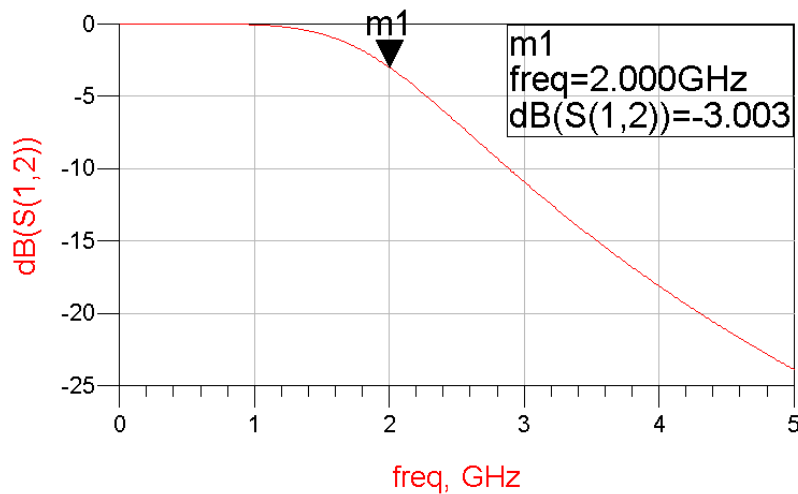
Figure 5.6 - Frequency response of the third order lowpass filter

The circuit is obtained and now the dimensions of the microstrip lines must be found. To obtain these dimensions the RT/duroid® 6006 substrate choice is made. The high (H) and low (L) impedance line length should be given regarding the wavelength considered, inductance, capacitance and characteristic impedance as seen in (3.8), (3.9), (3.10) and (3.11). Equations (3.9) and (3.11) are iterative correction procedures that take into account the fringing capacitances effects and try to adjust them. After this procedure, the characteristic impedance and effective dielectric constant are calculated as in equations (2.16) and (2.17).

Although, the width of the microstrip lines were calculated by *Linecalc* which is a tool incorporated in ADS, for length calculations the equations (3.8), (3.9), (3.10) and (3.11) are solved.

Hence, in Linecalc an electrical length of 360^0 was defined, meaning that the values for the length are exactly those of one single wavelength at 1 *GHz*.

Therefore the Table 2 present our Linecalc variables.

Line impedances	Electrical length(^{0})	W(mm)	L(mm)
20Ω (Z_{LOW})	360	7.2015	133.05
50Ω (Z_0)	360	1.8454	142.962
100Ω (Z_{HIGH})	360	0.3409	151.394

Table 2 - Variables values for microstrip line section constructions

First, equation (3.8) is used to determine the microstrip length referred to the inductance. The effective dielectric of the material must be determined for each line section and the respective wavelength in free space with $f_c = 2\,GHz$ as follows:

$$\lambda_0 = \frac{c}{f_c} = \frac{3\times10^8}{2\times10^9} = 0.15 \tag{5.5}$$

Referring to equation (2.16) the effective dielectric values for each line are:

$$\varepsilon_{eff_{LOW}} = \frac{6.15+1}{2} + \frac{6.15-1}{2} \times \frac{1}{\sqrt{1+12\times\left(1.27\times10^{-3}/7.20146\times10^{-3}\right)}} = 5.0337 \tag{5.6}$$

$$\varepsilon_{eff_{50}} = \frac{6.15+1}{2} + \frac{6.15-1}{2} \times \frac{1}{\sqrt{1+12\times\left(1.27\times10^{-3}/1.8454\times10^{-3}\right)}} = 4.4213 \tag{5.7}$$

$$\varepsilon_{eff_{HIGH}} = \frac{6.15+1}{2} + \frac{6.15-1}{2} \times \frac{1}{\sqrt{1+12\times\left(1.27\times10^{-3}/0.3409\times10^{-3}\right)}} = 3.9559 \tag{5.8}$$

The variables table is accordingly completed in Table 3.

Line impedances	Electrical length(0)	W(mm)	L(mm)	ε_{eff}
20Ω (ZLOW)	360	7.2015	133.05	5.0337
50Ω (Z0)	360	1.8454	142.962	4.4213
100Ω (ZHIGH)	360	0.3409	151.394	3.9559

Table 3- Variables values for microstrip line section constructions

$$\lambda_{LOW} = \frac{\lambda_0}{\sqrt{\varepsilon_{eff_{20}}}} = \frac{0.15}{\sqrt{5.0337}} = 0.0669\,m \tag{5.9}$$

$$\lambda_{50} = \frac{\lambda_0}{\sqrt{\varepsilon_{eff_{50}}}} = \frac{0.15}{\sqrt{4.4213}} = 0.0713\,m \tag{5.10}$$

$$\lambda_{HIGH} = \frac{\lambda_0}{\sqrt{\varepsilon_{eff_{HIGH}}}} = \frac{0.15}{\sqrt{3.9559}} = 0.0754\,m \tag{5.11}$$

The line section length of our filter is given by:

$$l_{INDUCTOR} = \frac{\lambda_{HIGH}}{2\pi} \sin^{-1}\left(\frac{2\pi f_c L_{HIGH}}{z_{HIGH}}\right) =$$
$$= \frac{0.0754}{2\pi} \sin^{-1}\left(\frac{2\pi \times 2 \times 10^9 \times 3.98 \times 10^{-9}}{100}\right) = 6.2853\,mm \tag{5.12}$$

$$C_L = \frac{1}{2\pi f_c Z_{HIGH}} \tan(\frac{\pi l}{\lambda_{HIGH}}) =$$
$$= \frac{1}{2\pi 2 \times 10^9 \times 100} \tan(\frac{\pi 6.2853 \times 10^{-3}}{0.0754}) = 0.2133\,pF \tag{5.13}$$

And the capacitor has the following length:

$$l_{CAPACITOR} = \frac{\lambda_{LOW}}{2\pi} \sin^{-1}\left(2\pi f_c C_k Z_{LOW}\right) =$$
$$= \frac{0.0669}{2\pi} \sin^{-1}\left(2\pi \times 2 \times 10^9 \times 3.18 \times 10^{-12} \times 20\right) = 9.8595\,mm \tag{5.14}$$

$$L_C = \frac{Z_L}{w} \tan\left(\pi l / \lambda_L\right) = \frac{20}{2\pi 2 \times 10^9} \tan\left(\frac{\pi 9.8595 \times 10^{-3}}{0.0669}\right) = 0.79448 \times 10^{-9} \tag{5.15}$$

The correction the effects of the adjacent lines:

$$L_1^{new} = 3.98 \times 10^{-9} \text{-} 0.7945 \times 10^{-9} = 3.1855 nH \tag{5.16}$$

$$C_2^{new} = 3.18 \times 10^{-12} \text{-} 2 \times 0.2133 \times 10^{-12} = 2.7534 pF \tag{5.17}$$

$$L_3^{new} = 3.98 \times 10^{-9} \text{-} 0.7945 \times 10^{-9} = 3.1855 nH \tag{5.18}$$

The goal of this method is to start this cycle all over again, however due to the facility provided by ADS there is no need to iterate several times. So we will continue with the initial values.

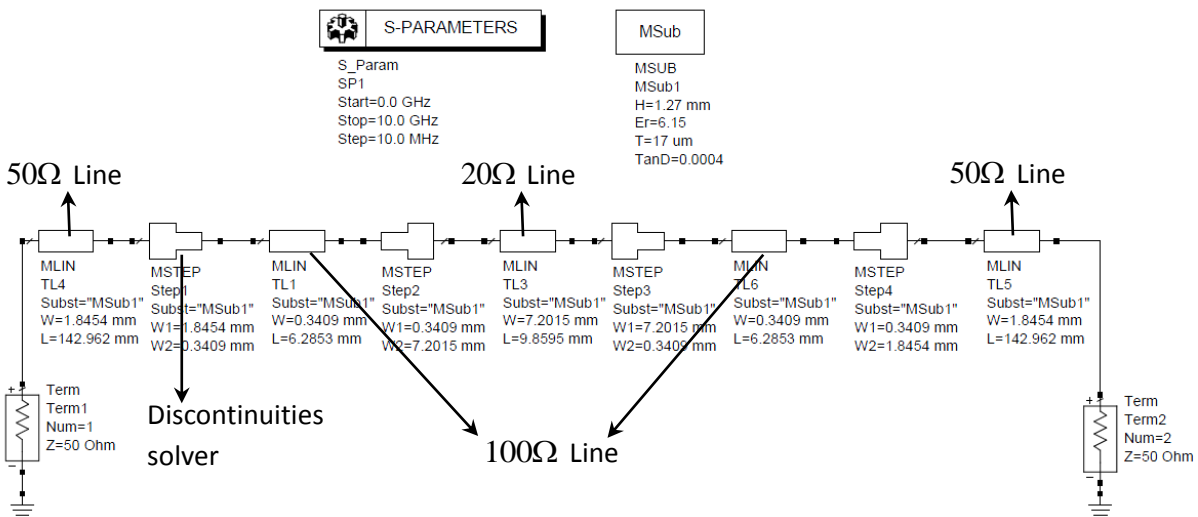The microstrip implementation is presented in Figure 5.7.

Figure 5.7 - Microstrip lowpass filter components

The $50\,\Omega, 20\,\Omega$ and $100\,\Omega$ lines were introduced by the Microstrip Line (MLINE) component with the specific width and length calculated previously. Microstrip Step in width (MSTEP) will model the discontinuities between two different width line sections. The substrate details are also specified by the component MSUB (Microstrip Substrate).

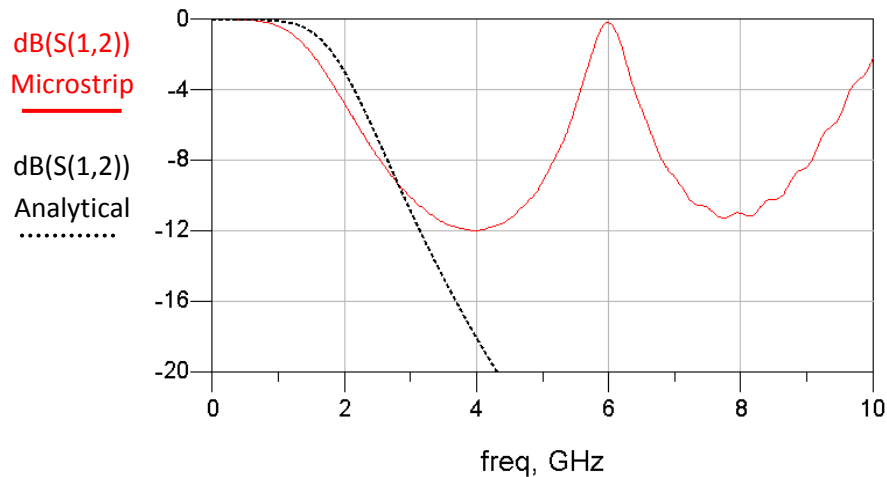After simulating the circuit the results are shown in Figure 5.8.

Figure 5.8 - Circuit Vs Microstrip implementation

At this point the similarities regarding the microstrip implementations are achieved. It is not important to equalize these responses because they will be brought to zero at the cut off frequency of the specified SRRCOS lowpass filter. For this purpose two open-circuit stubs are implemented at the end and beginning of the circuit. Plus, two components to model the discontinuities provided by the stubs are also needed. Therefore two Libra Microstrip T-junction (MTEE) are agglomerated in the circuit. The stub widths were initially set as the width of the $50\,\Omega$ line and the lengths were set to $20\,mm$.

The objective is to obtain the best equally frequency response regarding the SRRCOS one. So, the optimization was made (using the tuning facility of ADS) to all variables in the circuit except the width of the $50\,\Omega$ lines. An approximate frequency response was obtained as shown in Figure 5.10. For compact reasons the bends were introduced in the stubs as seen in Figure 5.9.
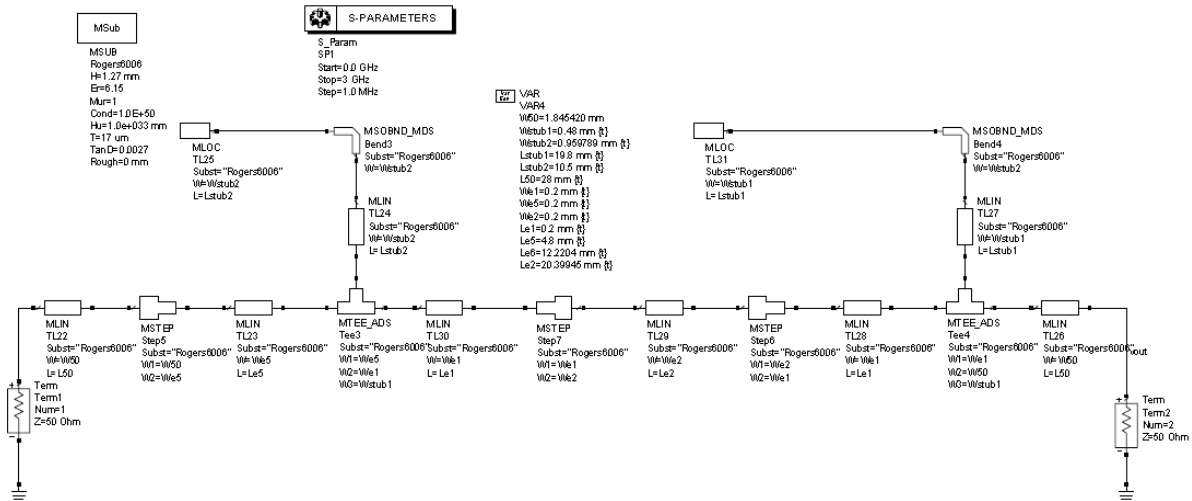
Figure 5.9 - Schematic of the SRRCOS lowpass filter

The filter response compared to the ideal square root raised cosine with a roll-off factor of 0.75 is:
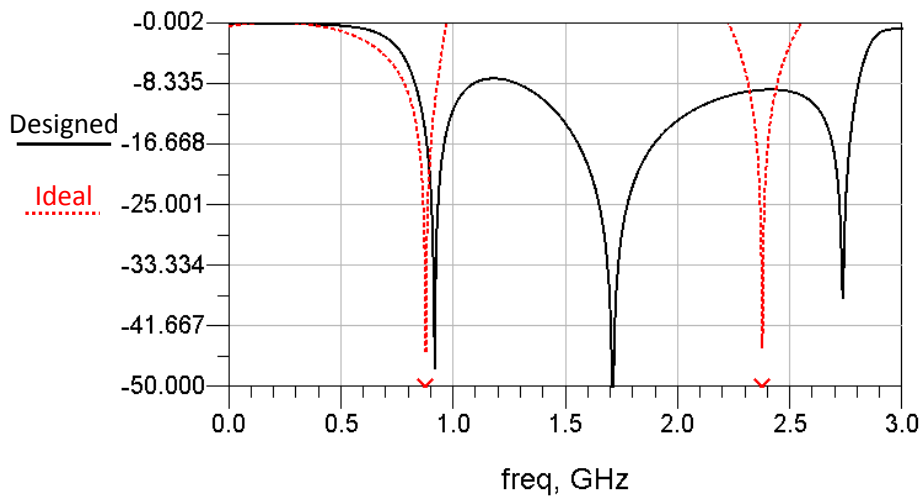
Figure 5.10 - Ideal SRRCOS lowpass filter response Vs Implemented version response

This response is further optimized as explained in the results section.

5.5. Bandpass filters design

The method adopted consists on parallel coupled lines. These resonators are coupled through the even and odd mode fields along the edges of the line. A broader bandwidth, a significant reduction of the component size and the fact that this method allows higher gaps (less interference) are the reasons to choose this design.

Filter performance are based on a good S-parameters analysis, bandwidth, center frequency, ripple, rejection, group delay, and power-handling capability. A specific transfer function which approximates the project desired filter response (Butterworth) is selected, and prior to the construction steps, some optimization is made. The optimizations consist on adjustments such as: modifying the offset symmetry, spacing, width, length, and thickness of the conductor resonators [24].

Seven bandpass filters were implemented in this project as illustrated in Figure 5.11. Two bandpass filters for initial trialing with 5.5 *GHz* and 4 *GHz* of bandwidth with center frequencies on 12 *GHz* and 16 *GHz* respectively, four bandpass filters with 2 *GHz* of bandwidth with center frequencies of 11, 13, 15 and 17 *GHz* and one narrow bandpass for the carrier with 9 GHz center frequency.
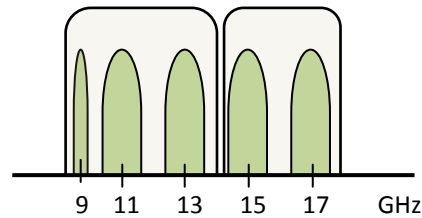

Figure 5.11 – BS downlink bandpass filters

5.5.1. 12 GHz centered frequency bandpass filter

First the *fractional bandwidth*[iii] must be obtained. Due to the 5.5 *GHz* required bandwidth it is assumed that at 17 *GHz* the filter must have attenuation higher than 30 *dB*. So the 3 *dB* fractional bandwidth of the filter is presented by equation (5.19):

$$\Delta = \frac{14 \times 10^9 - 8.5 \times 10^9}{11.25 \times 10^9} = 0.49 \tag{5.19}$$

The transformation of the normalized frequency is then obtained.

$$w = \frac{1}{0.49}\left(\frac{17 \times 10^9}{11.25 \times 10^9} - \frac{11.25 \times 10^9}{17 \times 10^9}\right) = 1.73 \tag{5.20}$$

$$w = \frac{w}{w_c} - 1 = 0.73 \tag{5.21}$$

So, from Figure 5.3 the order of the filter is:

$$N = 6 \rightarrow \; > 30dB \tag{5.22}$$

Another bandpass filter characteristic is that they must have a flat response at the bandpass. Thus, the element and admittance values can be chosen from equations (5.23), (5.24), (5.25) and (5.26).

$$Z_0 J_1 = \sqrt{\frac{\pi \times 0.49}{2 \times 1 \times 0.5176}} = 1.2194 = Z_0 J_7 \tag{5.23}$$

$$Z_0 J_2 = \frac{\pi \times 0.49}{2} \times \frac{1}{\sqrt{0.5176 \times 1.4142}} = 0.8996 = Z_0 J_6 \tag{5.24}$$

$$Z_0 J_3 = \frac{\pi \times 0.49}{2} \times \frac{1}{\sqrt{1.4142 \times 1.9318}} = 0.4657 = Z_0 J_5 \tag{5.25}$$

$$Z_0 J_4 = \frac{\pi \times 0.49}{2} \times \frac{1}{\sqrt{1.9318 \times 1.9318}} = 0.3984 \tag{5.26}$$

And the even and odd line impedances for each coupler are calculated through equations (3.18) and (3.19), and presented in Table 4.

Couplers	Even and Odd impedances (Ω)
1st and 7th	$Z_{0e} = Z_0\left(1 + JZ_0 + \left(JZ_0\right)^2\right) = 50\left(1 + 1.2194 + 1.2194^2\right) = 185.317$ $Z_{0o} = Z_0\left(1 - JZ_0 + \left(JZ_0\right)^2\right) = 50\left(1 - 1.2194 + 1.2194^2\right) = 63.377$
2nd and 6th	$Z_{0e} = Z_0\left(1 + JZ_0 + \left(JZ_0\right)^2\right) = 50\left(1 + 0.8996 + 0.8996^2\right) = 135.444$ $Z_{0o} = Z_0\left(1 - JZ_0 + \left(JZ_0\right)^2\right) = 50\left(1 - 0.8996 + 0.8996^2\right) = 45.484$
3rd and 5th	$Z_{0e} = Z_0\left(1 + JZ_0 + \left(JZ_0\right)^2\right) = 50\left(1 + 0.4657 + 0.4657^2\right) = 84.129$ $Z_{0o} = Z_0\left(1 - JZ_0 + \left(JZ_0\right)^2\right) = 50\left(1 - 0.4657 + 0.4657^2\right) = 37.559$
4th coupler	$Z_{0e} = Z_0\left(1 + JZ_0 + \left(JZ_0\right)^2\right) = 50\left(1 + 0.3984 + 0.3984^2\right) = 77.856$ $Z_{0o} = Z_0\left(1 - JZ_0 + \left(JZ_0\right)^2\right) = 50\left(1 - 0.3984 + 0.3984^2\right) = 38.0161$

Table 4 - Even and Odd impedance values

After obtaining Z_{0e} and Z_{0o}, the microstrip dimensions are calculated. ADS Linecalc tool is used for width, length and line spacing calculations. The first achieved values originated a bandpass filter dislocated from its centered frequency. This happened because line lengths do not consider all fringing capacitances effects between the end of the lines and the ground plane [25]. Fringing capacitances results from coupled lines longer than the actual physical lengths, so for implementation purposes the solution is to decrease the size of the line length to center the frequency.

The tuning tool was used to make these corrections and several optimizations. The final filter dimensions are presented in Table 5.

Coupler	1st & 7th	2nd & 6th	3rd & 5th	4th
W (mm)	0.3614	0.6474	1.0745	1.2087
S (mm)	0.2953	0.2	0.2	0.2
L (mm)	3.11	2.7988	2.8949	2.6268

Table 5 - Bandpass filter dimensions (fc=12 *GHz*)

The 50 Ω input/output lines are 10 *mm* long.

Using the dimensions presented in Table 5 the schematic in Figure 5.12 is achieved.
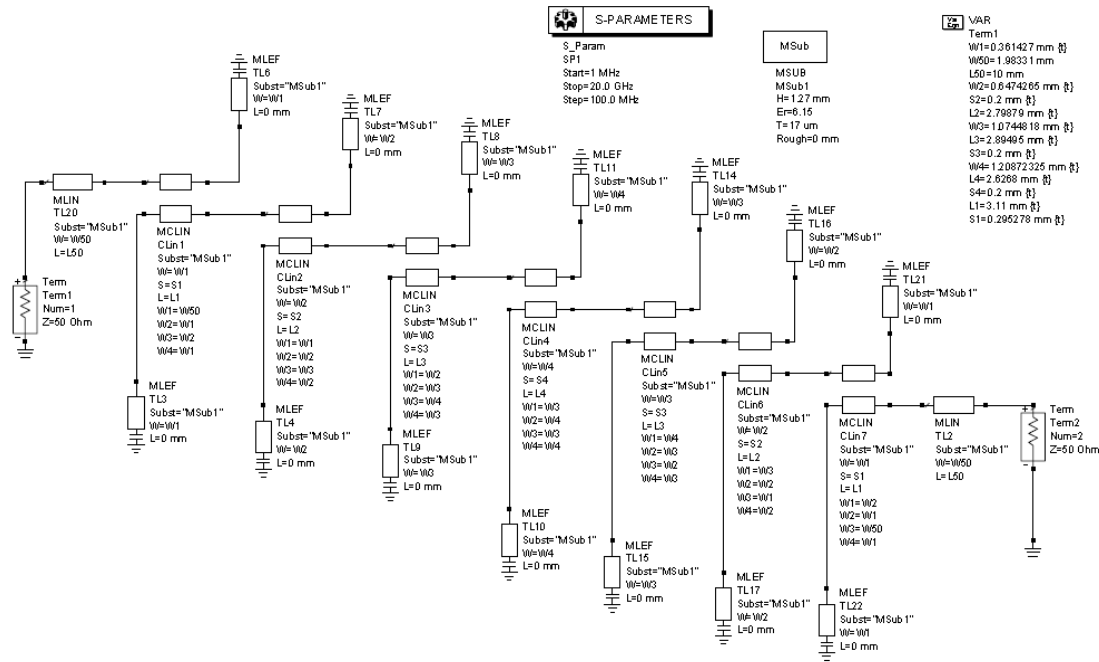

Figure 5.12 - Schematic of 12 *GHz* bandpass filter

The circuit components are selected from the Microstrip Elements Library, where MLIN represent the 50 Ω input and output connecting lines, Microstrip coupled line (MCLIN) simulates the couplers and Microstrip Line Open-End Effects (MLEF) represents the open ended effects of the open circuit coupled lines. It is very important to correct the non linearity's in the circuit, i.e. the lines width of each successive couplers must be all lined up to provide the best possible result.

The 3 *dB* attenuation points are deliberately designed with higher frequency values. When Momentum simulates this response it brings the response to zero more abruptly giving a more satisfactory attenuation. In fact, after the Momentum simulation all filters decrease their bandwidths, therefore wider bandwidth filters are considered at these design stages.

Figure 5.13 shows the circuit layout and its nomenclature using the dimensions presented in Table 5.
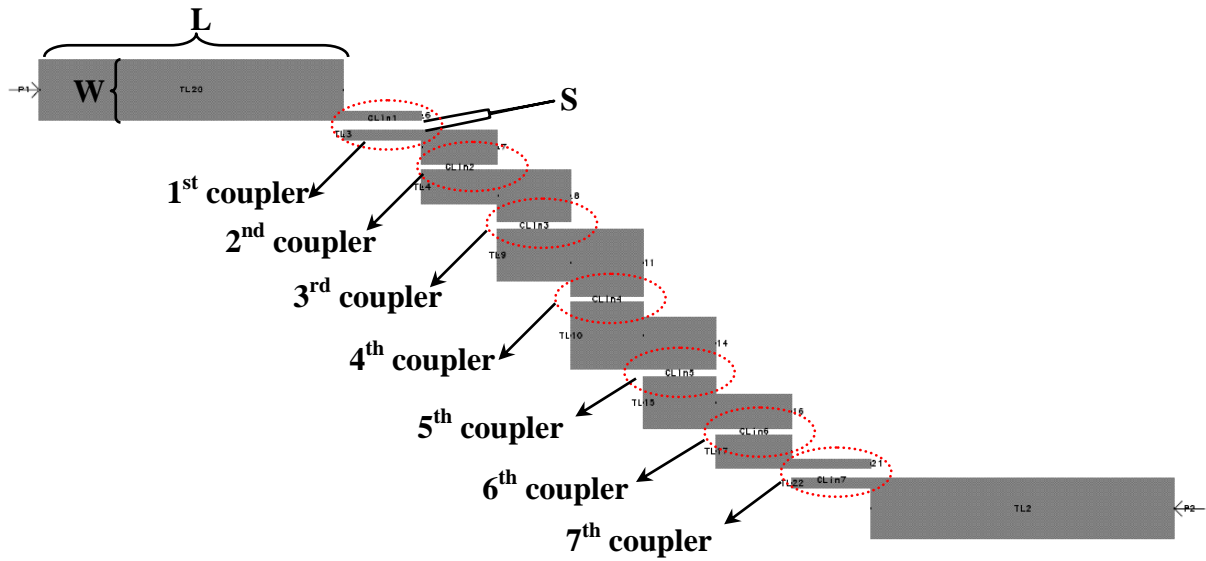

Figure 5.13 - Layout of the bandpass filter with f_c=12GHz

5.5.2. 16 GHz centered frequency bandpass filter

Using the same procedure as in 5.5.1 the dimension of the 16 *GHz* centered bandpass filter are presented in Table 6.

Coupler	1st & 7th	2nd & 6th	3rd & 5th	4th
W (mm)	0.2957	1.1099	1.6974	2.1994
S (mm)	0.3396	0.2	0.2512	0.2
L (mm)	2.6	2.4989	2.4045	2.3883

Table 6 - Bandpass filter dimensions with corrections (fc=12 *GHz*)

The schematic for all bandpass filters are similar. Only the number of couplers, lengths, widths and spacing between coupled lines can differ.

5.5.3. 9 GHz centered frequency bandpass filter

The bandpass filter centered at 9 *GHz* is used to filter the carrier. A very narrow bandwidth is required. The problem is to decrease the bandwidth a higher number of stages and bigger gaps are needed leading to higher losses. To minimize this disadvantage and because there are not significant signals behind 9 *GHz* a wider bandwidth will be used and

implemented near 9 *GHz* as observed in Figure 6.16. The dimensions of this narrow filter are presented in Table 7.

Coupler	1st & 5th	2nd & 4th	3rd
W (mm)	1.3513	1.8916	1.9149
S (mm)	0.3337	1.9938	3.0239
L (mm)	3.5334	3.3852	3.3758

Table 7 - Bandpass filter dimensions (fc=9 *GHz*)

5.5.4. 11 GHz centered frequency bandpass filter

This 2 *GHz* bandpass filter needs to have a large attenuation at the stop bands since it stands in the middle of the carrier and the 13 *GHz* centered signal. Thus, using the same procedure as in 5.5.1 plus two more couplers (to produce higher attenuation at the stop bands) the dimensions of the 11 *GHz* centered bandpass filter are represented in Table 8.

Coupler	1st & 9th	2nd & 8th	3rd & 7th	4th&6th	5th
W (mm)	1.0271	1.4651	1.8522	2.2484	0.9368
S (mm)	0.2	0.7783	1.2637	1.3192	2.1437
L (mm)	2.7521	2.6253	2.6253	2.5712	2.8712

Table 8 - Bandpass filter dimensions (fc=11 *GHz*)

The spacing between coupler 1 and 9 was taken to the limit of manufacturability as well as in others microstrip components. Thus, the main cause is the properties of the substrate and the needed response.

After making the same procedures as in 5.5.1 the measurements of the 13 *GHz* centered frequency bandpass filter were achieved as detailed in Table 9.

5.5.5. 13 GHz centered frequency bandpass filter

Coupler	1st & 7th	2nd & 6th	3rd & 5th	4th
W (mm)	0.7901	1.4651	1.6669	1.8737
S (mm)	0.2	0.5388	0.8424	0.8245
L (mm)	2.2225	2.111	2.0704	2.0655

Table 9 - Bandpass filter dimensions (fc=13 *GHz*)

The construction of a 15 *GHz* centered frequency bandpass filter with a desirable bandwidth of 2 *GHz* is also made and its dimensions are present in Table 10.

5.5.6. 15 GHz centered frequency bandpass filter

Coupler	1st & 7th	2nd & 6th	3rd & 5th	4th
W (mm)	0.7111	1.3023	1.8522	1.8737
S (mm)	0.3835	0.7783	0.7783	1.8139
L (mm)	2.0021	1.8092	1.7753	1.7712

Table 10 - Bandpass filter dimensions (fc=15 *GHz*)

Substrate characteristics at these high frequencies are very important, since they determine the dimensions of the microstrip component as well as its realistic behavior. This was taken into account specially when designing the 15 *GHz* and 17 *GHz* centered frequency bandpass filter, which leaded to the values shown in Table 11.

5.5.7. 17 GHz bandpass filter

Coupler	1st & 7th	2nd & 6th	3rd & 5th	4th
W	0.7111	1.3023	1.8522	1.8737
S	0.3835	0.5987	1.1232	1.1543
L	1.6021	1.4091	1.3753	1.3712

Table 11 - Bandpass filter dimensions (fc=17 *GHz*)

The length of the stub is related with the component frequency. At these high frequencies lengths have a higher tendency to shrink as it can be observed in the 16 and 17 *GHz* bandpass centered frequency.

5.6. Power divider

A single stage Wilkinson power divider is considered to work optimally at a single frequency or a relatively small frequency range, this is not the case in the projects where a wide frequency range between 9 *GHz* and 18 *GHz* is considered. In practice, the one stage Wilkinson divider (Figure 3.14) offers a bandwidth of about 10% which means that a center frequency of 12 *GHz* would produce an acceptable return loss between 10.8 and 13.2 which is not acceptable. Ports matching and isolation would not be achieved at certain frequencies. Consequently, a wideband power divider (multistage Wilkinson power divider) should be designed for of 10, 12 and 16 *GHz*.

5.6.1. Power divider at 10 *GHz*

The dimensions for the power divider with center frequency of 10 *GHz* were calculated by ADS tool (Linecalc) and analytically optimized (tuning option) to acquire a desirable response and are presented in Table 12.

Impedance (Ω)	θ (^{0})	Electrical Length	Width (mm)	Length (mm)
$Z_0=50$	360	λ	1.9833	8.106
$\sqrt{2}Z_0=70.71$	90	$\lambda / 4$	0.9896	3.5424

Table 12 - Dimensions of Wilkinson power divider

The ratio of the microstrip curve was introduced to give sufficient space for the resistor implementation. The ratio curve measurements after optimization with ADS tuning tool is 4.49 *mm*.

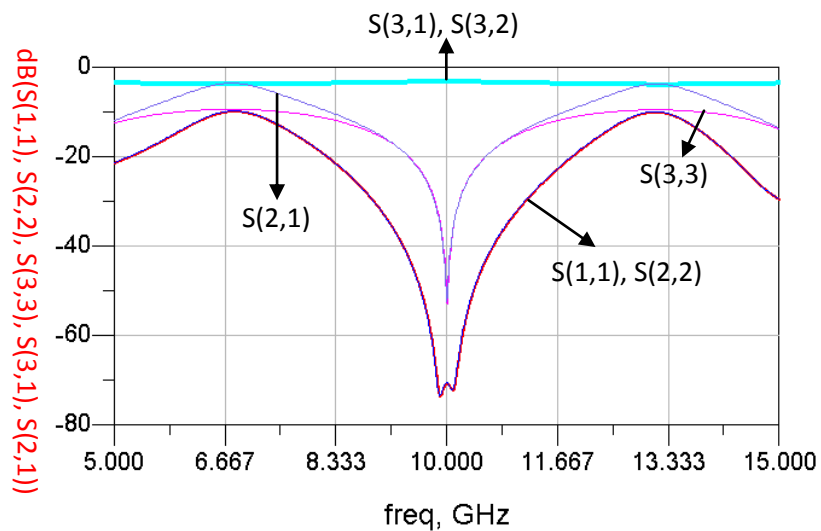The analytical S-parameters simulation is presented in Figure 5.14.

Figure 5.14 - S-parameters of the analytical Wilkinson power divider for 10 *GHz*

This divider has a bandwidth of about 20 %, which indicates an acceptable return loss between 8 *GHz* and 12.5 *GHz*.

5.6.2. Power divider at 12, 14 and 16 *GHz*

The first attempt for power division with the one stage Wilkinson has the measurements presented in Table 13.

Impedance (Ω)	θ (⁰)	Electrical Length	Width (mm)	Length (mm)
$Z_0=50$	360	λ	1.9833	10.8357
$\sqrt{2}Z_0=70.71$	90	λ / 4	0.9896	2.4797

Table 13 - Dimensions of Wilkinson power divider

The component curve ratio has 4 *mm* long.

The S-parameters analysis is performed concerning port matching (S(1,1), S(2,2), S(3,3)), transition, insertion loss (S(3,1),S(3,2)) and isolation S(2,1) around 12 *GHz* as illustrated in Figure 5.15 .
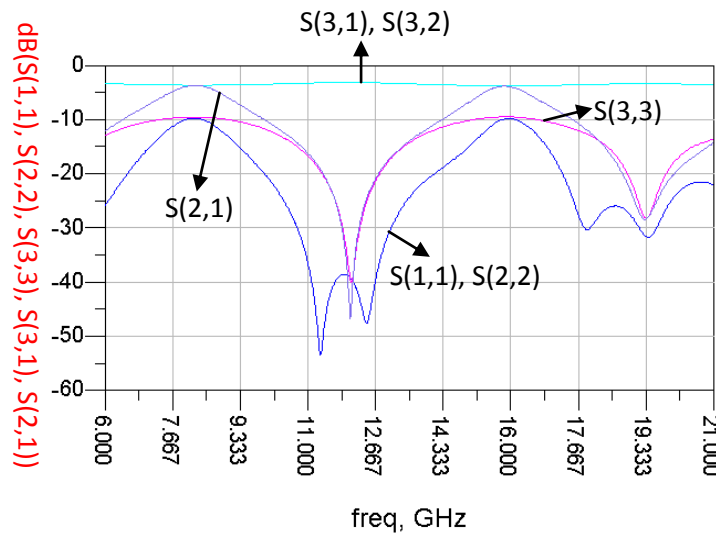
Figure 5.15 - S-parameters of the analytical Wilkinson power divider for 12 *GHz*

Regarding the network architecture (Figure 5.2) these theoretical values are not good because they do not provide the necessary bandwidth.

For a more wideband approach a multistage Wilkinson divider was designed as shown in Figure 5.16.
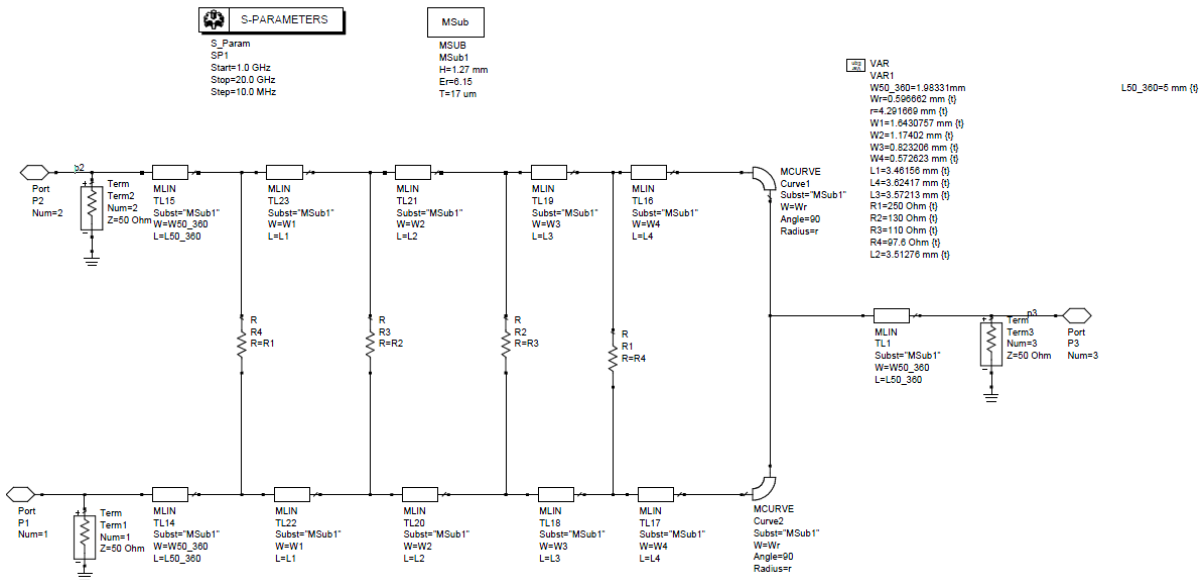
Figure 5.16 - Schematic of the multistage Wilkinson power divider

The architecture is based on the Wilkinson power divider methodology. However due to the length of its branches more resistors must be added due the increase of coupling effects and the isolation decrease. Although the number of sections (lines and resistors) is directly proportional to the bandwidth and inversely proportional to the attenuation, the filter design

has to take into account the filter length. A four section power divider was chosen and the analytical results of the S-parameters are presented in Figure 5.17.
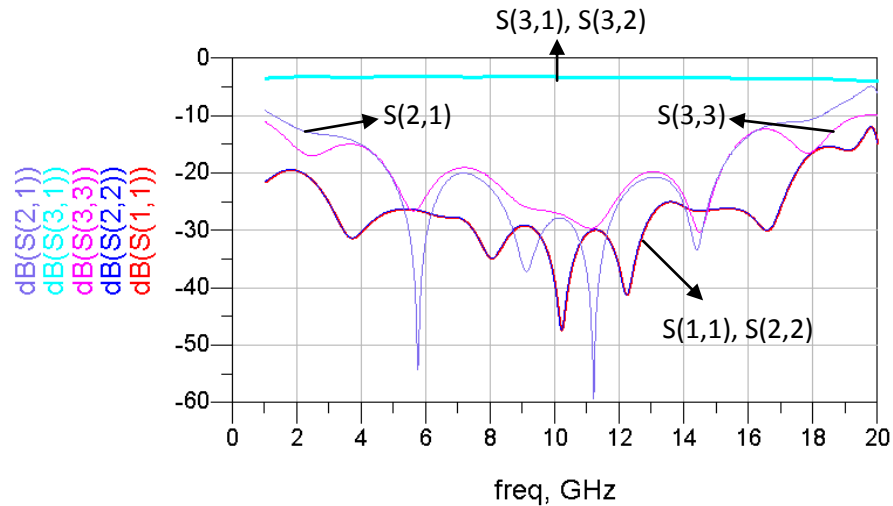
Figure 5.17 - S-parameters analysis of the multistage Wilkinson power divider

The bandwidth achieved with this architecture satisfies the project goals. From 6 *GHz* to 18 *GHz* port matching and isolation are well achieved. Also the power transition is made around 3 *dB* which is not perfect considering the first approach of the project (Figure 5.1) but is a very satisfying result regarding the wideband division scale.

However, in practice, these resistors are not ideal and will introduce distortions to the circuit, therefore some changes have to be made to the multistage Wilkinson power divider as discussed in this section.

5.7. Chapter summary

This chapter discusses filters and power dividers design methodologies. After specifying the desired attenuations and cut-off frequency the appropriate lumped element lowpass prototype is determined. The stepped-impedance method was chosen for the design of the lowpass filter. The design started with a third order lowpass filter. A stub was included in the design to bring the response to zero and the response was optimized in order to achieve a square root raised cosine with a roll-off factor off 0.75.

Parallel coupled lines were used to construct all bandpass filters in this project. Seven bandpass filters were constructed. For each one, fractional bandwidths were calculated, the

order determined, even and odd line impedances for each coupler were resolute and the widths and lengths of line sections were determined.

The power dividers were designed based on the two-way Wilkinson power divider. Due to the larger bandwidth requirements, a multistage Wilkinson power divider was implemented with 4 sections, each one with different optimized resistors for isolation purposes.

[iii] Fractional bandwidth is the bandwidth of a device divided by its center frequency. Example: consider a device that has 5 MHz bandwidth, and his center frequency is at 10MHz, this device will have a fractional bandwidth of $5/10$.

6. Momentum results

6.1. Introduction

This chapter presents the analytical and Momentum results of each microstrip component.

An evaluation of the SRRCOS filter is done by comparing the design response with the ideal one, and by analyzing the respective eye diagrams.

Bandpass filter responses are analyzed, and each 3 *dB* points were measured for performance studies. Power dividers are also tested regarding its S-parameters.

All components were simulated with Momentum due to its efficient and realistic performance in the overall network simulation.

6.2. Lowpass filter

The SRRCOS filter is presented in the following image:
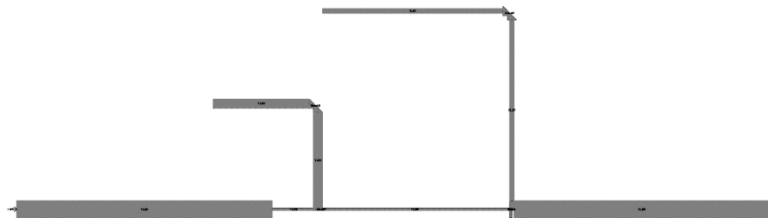
Figure 6.1 - Microstrip SRRCOS lowpass filter Layout

For realistic achievements Momentum simulation is performed. Momentum simulates undesirable effects that can distort the transmitted signals. Figure 6.2 represents the Momentum and analytical results for ideal SRRCOS lowpass filter response with 0.75 roll off factor.
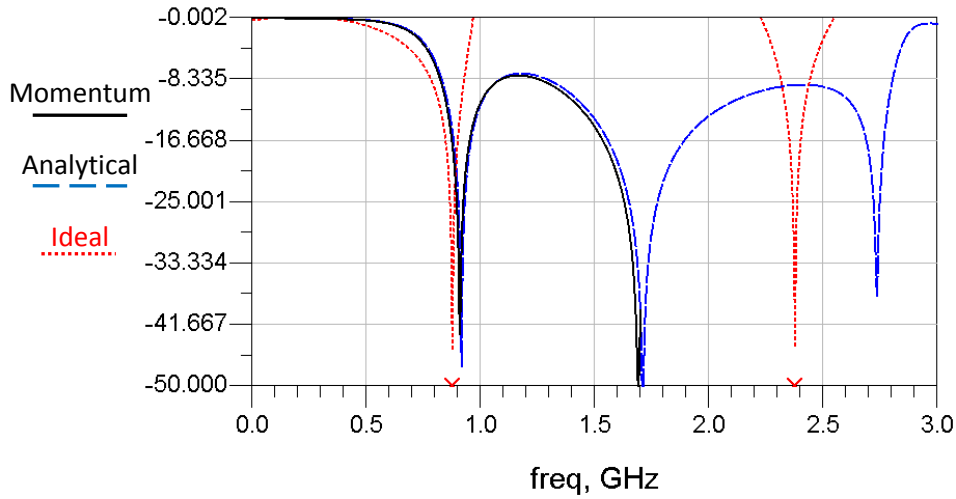
Figure 6.2 - Momentum *dB*(S(1,2)) results for the SRRCOS lowpass filter

The ideal curve is similar to the one designed. Signal distortion is very sensitive regarding the second harmonic of the designed curve. A relation between the first harmonic and the rest of the response had to be made to provide the best result possible.

The Momentum simulation was performed in this device and the response almost did not change regarding the frequencies used, dimensions of transmission lines and substrate chosen.

The S-parameters S(1,1) and S(2,2) are shown in Figure 6.3.
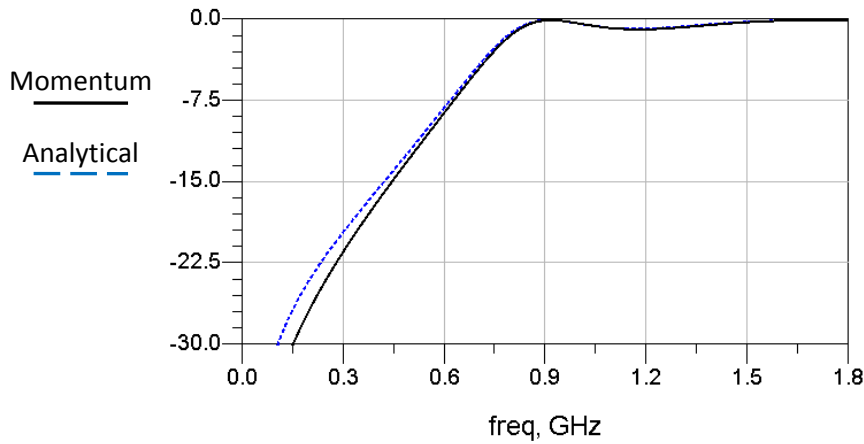
Figure 6.3 - Momentum *db*(S(1,1)) and *db*(S(2,2)) results for the SRRCOS lowpass filter

These results mean that a good matching occurs and a low interference will be expected in the manufactured component.
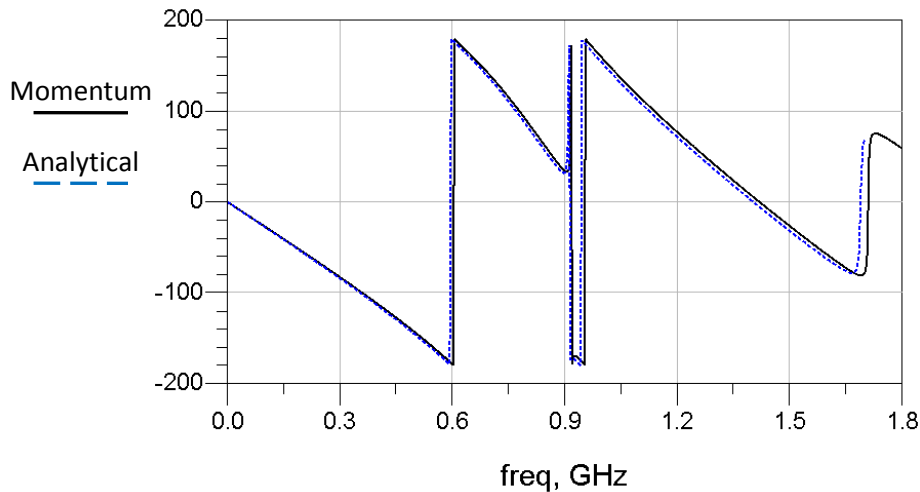
Figure 6.4 - Momentum *dB*(S(1,2)) phase results for the SRRCOS lowpass filter

The phase results confirm that a good signal will be delivered to the output.

For better analysis an eye diagram study was made. The eye diagram is an analysis tool for digital transmission. It evaluates system performance and can offer insight into the nature of channel imperfections [34].

An open eye pattern indicates minimal signal distortion. The eye closure is directly proportional to the distortion of the signal waveform (due to inter-symbol interference and noise) [35].

Thus, an eye diagram was visualized regarding an input data of 128 random bits and a time step of 0.128 during 100ns. The schematic of an ideal eye diagram with 0.75 roll off factor filtering random input data is showed in Figure 6.5 and the respective eye diagram illustrated in Figure 6.6.
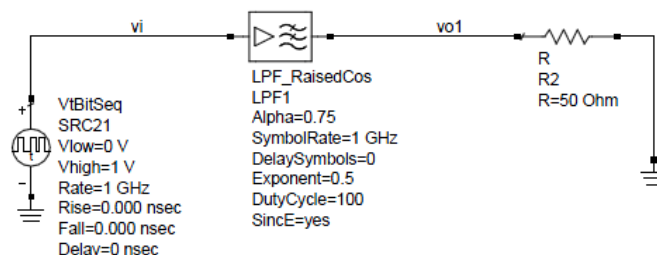
Figure 6.5 - Ideal schematic of the SRRCOS filter
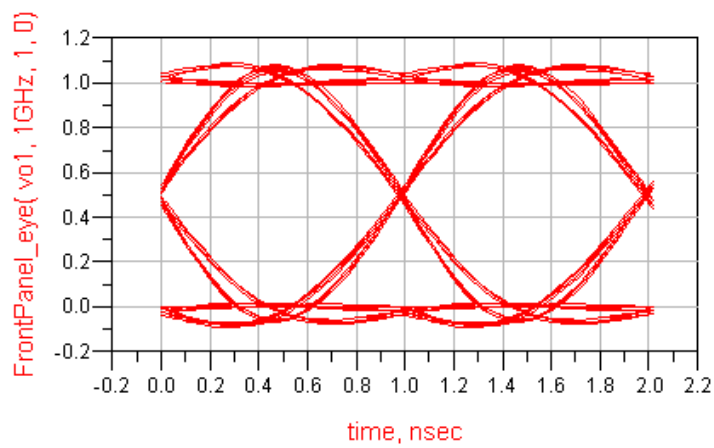
Figure 6.6 - Eye diagram of the ideal raised cosine filter

The schematic used for the practical approach is exactly like the ideal one except the designed filter component, as illustrated in Figure 6.7.
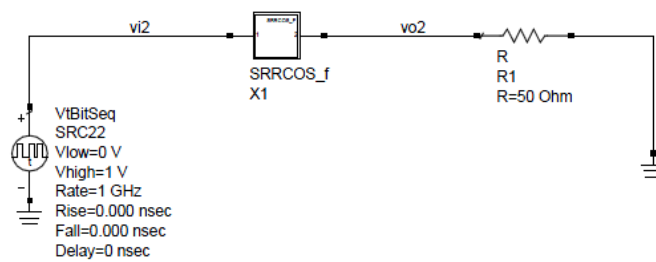

Figure 6.7 - Designed schematic of the SRRCOS filter

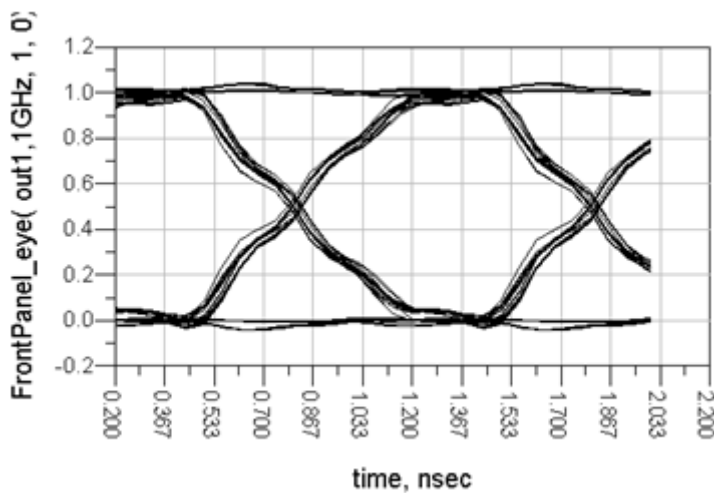The eye diagram of the designed SRRCOS lowpass filter is represented in Figure 6.8.

Figure 6.8 - Eye diagram of the designed raised cosine filter

This eye diagram has been achieved after a new optimization. Using the tuning tool and looking at the shape of the output filtered data the best resemblance was found. The solid line curve in Figure 6.2 represents the adapted response when compared to the ideal one. The second harmonic is the biggest problem in this design. The ideal achievement would consist on eliminating everything beyond 0.875, however it is not possible with microstrip technology, so the best relation between equivalence to the ideal response and well shaped output data had to be found.

The correspondent Momentum eye diagram after shaping the random binary sequence is presented in Figure 6.9.
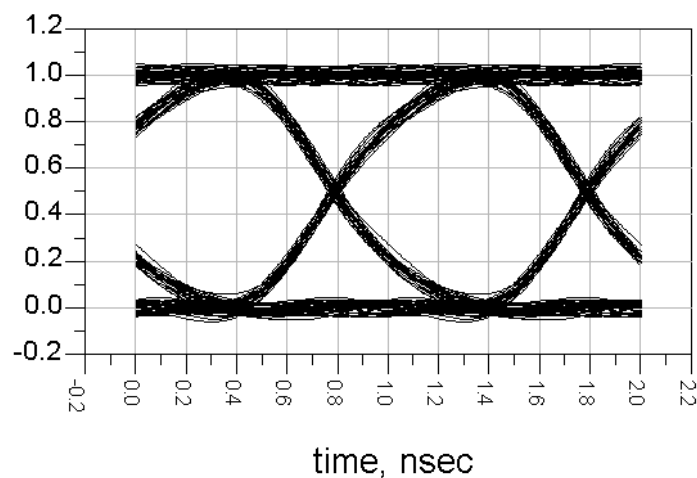
Figure 6.9 - Momentum eye diagram of the shaped pulses.

Momentum simulation improved the shape of the testing data because it caused more attenuation to the second and third harmonics of the filter response.

6.3. Bandpass filter

All the bandpass filters designs in the projected were simulated in Momentum and its responses compared to the analytical design although what matters most is the Momentum results due the credibility of its calculations.

6.3.1. 12 *GHz*

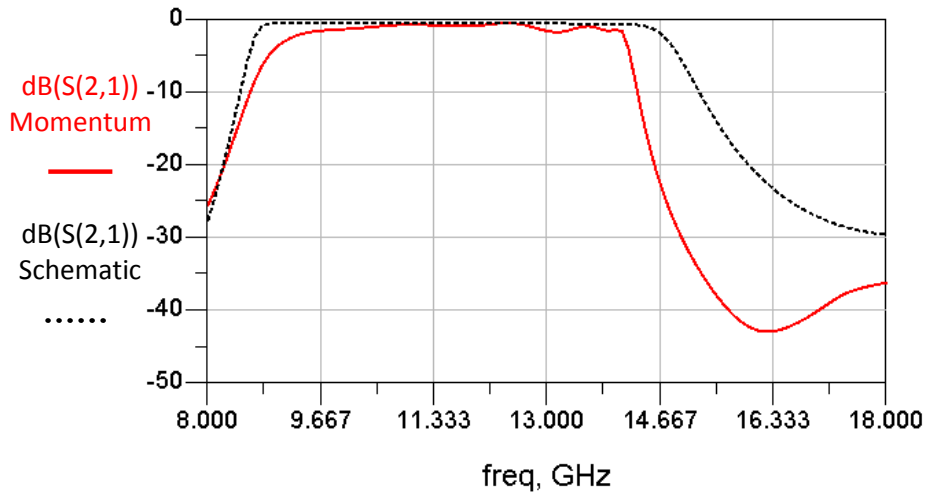Momentum simulation results for the 12 *GHz* centered frequency bandpass filter is presented in Figure 6.10.

Figure 6.10 - S(1,2) *dB* of 12 *GHz* bandpass filter (Schematic Vs Momentum)

Figure 6.10 analysis reveals an acceptable bandwidth between 8.6 *GHz* and 14.3 *GHz*. The wider analytical result was deliberately introduced regarding the Momentum tendency for narrowing the bandpass filters. Thus, after 14 *GHz* the response quickly turns to zero.

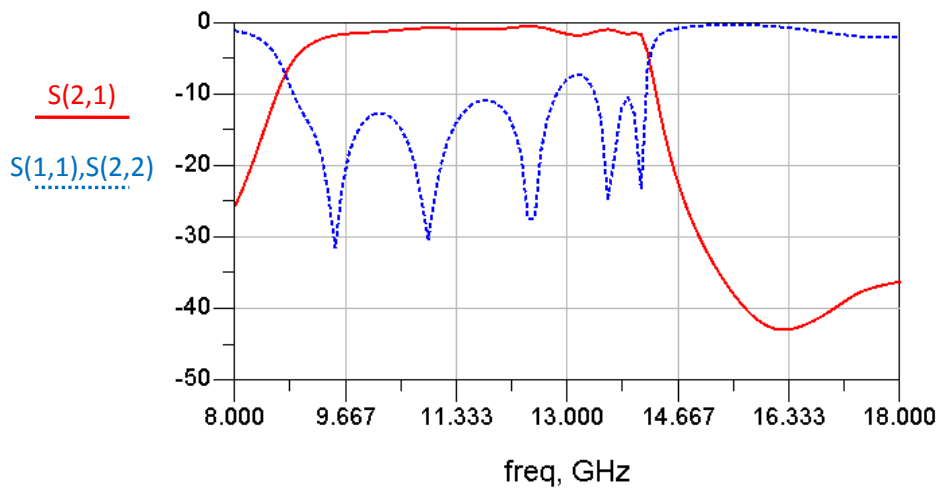Port matching between input and output ports (S(1,1) and S(2,2)) is also studied and presented in Figure 6.11.

Figure 6.11 - Port matching and Insertion loss analysis (12 *GHz* centered filter)

A good transition and port matching is achieved between the input and the output port.

The layout of the bandpass filter with dimensions presented in Table 6 is represented in Figure 6.12.
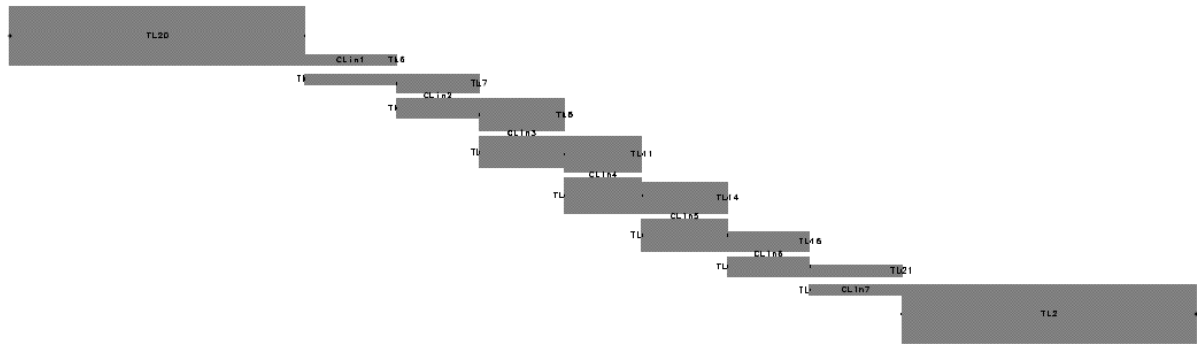
Figure 6.12 - 12 *GHz* centered frequency bandpass filter Layout

Small gaps are observed in this type of filter due to its high bandwidth of 5.5 *GHz*. The longest lines are the input 50 Ω characteristics impedances and the smaller ones correspond to the coupled lines that produce the bandpass response.

6.3.2. 16 *GHz*

The analysis of the 16 *GHz* bandpass filter was done by comparing the analytical response to the Momentum response. The equivalences are shown in Figure 6.13.
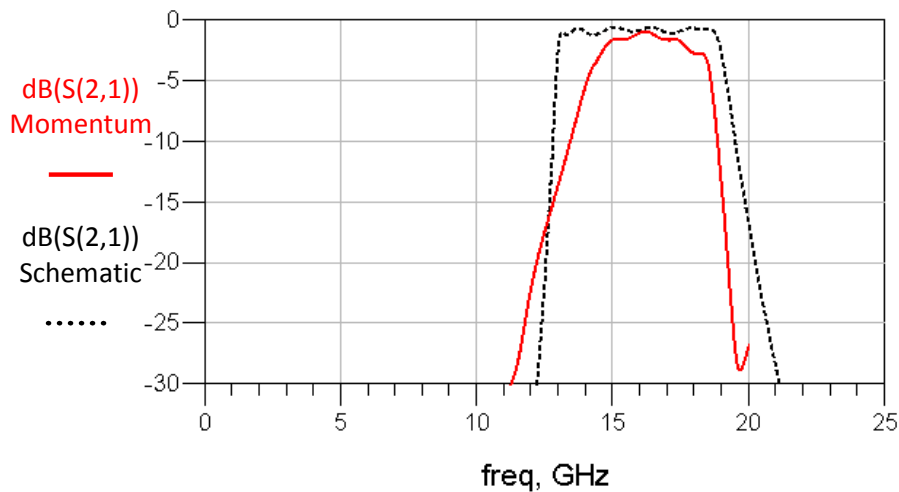

Figure 6.13 - S(1,2) *dB* of 16 *GHz* bandpass filter (Schematic Vs Momentum)

A satisfying portion of bandwidth is achieved after Momentum analysis is made.

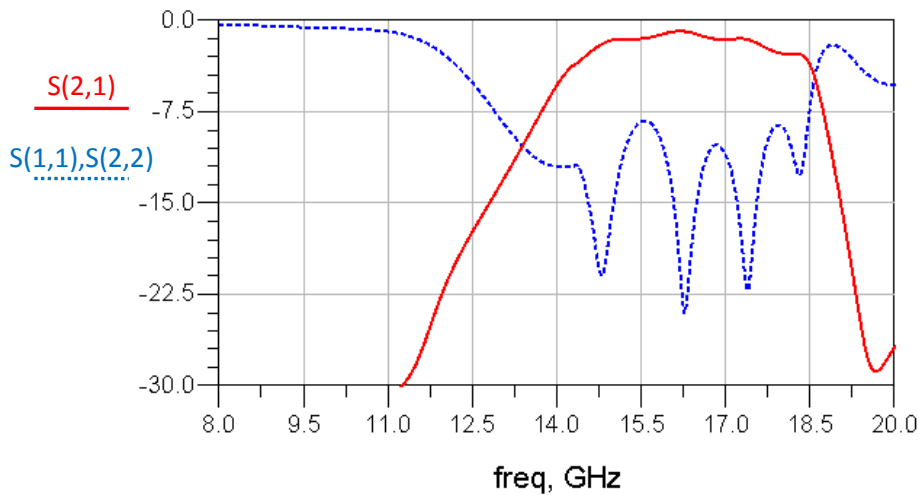The reflected waves are also studied and represented in Figure 6.14.

Figure 6.14 - Port matching and Insertion loss analysis (16 *GHz* centered filter)

It reveals a good isolation achievement in the input and output ports.

In the schematic and in the layout there are some components that need to be implemented in order to acquire a desirable response. These components (MLEF) line up the coupled lines and prevent changes in width discontinuities, which at these frequencies can damage the entire signal. The widths linearity is shown in Figure 6.15.
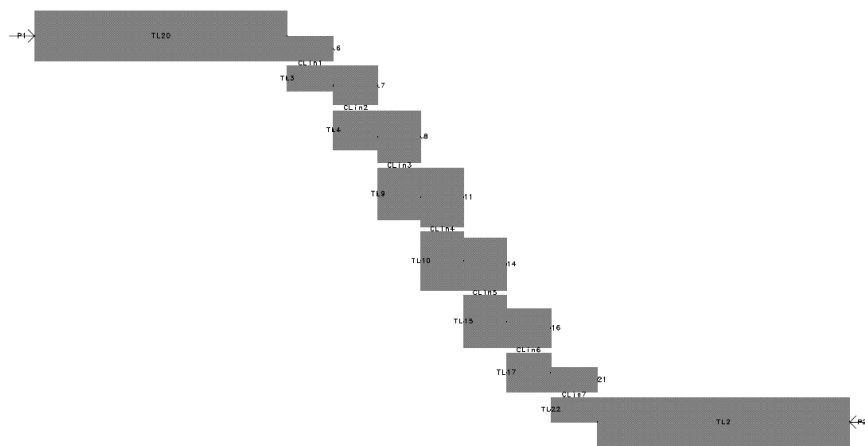

Figure 6.15 - Layout of the bandpass filter with f$_c$=16 *GHz*

The gap between the coupled lines still remains very low because of the high bandwidth that must be achieved by filter.

6.3.3. 9 *GHz*

The 9 *GHz* centered bandpass filter was performed in several interactions. This filter was supposed to be very narrow, however in microstrip technology this is a very difficult task to achieve especially if frequencies and the substrate thickness are high. Thus a design has

been made with a wider bandwidth once the spectrum at frequencies lower than 9 *GHz* does not have data to consider. The Momentum analysis of the bandpass filter to capture the carrier is illustrated in Figure 6.16.
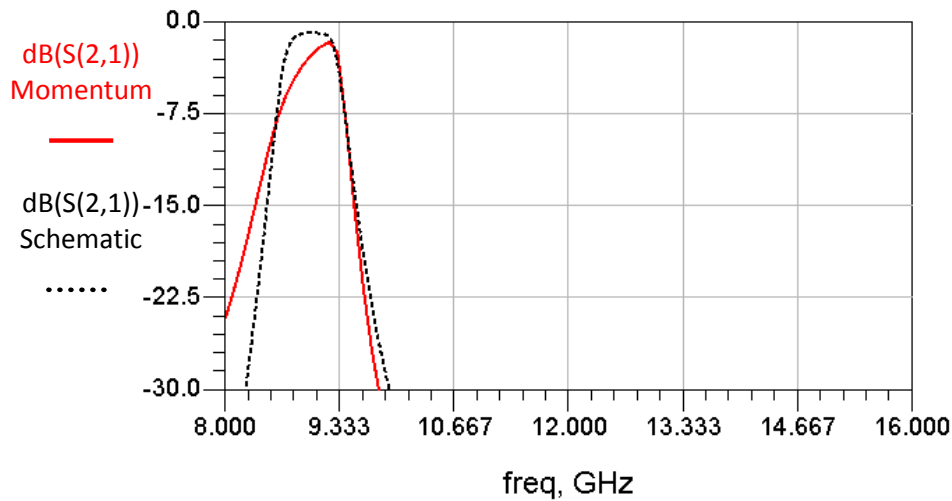

Figure 6.16 - S(1,2) *dB* of 9 *GHz* bandpass filter (Schematic Vs Momentum)

The study regarding the S-parameters S(1,1) and S(2,2) is also made and presented in Figure 6.17.
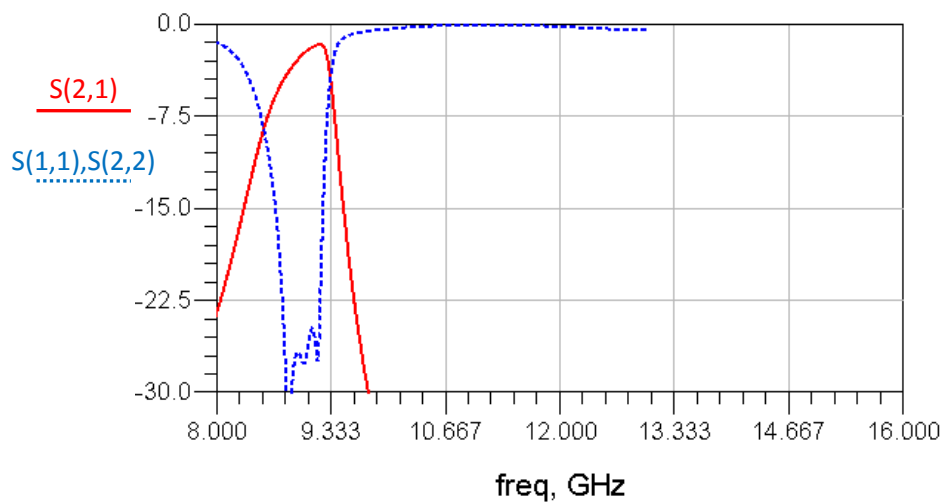

Figure 6.17 - Port matching and Insertion loss analysis (9 *GHz* centered filter)

Figure 6.17 reveals that when the carrier is captured (9 *GHz*) no significant interference in the input and output ports exists.

The layout of the 9 *GHZ* centred frequency bandpass filter is shown in Figure 6.18.

Figure 6.18 - Layout of the bandpass filter with f_c=9 *GHz*

In this layout the bandwidth is notorious smaller than the others bandpass filters. This can be seen by looking at the existing space between the coupled lines. However, this implicates higher attenuation in the signal as discussed before.

6.3.4. 11 *GHz*

The bandpass filter with center frequency at 11 *GHz* was also analyzed by Momentum. The results of this analysis are present in Figure 6.19.
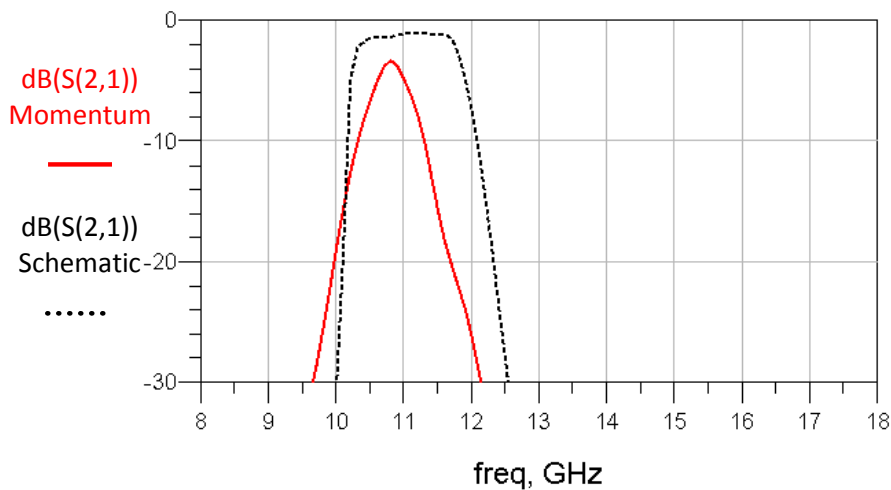

Figure 6.19 – 11 *GHz* centred bandpass filter (Schematic Vs Momentum)

This filter had to be designed with a very high attenuation at the cut off frequency points because it stands in the middle of the carrier and the 13 *GHz* centered signal.
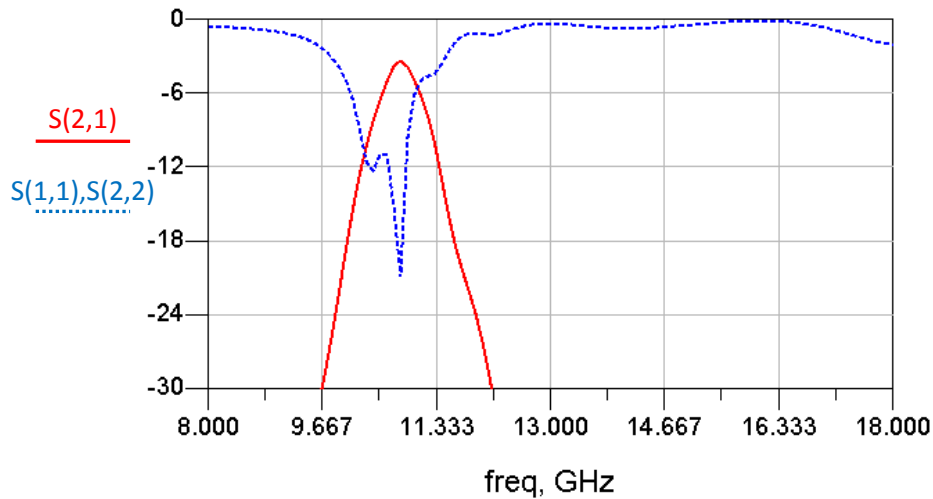
Port matching is also studied in Figure 6.20.

Figure 6.20 - Port matching and Insertion loss analysis (11 *GHz* centered filter)

The relation between the filter attenuation and port matching is less than ideal, however, it still provides a satisfactory isolation in the input and output ports regarding the reflected waves in the transmission lines.

Once again the coupling is very linear as it can be seen by Figure 6.21.
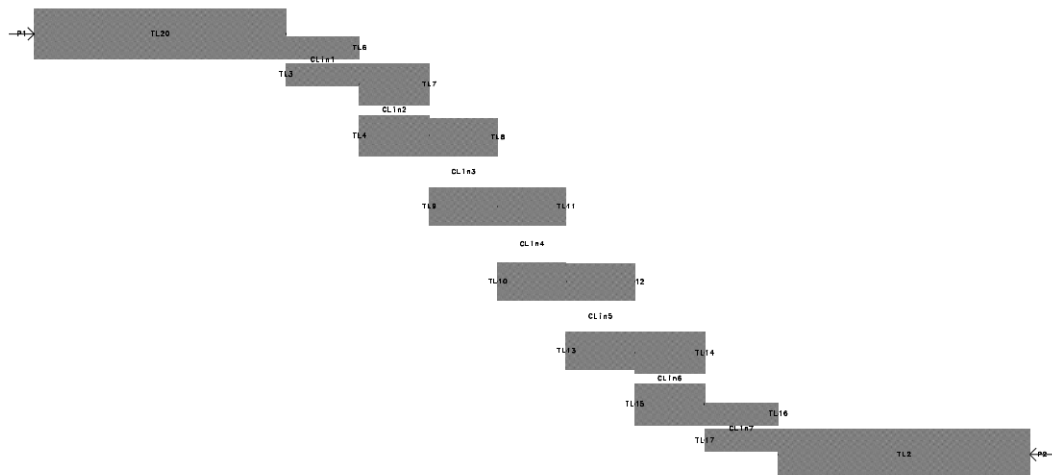

Figure 6.21 - Layout of the bandpass filter with f$_c$=11 *GHz*

The linearity is produced by the MLEF component. Without this component this optimization would be done in Momentum by dislocating each section to the correct place.

6.3.5. 13 *GHz*

At 13 *GHz* the Momentum and analytical responses are compared in Figure 6.22.
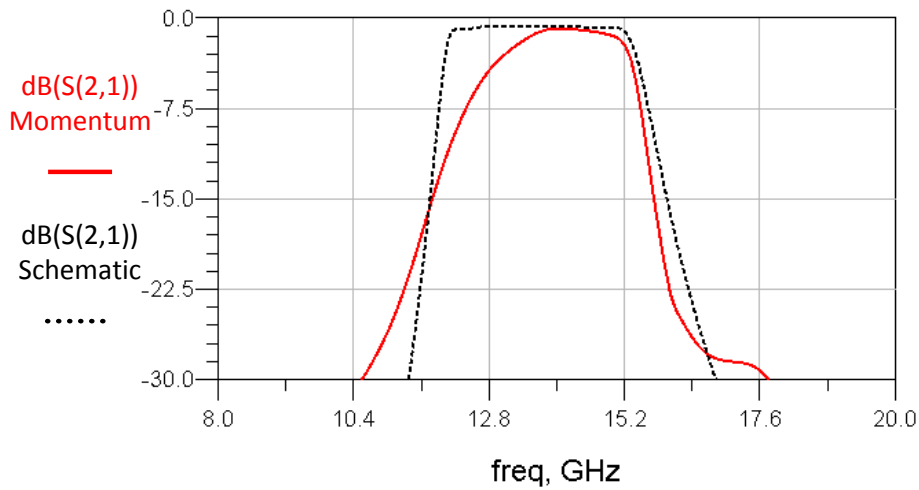
Figure 6.22 - S(1,2) *dB* of 13 *GHz* bandpass filter (Schematic Vs Momentum)

The response has the desirable bandwidth and attenuation at the stop bands and at the pass band.

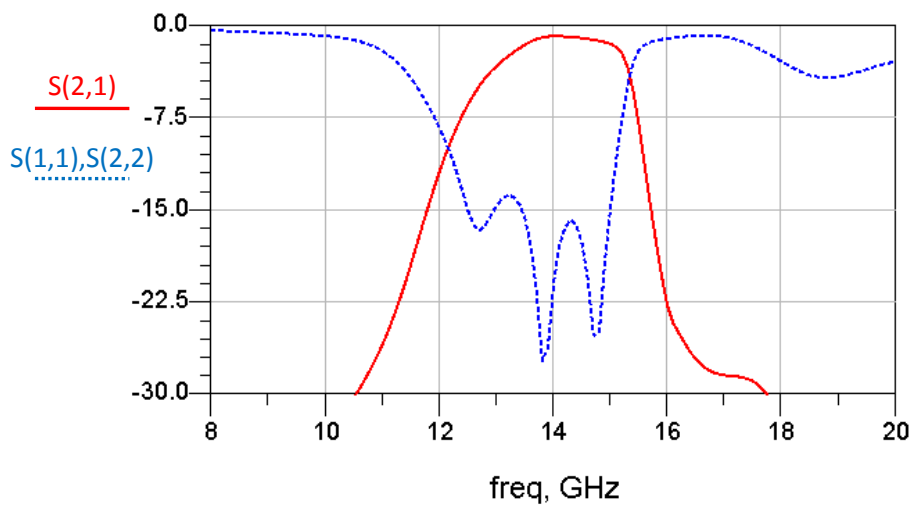Reflected transmission waves are taken into account as shown in Figure 6.23.

Figure 6.23 - Port matching and Insertion loss analysis (13 *GHz* centered filter)

Port matching is successfully implemented in the 13 *GHz* centered filter. No interference will occur at the desirable pass band frequencies.

The layout appearance is introduced in Figure 6.24. Linearity and small spaces between coupled lines are once again observed.
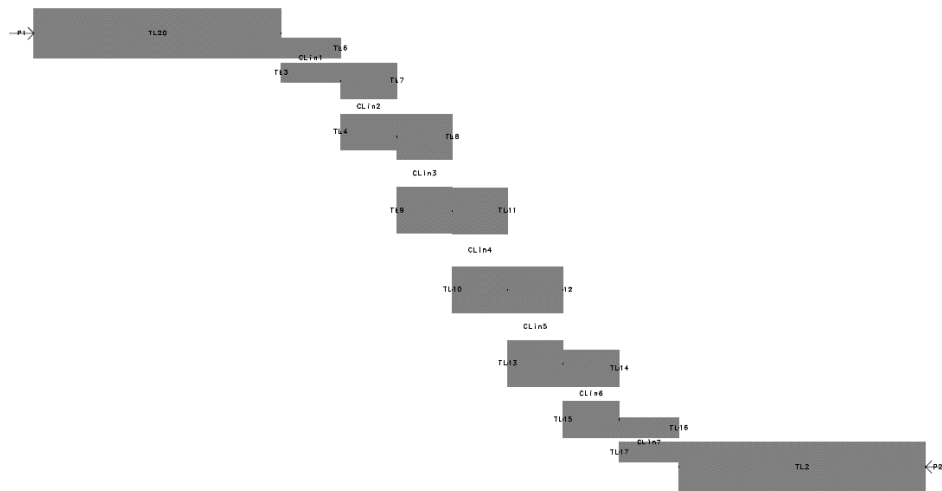
Figure 6.24 - Layout of the bandpass filter with f$_c$=13 *GHz*

6.3.6. 15 *GHz*

As frequency increases Momentum computation becomes harder and it takes longer to simulate the components. In addition, differences between the analytical and Momentum designs are more common, so several designs were made and simulated to achieve a desirable response. The 15 *GHz* centered frequency response is compared in Figure 6.25.
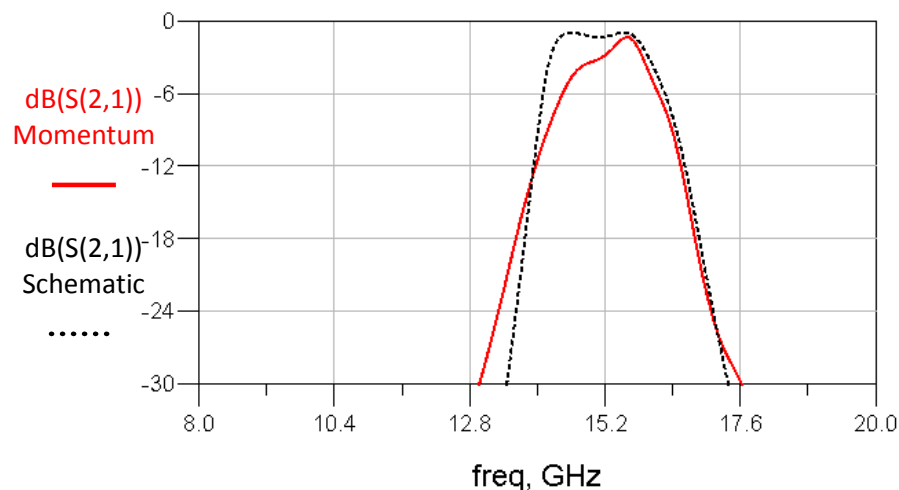

Figure 6.25 - S(1,2) *dB* of 15 *GHz* bandpass filter (Schematic Vs Momentum)

The upper stop band has low interference with the 17 *GHz* centred signal and the lower stop band has the influence of the preliminary filters introduced in the network to ease the filtering achievement, so a good filtering is accomplished.

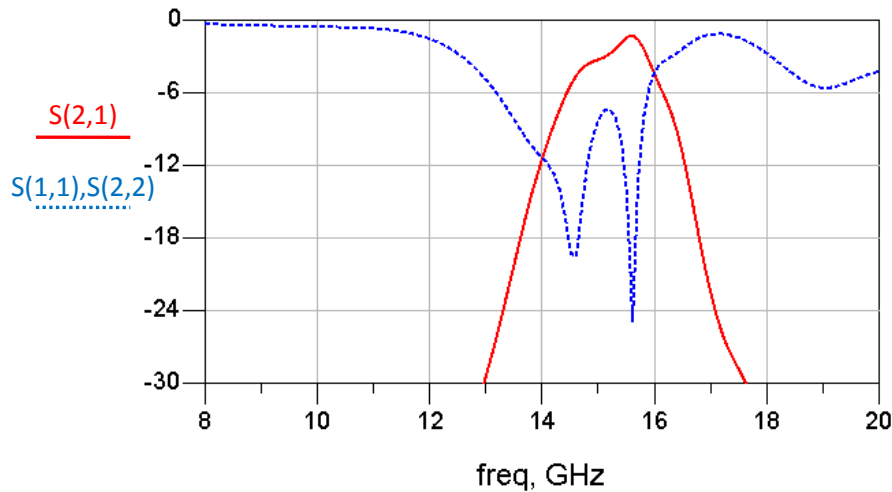Port matching is represented in Figure 6.26.

Figure 6.26 - Port matching and Insertion loss analysis (15 *GHz* centered filter)

From 14 *GHz* to 16 *GHz* little interference is observed by the reflected waves improving the transmission quality.

The respective layout is showed in Figure 6.27.

Figure 6.27 - Layout of the bandpass filter with f$_c$=15 *GHz*
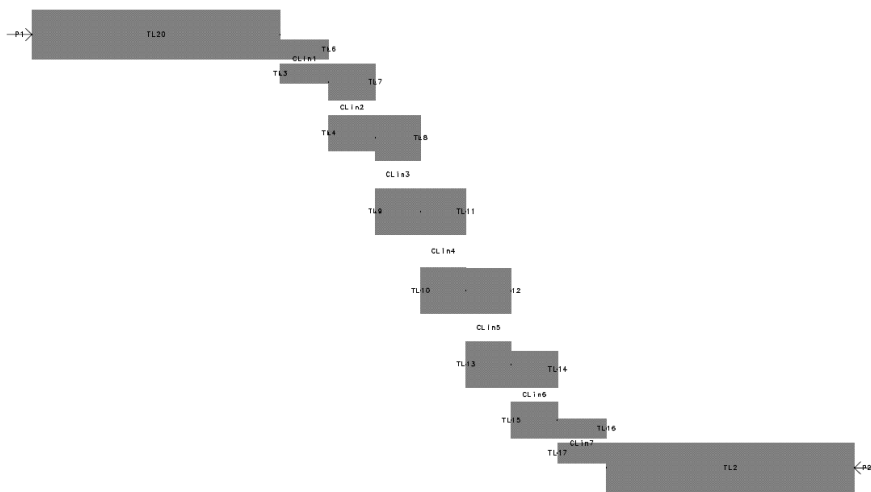
It is notary the coupler spacing of this filter regarding the wideband and narrowest filters as well as the attenuation induced by these components. As the needed bandwidth enlarges the spacing between coupled lines becomes smaller and the attenuation lower.

6.3.7. 17 *GHz*

The 17 *GHz* cantered frequency bandpass filter results are shown in Figure 6.28.
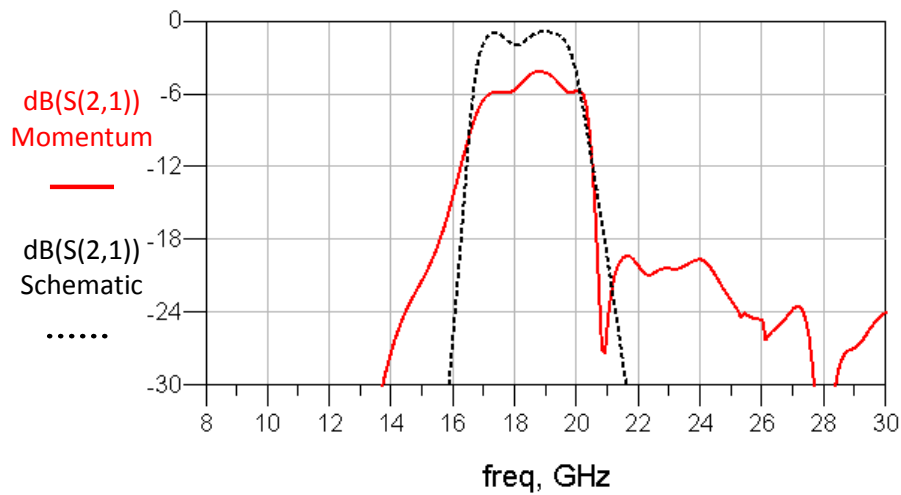
Figure 6.28 - S(1,2) *dB* of 17 *GHz* bandpass filter (Schematic Vs Momentum)

Figure 6.28 shows that the filter induces a high attenuation regarding all other designed filters, however the difference is not relevant once a lower interference between adjacent channels is satisfied.

The reflected waves take the form illustrated in Figure 6.29.

Figure 6.29 - Port matching and Insertion loss analysis (17 *GHz* centered filter)

Thus, from 16.4 *GHz* to 19.8 *GHz* a good port matching is satisfied.

The layout is similar to the previous bandpass filter and is presented in Figure 6.30.
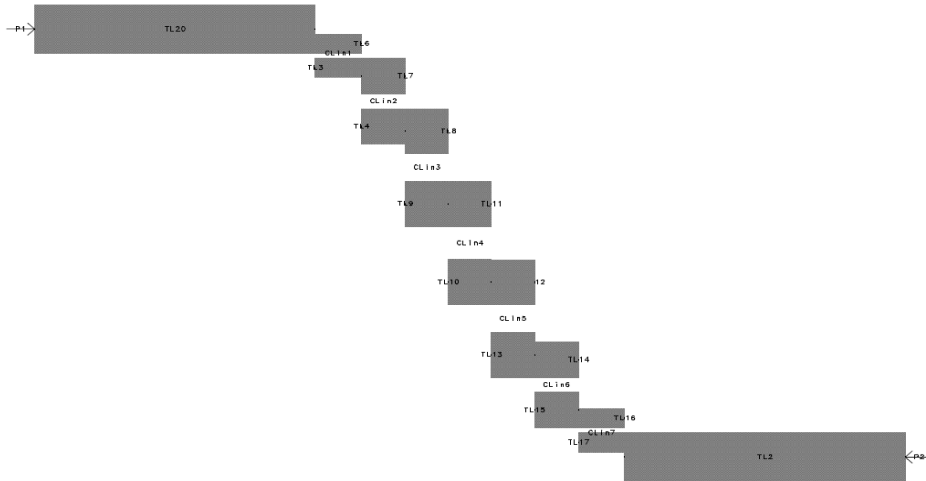
Figure 6.30 - Layout of the bandpass filter with f$_c$=17 *GHz*
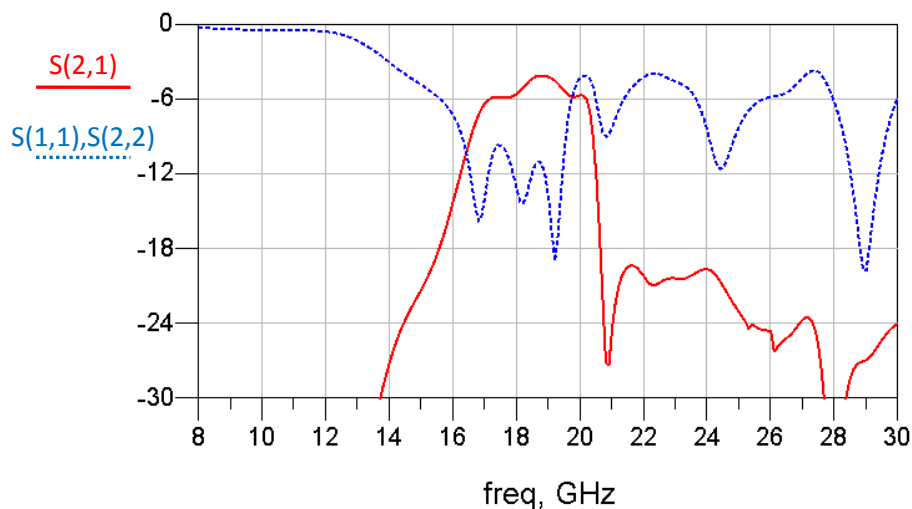
6.4. Power Divider

6.4.1. 10 *GHz*

This 10 *GHz* power divider is supposed to work at 9 *GHz* and 11 *GHz*.

The Electromagnetic-Circuit co-simulation feature of ADS allows the combination of Momentum and circuit simulations from the schematic. Basically, it allows the insertion of a layout component in a schematic.

To run an EM simulation together with circuit components a layout lookalike component from the Momentum structure must be created and placed in the schematic where the rest of the circuit components will be added as illustrated in Figure 6.31.
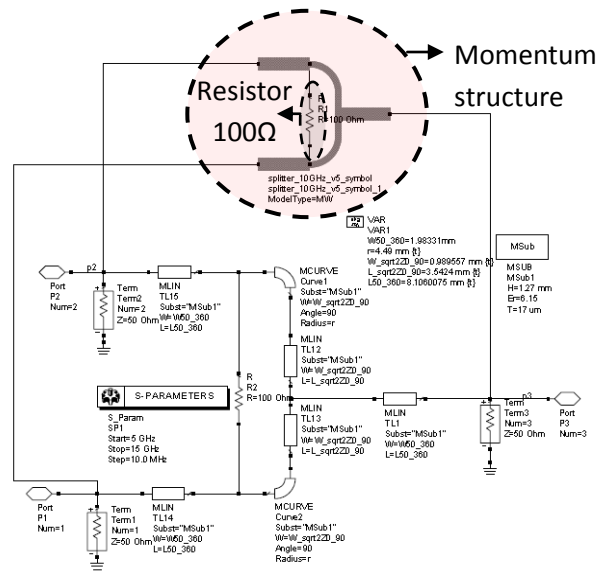
Figure 6.31 - Co-simulation of 10 *GHz* power divider

Thus port matching (S(1,1), S(2,2), S(3,3)), transition, insertion loss (S(3,1),S(3,2)) and isolation S(2,1) are the S-parameters that will be analyzed. At 10 *GHz*, the power divider S-parameters are present in Figure 6.32.
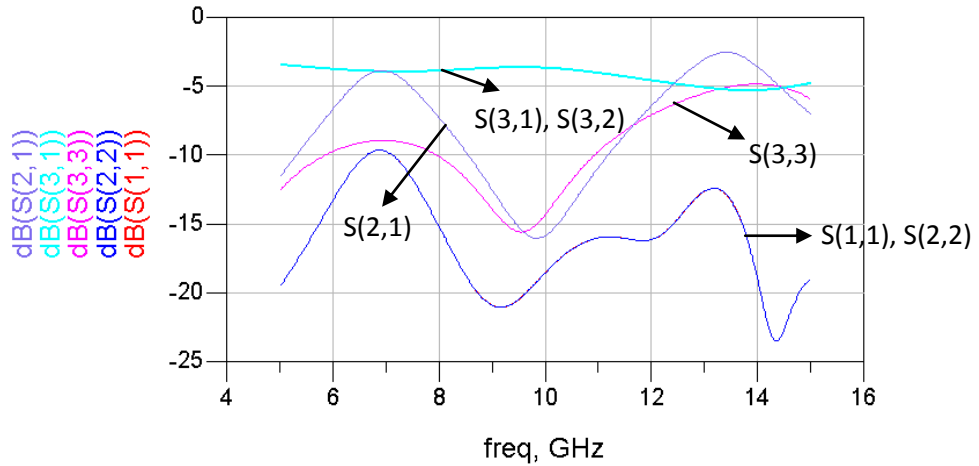
Figure 6.32 - S-parameters of the designed Wilkinson power divider for 10 *GHz*

This reveals a good attenuation regarding port matching and isolation issues. However the resistor simulated is an ideal one and not a thin film resistor properly simulated.

6.4.2. 12 *GHz*, 14 *GHz* and 16 *GHz*

The co-simulation for the multistage Wilkinson power divider is illustrated in Figure 6.33.

Figure 6.33 - Layout of the multistage Wilkinson power divider

This power divider has (28.5x10.5) *mm* length which is an acceptable size for a project component. Each change in width represents a new section where t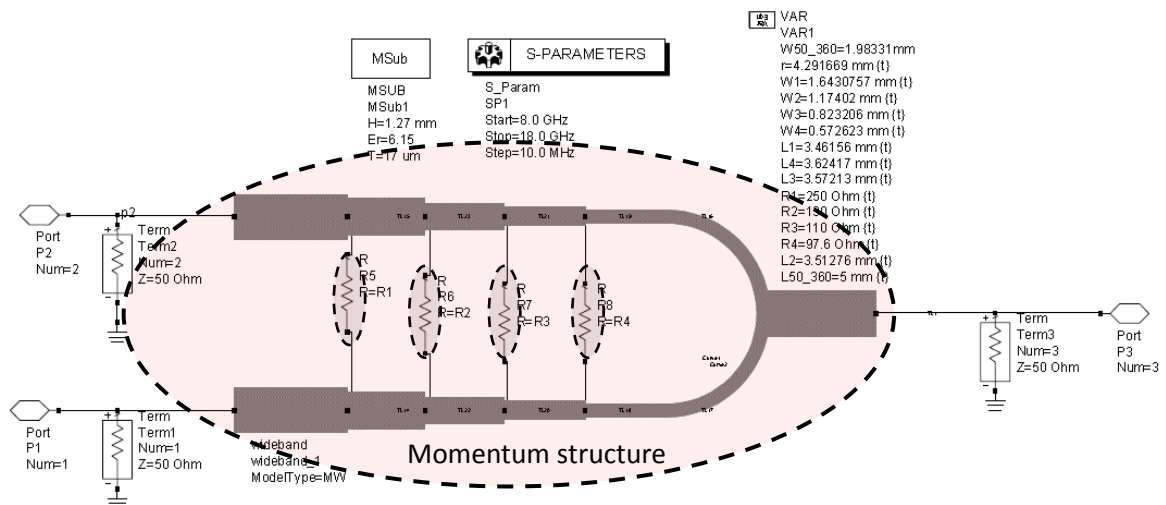he isolation resistor is implemented. From R_4 to R_1 the coupling between the output transmission lines becomes greater so the resistors need to compensate this effect be raising its values.

The co-simulation results for these Wideband power dividers are shown in Figure 6.34.
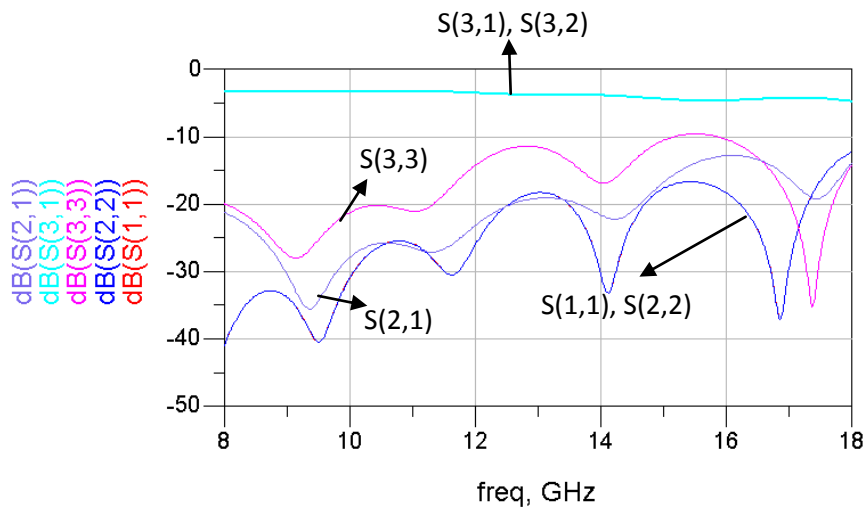
Figure 6.34 - Momentum S-parameters results without resistors

The S-parameters reveals acceptable insertion loss, port matching and isolation at higher frequencies and very good results at lower frequencies. Port matching and isolation are improved when resistors are added as seen in Figure 6.33. For better results a substrate with a thickness less than 1.27 *mm* would be required.

In practice the thin film resistors will be used to provide the required isolation. These components may introduce degradation in the signal if accompanied with connecting stubs, or if their dimensions are greater than it should be.   One other issue is the smoothness of the output transmission lines that may cause undesirable interferences in the output signal. Thus, an incorporated thin film resistor in a Momentum structure based on the multistage Wilkinson power divider is implemented as illustrated in Figure 6.35.
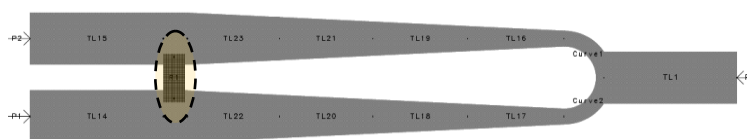
Figure 6.35 - Power divider with thin film resistor

The output transmission lines were brought together with sufficient space between them to allow the connection of a 10 *KΩ* thin film resistor with a length of 1.6 *mm* and width of 0.8 *mm* without signal degradation. More than one resistor would produce undesirable distortions due to the significant dimension of these components.

The S-parameters of the designed power divider are presented in Figure 6.36.
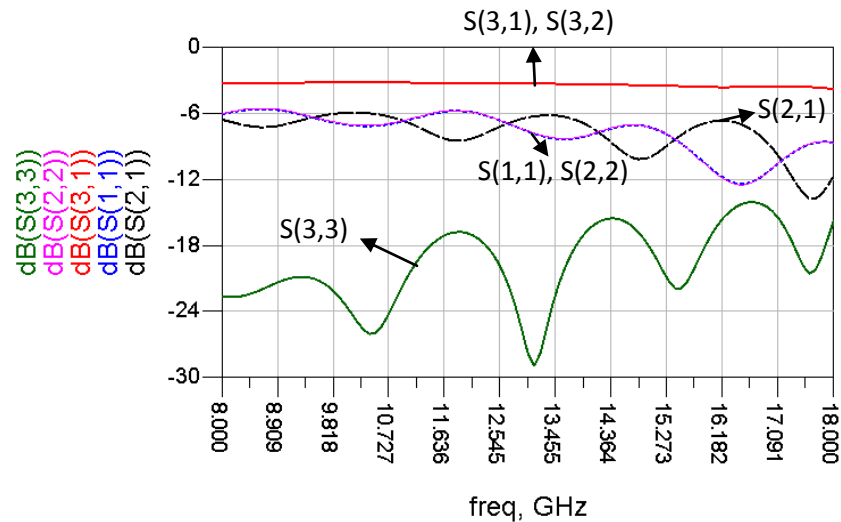
Figure 6.36 - Momentum simulation results of the power divider with a 10 *KΩ* thin film resistor

A good transition is made between the output ports as described in Figure 6.36. Transmission data at 11 *GHz* and 15 *GHz* can take a small disadvantage of this divider regarding isolation issues (S(2,1)), however it is almost insignificant.

The Momentum results of the power divider are tested as seen in Figure 6.37.
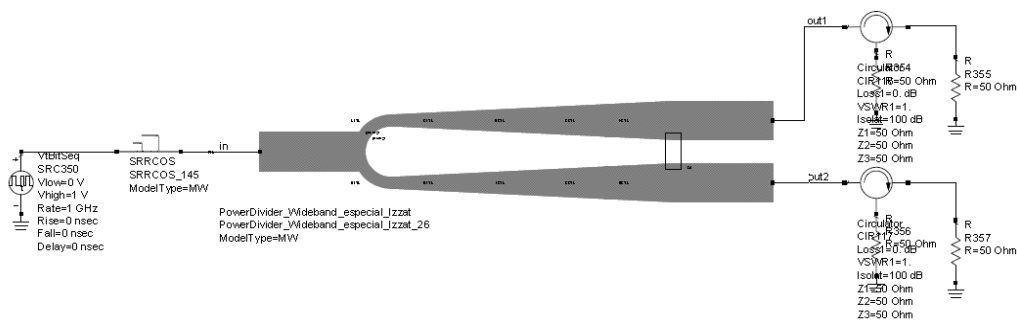
Figure 6.37 - Testing schematic of the designed power divider

The generated random data is filtered by the design SRRCOS lowpass filter and then equally divided to the two output ports. This structure provides the result illustrated in Figure 6.38.
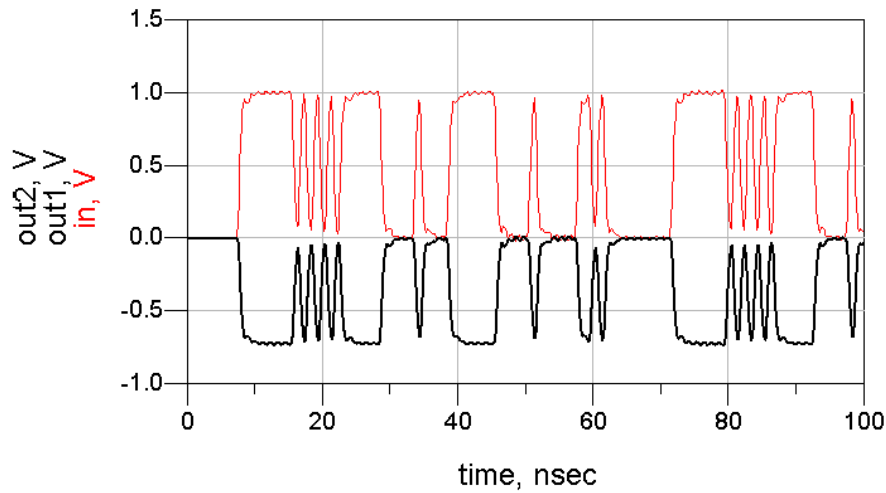
Figure 6.38 - Power divider outputs

Power is divided and inverted to each of the output ports. The inversion can be seen in the output/input port phase analysis. Between 12.5 *GHz* and 13 *GHz* it is expected a 180 phase shifting as seen in Figure 6.39.

Figure 6.39 - Power divider phase analysis

As observed in the Momentum analysis this divider has a good behaviour regarding isolation, port matching and insertion loss so a good performance is expected for this component.

Only this transient analysis would be insufficient and unrealizable after the products been manufactured.

6.5. Chapter summary

The equivalence between the SRRCOS filter response and the ideal filter is notary. The amplitude of the second harmonic is very important for the transmission quality, so the curve equivalence was carefully designed.

The stub revealed to be a fundamental part of the lowpass filter construction, as well as essential in the equalization of the two responses (Ideal and designed).

Bandpass filters were designed for each specific frequency. When higher frequencies are used the design becomes more difficult to achieve, i.e. the Momentum simulation distorts more at high frequencies as in the lower ones. This distortion is provoked by differences in the wavelengths of each frequency, so a lower wavelength means higher number of subdivisions in the mesh analysis and longer simulation time, thus with a good control of the dielectric constant, height and width of the transmission lines, distortion can be decreased.

The power splitter used in the dissertation was based on the Wilkinson power divider. Wilkinson divider is considered to work optimally at a single frequency or a relatively small frequency. Although a single splitter would work at multiples of a quarter-wave, at higher frequencies like above 15 *GHz* higher order modes would start to appear as well as substrate and space radiation. So, an analysis of the analytical S-parameters of these devices was done and compared with Momentum S-parameters results. Concluding that a new approach had to be made that took into account the inaccuracy of the resistors and the large bandwidth interval. After generating a regular multistage Wilkinson power divider the output transmission lines were smooth and only one resistor (thin film) was implemented at end of the power divider.

7. System simulation with the Designed Microstrip components

7.1. Introduction

In this chapter the performance evaluation of the RoFnet base station downlink base was done. Figure 7.1 represents the overall simulation.

7.2. Network Microstrip components
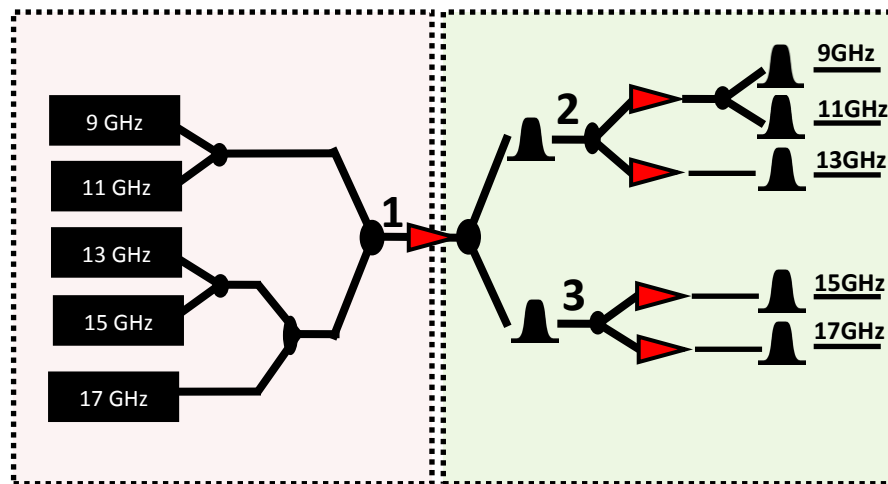
Figure 7.1 - Overall simulation

Each black box in Figure 7.1 represents a high frequency data channel. Each high frequency data channel consists on a random bit sequence that is filtered by the SRRCOS lowpass filter and modulated with BPSK format (binary phase shift keying) in a specific frequency as illustrated in Figure 7.2.
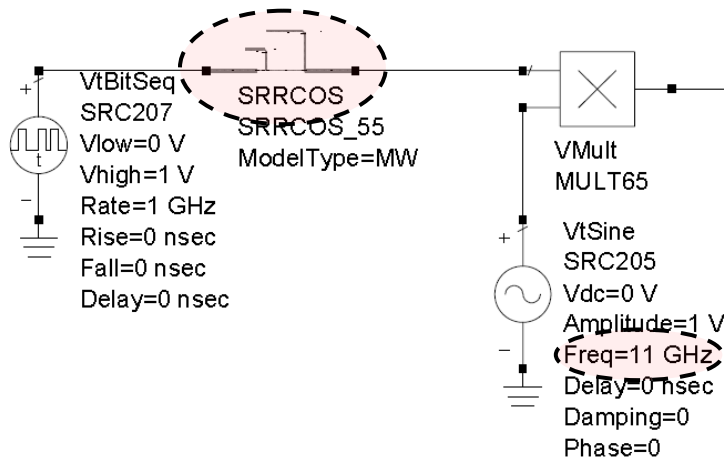
Figure 7.2 - Frequency shifting description

In order to provide a more realistic approach it has been included the Momentum results of the SRRCOS lowpass, bandpass and power divider components as well as the noise figure of the amplifiers.

The random bit sequence present in Figure 7.2 is shaped by the SRRCOS filter as showed in Figure 7.3.
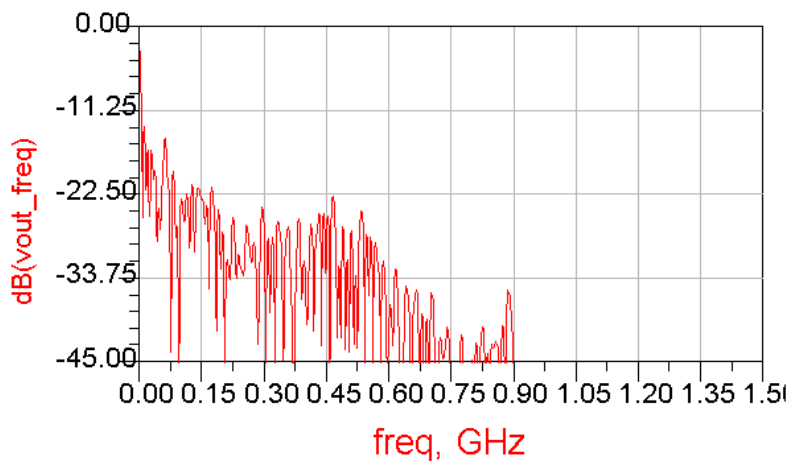
Figure 7.3 - SRRCOS filter shaped data

Results only appear till 0.9 *GHz* due to the roll off factor implemented ($\alpha=0.75$). Figure 7.4 represents all frequencies used in the project downlink channel. This spectrum refers to point 1 of Figure 7.1.
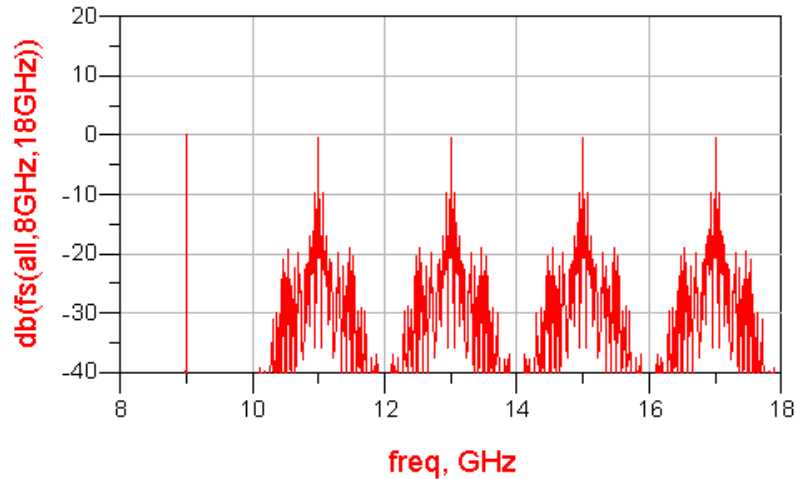
Figure 7.4 - Spectrum of all downlink channel frequencies

The signal is then splitted and amplified to compensate the attenuation imposed by the previous components. The amplifier has 20 *dB* gain, noise figure of 2 *dB* and 50 Ω matched input impedance. The splitter used is the wideband power divider based on the multistage Wilkinson power divider.

At point 2 and 3 (see Figure 7.1) the signal is divided by two outputs. Point 2 has been submitted to a bandpass filter with a centred frequency of 12 *GHz* and 5.5 *GHz* bandwidth and point 3 with a bandpass filter that only allows frequencies between 14 and 18 *GHz*. These two components were combined and tested as one single device, in order to minimize the signal distortion produced by the physical connection of two different components. Figure 7.5 and Figure 7.7 illustrates the combined components.
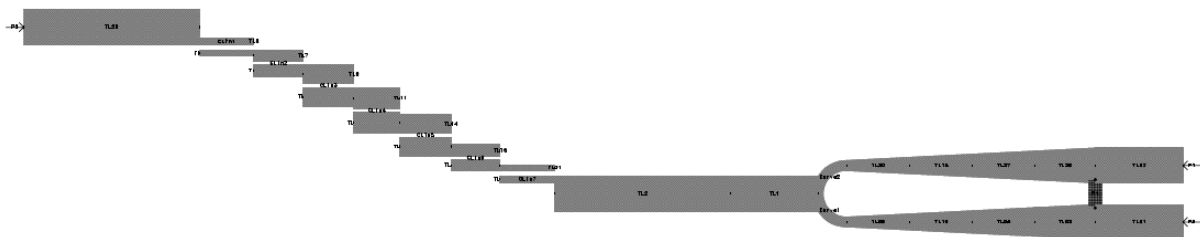
Figure 7.5 - Combined bandpass filter with 12 *GHz* centred frequency and power divider

After the junction some optimizations had to be made although it didn´t drastically degraded the signal.

The output signal spectrum at the end of this junction is represented in Figure 7.6.
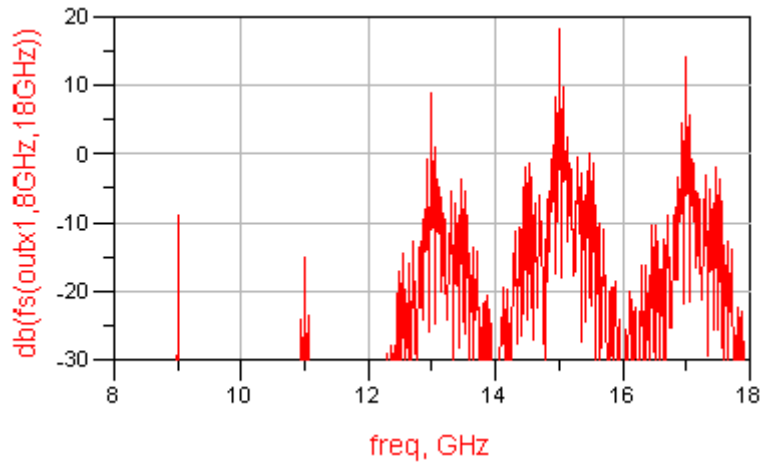
Figure 7.6 - Combined structure (16 *GHz*) output

The spectrum shows a good attenuation of signals at 9, 11 and 13 *GHz*. This is the preliminary filter that will only help the signals achievement at the end of the network.

The same procedure is made for the 12 *GHz* structure represented in Figure 7.7.
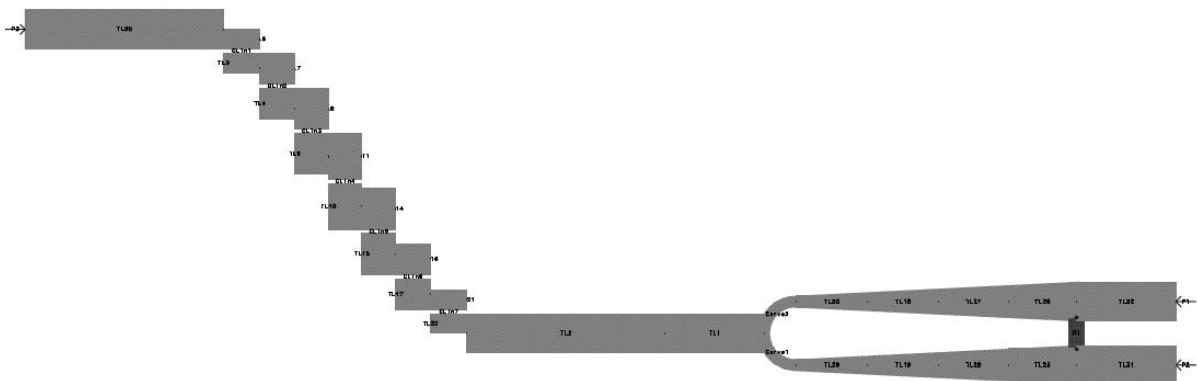
Figure 7.7 – Combined bandpass filter with 16 *GHz* centred frequency and power divider

This architecture presents the spectrum illustrated in Figure 7.8.
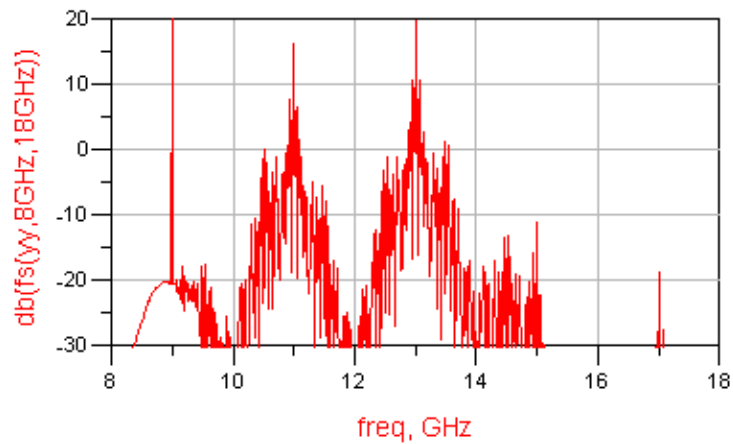
Figure 7.8 - Combined structure (12 *GHz*) output

The filter capture the 9, 11 and 13 *GHz* centered signals and severely attenuates the rest of the channel data.

After this stage, the signal is specifically filtered and properly received. The received information at the downlink output is presented separately for each frequency in Figure 7.9 and Figure 7.10.
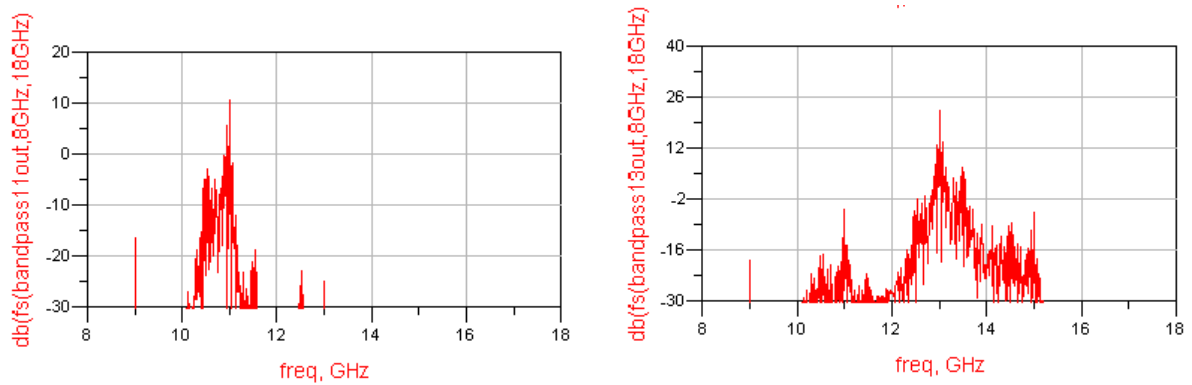
Figure 7.9 – 11 and 13 *GHz* centered signals spectrums
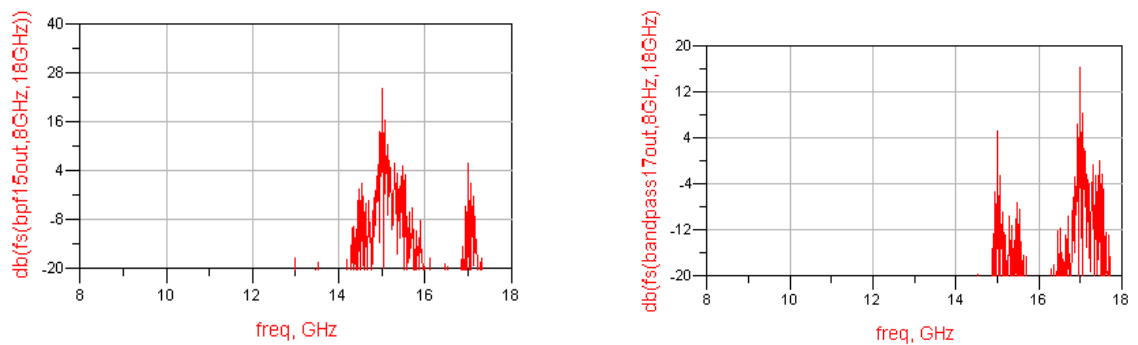
Figure 7.10 – 15 and 17 *GHz* centered signals spectrums

As expected the 9 and 11 *GHz* centered signals (see Figure 7.1) have more attenuation regarding the extra power divider that is submitted to it. Each standalone power divider presents attenuation around 5 *dB* and each bandpass filter attenuates the signal in 3 *dB*. Thus, the combined structures have an attenuation around 8 *dB* for each output channel.

Finally the eye diagram is analysed at the end of each bandpass output as illustrated in Figure 7.11.
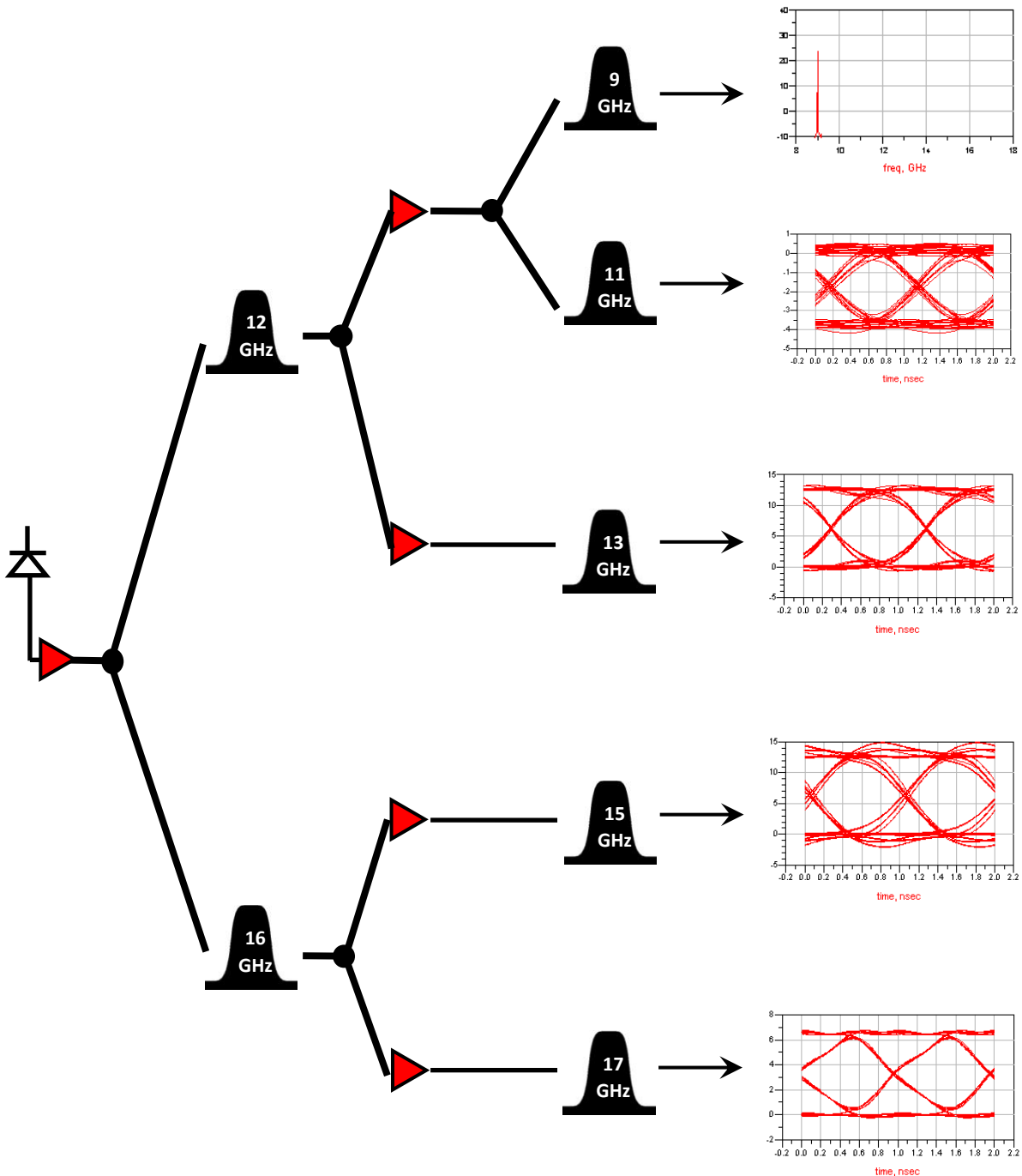
Figure 7.11 - Eye diagrams of the received signals

These eye diagrams are obtained after downconversion filtering again with the SRRCOS lowpass filter. At 11 *GHz* it has some distortion due to the unified carrier power. A very narrow filter was designed to achieve this satisfactory response. The 13, 15 *GHz* produced good results showing a few ISI in the transmission signals and at 17 *GHz* the best result is achieved, mainly because of the degree of freedom offered by the non existing upper adjacent signal.

The carrier was also captured with success at the end of the network. This will be integrated in the uplink channel of the RoFnet project.

7.3. Chapter summary

A network simulation was done with the Momentum results of all designed microstrip components. It was found that although a single and isolated component may appear to work satisfactory, when it is introduced and connected to other elements in a whole network environment the results are always less satisfactory. Thus, several iterations were made with all network components to achieve the better eye diagrams possible.

8. Conclusions and further work

8.1. Conclusions

This dissertation starts by introducing the RoFnet project and to discuss the BS architecture. Since the main components studied in this dissertation are the BS filters and power splitters, the theory behind microwave filters have been thoroughly studied as well as the microstrip transmission lines theory. Some fundamental concepts of digital communications have been presented and the design strategies discussed.

The lowpass filter required for testing and the bandpass filters required for the operation of the BS downlink have been designed and simulated using both ADS and Momentum simulators. Additionally, two power splitters have been designed.

The construction of the lowpass filter was based on finding the appropriate lumped-element prototype and implementing it in microstrip form employing the stepped impedance method. The necessary transmission zeros were introduced by open-circuited stubs $\lambda/4$ long at the frequency for which the transmission zero is desired. The equivalence between the analytical SRRCOS filter response and Momentum response was very good .To achieve an ideal microstrip response plenty of iterations must be made. Spurious bands are very important to consider when optimizing the microstrip SRRCOS lowpass filter. An agreement between the ideal response equivalence until 0.875 GHz and the spurious bands must be made without ever forgetting that the structure might change after Momentum analysis.

Bandpass filters needed more attention regarding Momentum simulation than the lowpass filter due to the different architecture and higher operational frequencies. Thus, schematic results of the bandpass filters are a little wider than expected to prevent bigger distortion when simulating with Momentum. Other important issue in bandpass filters is that narrow bandwidth implicates a higher number of stages and bigger gaps and therefore higher loss as it can be seen by the previous implementations. Frequencies values are also an important factor to consider due to the attenuation that it produces to the pass band.

Higher frequencies and larger components areas make the Momentum simulation run slower. The final bandpass filter with center frequency of 17 GHz was harder to design

because of the operational frequency value. More attenuation and degradation of the signal are considerations that need to be taken into account at this range of frequencies.

Results obtained with Momentum are not exactly as the theoretical ones. This software achieves a realistic performance since it considers more undesirable effects and interferences.

Power dividers are classified as reciprocal devices, i.e. they can also be used as a low loss power combiner of identical signals. The analysis for these devices is done based on the S-parameters (power division, insertion loss, isolation and port matching). A good performance was achieved as seen in the power divider results, however if expenditures were not an issue several types of substrate would be used and surely even better results (performance and dimensions) would occur in some components. More stages in the multistage Wilkinson power divider mean more bandwidth, however an optimal value must be considered for length reasons. The Momentum simulation of these devices presented good behaviors at the required operational bandwidth.

A limitation of this work was the minimum design dimensions imposed by the manufacture. Also, a different substrate for the higher frequency components would improve some performances and the layout of the design components.

The overall simulation had some difficult points. To acquire sufficient knowledge to build, create, perform analytical and Momentum simulations, took long weeks of practice and long manual readings. After this barrier was crossed, better results and more interesting details were achieved. Thus the overall simulation was made with Momentum, i.e. the results of the electromagnetic simulator were used in the final simulation as well as the physical characteristics of the amplifier. This analysis produced good eye diagrams at the projects network output.

8.2. Further work

The physical implementation of the components should be made and a comparison to the simulated values is advised. Some of these components are built to operate alone in a single substrate and the utilization of a different substrate for higher frequency components will bring better results.

Passband filters were taken to the limit with this architecture. RF filters that require a bandwidth much greater than 10% of the centre frequency are difficult to implement, since

conventional filter design techniques such as those for coupled line are applicable to filters with less than 10% bandwidth, thus for further work and if expenditures are not a great issue it is recommended the use of dual output amplifiers to avoid this initial trialing and improve the network performance.

A study regarding the contribution of noise to the overall system performance may also be quite interesting as well as the uplink behaviors of the RoFnet network. After the carrier is captured it would be appealing to study the uplink performance of the BS architecture.

9. References

[1] J. O'Reilly, P.M. Lane, J. Attard and R.Griffin, "Broadband Wireless Systems and Networks: an Enabling Role for Radio-over-Fibre," Philosophical Transactions of the Royal Society, London, No. 1773, 2000.

[2] W. A. Davis, K. Agarwal, "Radio Frequency Circuit Design," John Wiley & Sons, Inc, New York, 2001.

[3] David M. Pozar, "Microwave Engineering," John Wiley & Sons, New York, 2005.

[4] Mircowaves&RF, http://www.mwrf.com/Articles/ArticleID/19725/19725.html, visited at January 2009.

[5] Effy Deal Global Co., Ltd, http://www.pcbprototype.net/article/Design_Techniques_ 4. html, visited at October 2008.

[6] T. C. Edwards, M. B. Steer, "Foundations of Interconnect and Microstrip Design," John Wiley & Sons, New York, 2000.

[7] Mircowaves&RF, http://www.mwrf.com/Articles/ArticleID/20743/20743.html,visited at January 2009.

[8] E. H. Fooks, R. A.Zakarevicius, "Microwave Engineering Using Microstrip Circuits," Prentice Hall, New York, 1990.

[9] Microwave Encyclopedia, http://www.microwaves101.com/encyclopedia/propagation .cfm, visited at February 2009.

[10] P. Russer, "Electromagnetic, Microwave Circuit and Antenna Design for Communi-cations Engineering," Artech House Publishers, New York, 2003.

[11] A. P. Martin, "Applied Electromagnetics," McGraw-Hill Book Company, New York, 1978.

[12] F. Nibler, "High Frequency Circuit Engineering," IEEE Circuit and Systems Series 6, UK, 1996.

[13] Microwave Encyclopedia, http://www.microwaves101.com/encyclopedia/sparamete rs.cfm, visited at February 2009.

[14] 0. P. Sharma, V. Janyani, S. Sancheti, "Analysis of Raised Cosine Filtering in Communication Systems," Proceedings of the Third International Conference of IEEE on Wireless Communication and Sensor Networks (WCSN-07), IEEE, Allahabad, 2007.

[15] Proakis, J. G., Salehi, M., "Communication Systems Engineering," Prentice Hall, New Jersey, 2002.

[16] I. A. Glover, P. Grant, "Digital Communications," Prentice Hall, 1998.

[17] J. Proakis, "Digital Communications," McGraw- Hill, New York, 1995.

[18] Edwards, T., "Foundations for Microstrip Circuit Design," John Wiley & Sons, West Sussex, 1992.

[19] G. van Ruymbeke, "Filtres continus integres programmables," Ph.D. thesis, EPFL, Lausanne, 1995.

[20] G. Ruymbeke, C. C. Enz,, F. Krummenacher, and M. Declercq, "A BiCMOS Programmable Continuous-Time Filter Using Image-Parameter Method Synthesis and Voltage-Companding," IEEE Journal of solid-state circuits, No. 3, 1997.

[21] F.F. Kuo, "Network analysis and synthesis," John Wiley & Sons, New York, 1966.

[22] G.C. Temes, J.W. LaPatra, "Introduction to circuit synthesis and design", McGraw-Hill, New York, 1977.

[23] G.L. Matthaei, L. Young and E.M.T. Jones, "Microwave filters, impedance-matching networks, and coupling structures," McGraw-Hill, New York, 1964.

[24] Mircowaves&RF, http://www.mwrf.com/Articles/ArticleID/20743/20743.html, visited at April 2009.

[25] S. B. Cohn, "Parallel-Coupled Transmission-Line-Resonator Filters," IRE Trans. Microwave Theory and Techniques, No. 2, 1958.

[26] K. M. Cheng and F. Wong, "A New Wilkinson Power Divider Design for Dual Band Application," IEEE microwave and wireless components letters, No. 9, 2007.

[27] Electromagnetic Problems, http://www.ee.bilkent.edu.tr/~microwave/programs/ magnetic/mwpower/wilk1.htm, visited in April 2009.

[28] B. C. Seymour, "A class of Broadband Three-Port TEM-Mode Hybrids," IEEE transactions on microwave theory and techniques, No.2, 1968.

[29] Agilent, http://www.home.agilent.com/agilent/product.jspx?nid=4346.0.00&cc= US &lc=eng, visited at April 2009.

[30] Agilent, http://edocs.soco.agilent.com/display/ads2008U1/Tuning+and+Optimi-zing+Designs, visited at March 2009.

[31] Agilent, http://edocs.soco.agilent.com/display/ads2008U2/Momentum+Basics, visited at February 2009.

[32] RF Globalnet, http://www.rfglobalnet.com/product.mvc/Agilent-EEsof-EDA-Momentum-3-D-planar-EM-simu-0001, visited at February 2009.

[33] Hittite Microwave Corporation, http://www.hittite.com/products/index.html/category/1, visited at March 2009.

[34] Gary Breed, "Analyzing Signals Using the Eye Diagram," High Frequency Electronics, 2005.

[35] Glossary of telecommunications terms, http://www.its.bldrdoc.gov/fs-1037/fs-1037c.htm, visited at April 2009.

10. Apendix

Appendix 1 - Rogers RO6006 datasheet

PROPERTY	TYPICAL VALUE [2]		DIRECTION	UNITS [1]	CONDITION	TEST METHOD
	6006	6010LM [3]				
Dielectric Constant, ε_r	6.15 ± 0.15	10.2 ± 0.25 10.5 ± 0.25 10.8 ± 0.25	Z		10 GHz/A	IPC-TM-650 2.5.5.5
Dissipation Factor, tan δ	0.0027	0.0023	Z		10 GHz/A	IPC-TM-650 2.5.5.5
Thermal Coefficient of ε_r	-410	-425	Z		-50 to 170°C	IPC-TM-650 2.5.5.5
Surface Resistivity	7x10⁷	5X10⁶		Mohm	A	IPC 2.5.17.1
Volume Resistivity	2X10⁷	5X10³		Mohm cm	A	IPC 2.5.17.1
Young's Modulus under tension	627 (91) 517 (75)	931 (135) 559 (81)	X Y	MPa (kpsi)	A	
ultimate stress	20 (2.8) 17 (2.5)	17 (2.4) 13 (1.9)	X Y	MPa (kpsi)	A	ASTM D638 (0.1/min. strain rate)
ultimate strain	12 to 13 4 to 6	9 to 15 7 to 14	X Y	%	A	
Young's Modulus under compression	1069 (155)	2144 (311)	Z	MPa (kpsi)	A	
ultimate stress	54 (7.9)	47 (6.9)	Z	MPa (kpsi)	A	ASTM D695 (0.05/min strain rate)
ultimate strain	33	25	Z	%		
Flexural Modulus	2634 (382) 1951 (283)	4364 (633) 3751 (544)	X Y	MPa (kpsi)	A	ASTM D790
ultimate stress	38 (5.5)	36 (5.2) 32 (4.4)	X Y	MPa (kpsi)		
Deformation under load	0.33 2.10	0.26 1.37	Z Z	% %	24 hr/50°C/7MPa 24 hr/150°/7MPa	ASTM D621
Moisture Absorption	0.05	0.05		%	24hr/23°C 0.050" (1.27mm) thick	IPC-TM- 650 2.6.2.1
Density	2.7	3.1				ASTM D792
Thermal Conductivity	0.48 (3.3)	0.78		W/m/K (BTU/in/ft²/hr/°F)	23 to 100°C	ASTM D2214, Modified
Thermal Expansion	47 34, 117	24 24, 24	X Y,Z	ppm/°C	0 to 100°C	ASTM 3386 (5K/min)
Td	500	500		°C TGA		ASTM D3850
Specific Heat	0.97 (0.231)	1.00 (0.239)		J/g/K (BTU/lb/°F)		Calculated
Copper Peel	14.3 (2.5)	12.3 (2.1)		pli (N/mm)	after solder float	IPC-TM-650 2.4.8
Flammability Rating	94V-0	94V-0				UL
Lead-Free Process Compatible	Yes	Yes				

STANDARD THICKNESS:	STANDARD PANEL SIZE:	STANDARD COPPER CLADDING:
0.010" (0.254mm) 0.025" (0.64mm) 0.050" (1.27mm) 0.075" (1.90mm) 0.100" (2.50mm)	10"X 10" (254 X 254mm) 10"X 20" (254 X 508mm) 20"X 20" (508 X 508mm)	¼ oz. (8 μm) electrodeposited copper foil. ½ oz. (17μm), 1 oz. (35μm), 2 oz. (70μm) electrodeposited and rolled copper foil. Heavy metal claddings are available. Contact Rogers Customer Service.